R. & M. No. 3558

R. & M. No. 3558

MINISTRY OF TECHNOLOGY

AERONAUTICAL RESEARCH COUNCIL
REPORTS AND MEMORANDA

Flight Tests on the Short SB5 with 60° Sweepback and Low Tailplane
Part I – Forces and Moments

By K. J. Staples, B.Sc.(Eng.), A.F.R.Ae.S., F.B.I.S.

LONDON: HER MAJESTY'S STATIONERY OFFICE
1969
PRICE £2 0*s.* 0*d.* NET

Flight Tests on the Short SB5 with 60° Sweepback and Low Tailplane
Part I – Forces and Moments

By K. J. Staples, B.Sc.(Eng.), A.F.R.Ae.S., F.B.I.S.

Reports and Memoranda No. 3558*
May, 1967

Summary.

The Short SB 5 is a low-speed research aircraft capable of operation with wing sweepback angles of 50°, 60°, or 69°, various wing leading-edge configurations, and a high or low tailplane. Extensive flight measurements have been made in the 60° sweepback, low-tail configuration and these included tests with inboard nose flaps undeflected, with nose flaps deflected 4° and 20·2°, and with full-span leading-edge droop. Other variations included the incorporation of a small leading-edge notch at 70 per cent semispan, and 20° deflection of the trailing-edge flaps. This Report is restricted to consideration of the forces and moments acting on the aircraft and those produced by the control surfaces; fluid motion investigations are to be reported separately.

Comparisons are made of the flight results with three different series of wind-tunnel tests, and with estimates and theory. Pilots' opinions of the general handling characteristics of the aircraft are also reported.

CONTENTS

*Replaces R.A.E. Tech. Report 67 116—A.R.C. 29 529.

---

1. *Introduction.*

The continual increase in the speed of aircraft has led to wing planforms with increasing sweepback and lower aspect ratios. These particular planform characteristics have been adopted largely from performance considerations. It is, of course, necessary that aircraft be controllable throughout their operating speed range and the fact that the wing design has been determined in the first instance by high speed requirements might be expected to cause problems in the 'low' speed regime of take-off and landing.

A fairly thorough background of experience has been obtained of the low speed characteristics of aircraft with wings of substantially unswept planform and moderate to large aspect ratio. Approach and landing speeds in particular, are determined by allowing a suitable safety margin above the speed corresponding to the wing maximum lift coefficient, which may be increased above that of the basic wing by one or more of a variety of high-lift devices. Any attempt to exceed the maximum lift coefficient results in sudden loss of control, caused by a general breakdown of the ordered flow over the wings, i.e. the conventional stall.

The introduction of moderate amounts of wing sweepback, say roughly between 20° and 45° on the quarter-chord line, results in less precisely defined limits to the minimum flying speed in that, at values of lift coefficient below the maximum, local areas of flow breakdown occur and increase in extent as the lift coefficient is increased. There is a consequential deterioration in stability and/or control, generally gradual, but often sufficient to make unrealistic the definition of an approach speed based on a margin from the maximum lift coefficient. The approach speed is then determined by some minimum stability and control requirements, which can finally be defined only by flight experience.

With still larger angles of sweepback, and particularly where the wing has a sharp leading edge, the transition from attached to 'separated' flow may occur at quite a low lift coefficient; this 'separated' flow, however, can be ordered and stable and satisfactory operation in this regime can be achieved. The concept of a maximum lift coefficient has no practical significance, and the breakdown of the flow from an ordered, but 'separated', to a disordered state may occur only at a very high angle of incidence.

Assuming there are no limitations to the approach speed due to vision from the cockpit, tail 'clearance', or some such geometric characteristic of the aircraft, the limiting factors will again be stability and control.

At the time of the initial conception of the Short SB 5 research aircraft (1949), it was recognised that the trend towards higher angles of sweepback was likely to continue, and this was emphasised by the existence of a design for an operational fighter aircraft, the English Electric P1 (Lightning), which was to have a sweepback of 60°. There was then no flight experience with wings of this amount of sweepback. The SB 5 was designed to allow a gradual approach to this configuration, flying initially with 50° sweepback before conversion to 60° when it would resemble, aerodynamically, a seven-eights scale model of the Lightning. To increase its usefulness as a research vehicle the aircraft was capable of further modification to operate with 69° of wing sweepback.

This Report is concerned with tests made in flight on the aircraft with 60° of wing sweepback. It is confined to force and moment measurements, as distinct from fluid-motion investigations, (pressure plotting, flow visualisation, etc.), which will be presented in a later report (Part 2). An extensive series of tests was made with various wing configurations, including the plain wing, two different inboard nose-flap deflections, or alternatively, a full-span drooped leading edge. The tests covered measurements of lift and drag, static longitudinal stability and static and dynamic lateral stability, and the control power of all surfaces except the rudder. The report is divided by subjects into self-contained sections, each section covering all the configurations tested and including a comparison with wind-tunnel results (from up to three different tunnels), estimates and theory, where applicable. Section 13 gives a general discussion of all the results presented and outlines such features of the flow as are necessary for the examination of the comparisons between wind tunnel and flight. Pilots' comments on the general handling characteristics of the aircraft are given in Appendix F.

2. *Description of the Aircraft.*

The Short Brothers and Harland SB 5, ER 100, is a single seat research aircraft powered by one Derwent Mk. 8 turbojet engine, located in the rear fuselage, with a nose intake and single jet exhaust pipe. A three view general arrangement drawing of the aircraft is given in Fig. 1 and photographs of the aircraft in Fig. 2. Details of the various modifications made during the tests described here are shown in Figs. 3, 4 and 5. A brief description of the components and configurations of the aircraft is given below; full details of the relevant geometric data are given in Table 1.

The settings of the wings can be adjusted on the ground to give leading-edge sweepback angles of 50°, 60° and 69°; but only the 60° configuration is considered here. The wing trailing edge is sweptback out to approximately 55 per cent of the semispan but the outermost portion containing the ailerons is unswept in the 60° leading-edge sweep configuration. The wings have no twist or camber. They are made of plywood, except for light alloy sheeting at the leading and trailing edges.

Part span split-cum-Zap flaps are fitted, Fig. 1. On deflection of the flaps the hinge line rotates, so as to decrease its sweepback, about a fixed pivot at the outboard end. Part span inboard leading-edge nose flaps, Fig. 3, are fitted, the deflection being adjustable on the ground only. Alternatively, the wing leading edges can be drooped over the full span, Fig. 4. A notch, Fig. 5, which can be sealed to give the normal plain leading edge, is cut at 70 per cent semispan.

The complete rear fuselage, just aft of the engine, is detachable and two alternative rear fuselages are available, one with the tailplane set on top of the fin and the other with the tailplane set below the fuselage. The tailplane angle is adjustable in flight, being electrically actuated.

All control surfaces are manually operated, having set back hinges and, with the exception of the starboard elevator, geared balance tabs. The starboard elevator has a pilot operated trim tab.

The aircraft is fitted with a fixed undercarriage and Maxaret brakes operated by toe pedals on the rudder bar. Two 20 ft circumference brake parachutes and one 20 ft anti-spin parachute are housed in the rear fuselage above the jet pipe.

Wing canisters, Fig. 3, each capable of carrying up to 400 lb of ballast, and mounted on pylons, can be fitted to each wing undersurface.

The centre of gravity location can be altered within the range 0·341 $\bar{c}$ (stressing limit) and 0·435 $\bar{c}$ (zero

nose ballast) by the removal or addition of ballast weights located in the nose above the intake. The fuel is contained in a fuselage tank with a maximum capacity of 300 gallons and having its centre of gravity located at 0·423 $\bar{c}$. The movement of centre of gravity position with fuel consumption is therefore small.

The endurance of the aircraft with full fuel load is about 45 min. The all up weight at take-off varies between 11 500 lb and 12 700 lb, according to centre of gravity position and wing cannister loads.

3. *Instrumentation.*

During the course of the flight tests the aircraft instrumentation underwent a number of changes. Initially, and for the majority of the tests reported here, an auto-observer panel was fitted in the fuselage just forward of the fuel tank and photographed by a Bell and Howell A4 camera running at approximately 8 frames per second. The auto-observer panel contained instruments to measure the following quantities:

(i) Indicated airspeed, both from aircraft and trailing static systems.

(ii) Altitude.

(iii) Angular displacement of all control surfaces and the elevator trim tab.

(iv) Tailplane setting relative to fuselage datum.

(v) Trailing edge flap deflection.

(vi) Stick force, longitudinal and lateral.

(vii) Angles of pitch, bank and sideslip.

(viii) Rates of roll and yaw.

(ix) Normal acceleration.

(x) Engine speed.

(xi) Ambient and jet pipe temperatures.

(xii) Fuel gallons gone.

(xiii) Attitude by liquid bubble.

(xiv) Time base by clock.

For tests of the lateral oscillation with full-span leading-edge droop two S.F.I.M. A.22 Hussenot continuous trace recorders were fitted. These recorded normal acceleration, indicated airspeed, rudder deflection, angle of sideslip, angles of roll and yaw and rates of roll and yaw.

Prior to the stability and control measurements with the plain leading edge (no droop, 0° nose flap) the aircraft was completely re-instrumented. The two A22 recorders were replaced by two Beaudouin A13 recorders indicating the following quantities:

(a) Indicated airspeed.

(b) Altitude.

(c) Angular displacement of all control surfaces.

(d) Angles of bank, yaw and sideslip.

(e) Rates of roll and yaw.

(f) Normal and longitudinal acceleration.

The auto-observer panel was retained but no longer indicated items (iii), (vii) and (viii) listed above.

The aircraft airspeed was sensed by a pitot-static head mounted at the end of a six foot boom projecting from the nose of the aircraft on the starboard side. The head was deflected down 15° relative to fuselage datum so as to reduce the position error at high angles of incidence. A similar boom on the

port side carried the sideslip vane.

For position-error measurements a trailing static, raised and lowered by an electrically powered winch, under the control of the pilot, was fitted forward of the fuel tank in the fuselage. This was connected across an airspeed indicator to a venturi pitot on the starboard side of the fuselage.

4. *Programme of Tests.*

4.1. *Historical.*

The first flight of the aircraft was made in December 1952, with wing leading-edge sweepback of 50°, full-span drooped leading edge of 20·1° measured in the line of flight, and the tailplane in the high position on top of the fin. The aircraft was operated from the Aeroplane and Armament Experimental Establishment Airfield at Boscombe Down. The first flight with the wing sweepback increased to 60°, retaining the drooped leading edge and high tail, was made in July 1953. In January 1954, testing commenced in the low-tail configuration with the English Electric Lightning (P.1A) type of nose flap and leading-edge droop outboard of the flap. The amount of flying in these early configurations was restricted to the minimum essential for flight clearance, in order that the English Electric Lightning configuration might be tested before that aircraft made its first flight. This important aim was achieved when the outboard leading-edge droop was removed in February 1954. The aircraft then resembled a seven-eighths scale model of the Lightning with nose flap down. It was transferred from A & A.E.E., Boscombe Down to R.A.E., Farnborough in June 1954, and to R.A.E., Bedford in August 1956. Testing in the 60° sweep configuration was completed in April 1958.

4.2. *Present Series of Tests.*

The purpose of the investigation reported here was to determine the general performance and stability characteristics of the aircraft in the 60° wing sweepback, low tail configuration. Excluded from the present Report is a considerable programme of general flow studies, which will be reported separately. The aircraft was tested in the following conditions:

(A) Basic configurations, nose flaps deflected 4° (in line of flight), trailing-edge flaps up, leading-edge notch both cut and sealed.

(B) Nose flaps deflected 4°, trailing-edge flaps deflected 20°, leading-edge notch both cut and sealed.

(C) Nose flaps deflected 20·2°, trailing-edge flaps up, leading-edge notch both cut and sealed.

(D) Full-span drooped leading-edge deflected 10·7° (in line of flight), trailing-edge flaps up, leading-edge notch sealed.

(E) Undeflected leading edge (0° droop, 0° nose flap), trailing-edge flaps up, leading-edge notch both cut and sealed.

Configuration (C) represents the prototype English Electric Lightning (P.1A) with nose flaps deflected. Configurations (A) and (B) have a nose-flap deflection representative of the undeflected, but cambered nose flaps on the P.1A and were tested at the request of the English Electric Company to determine whether it would be possible to delete the nose flap, used for landing, on this aircraft. Production versions of the Lightning (P.1B) have, in fact, no nose flaps. Configuration (D) simulates an application of conical camber to the Lightning, primarily intended to reduce the induced drag at moderate and high values of lift coefficient. Configuration (E) was obtained simply by removing the leading-edge droop of configuration (D) and was used primarily for flow studies. There was then no merit in replacing the nose flaps for this work.

The tests covered a lift-coefficient range from $C_L = 0{\cdot}13$ to $C_L \simeq 1{\cdot}2$ and are summarised below, the letters in brackets indicating the configuration tested:

(i) Position error measurement, at maximum continuous cruise engine speed 14 100 r.p.m. (ABCD), and idling (ABCD).

(ii) Lift and drag from partial glides, at engine speeds 14 100 r.p.m. (CD) and idling (ABCD).

(iii) Minimum speed (C).

(iv) Stick fixed and stick free longitudinal stability (ABCE).

(v) Rolling performance including damping in roll (C) and aileron effectiveness (CE).

(vi) Lateral stability, static (ACD) and dynamic (DE).

The total experimental flying on the aircraft in the 60° swept-wing, low-tail configuration and excluding miscellaneous flying (pilot's handling, post-inspection air tests, etc.) covered 185 hours of which the tests covered by this report took 118 hours.

5. *Position Error.*

Analysis of the flight test results necessitated accurate knowledge of the position error. Measurements were made using a winged trailing static and a venturi pitot connected across a test airspeed indicator which was then compared with the standard aircraft indicator. Results were obtained with two engine settings, 14 100 r.p.m. and idling, and all other flight results, with the exception of the minimum speed tests, were obtained at one or other of these engine settings.

Pressure lag[2] in the tubing between the trailing static head and the automatic observer was appreciable; the total correction that had to be applied amounted to a maximum of 3·7 knots in the most severe case, that of engine idling tests at low speed, where the rate of descent was highest. It was unnecessary to account for the lag in the aircraft system separately, since the position-error measurements were made under the same flight conditions of altitude and rate of descent as were used later in the aerodynamic measurements. The effect of the aircraft system lag was thus automatically included in the calibration.

Fig. 6 gives the position-error results obtained. It will be noted that in all cases there is a large effect of power. This is mainly due to changes in fuselage blockage with variation in engine intake mass flow; it should be noted that the effect of lag in the aircraft system, associated with the differing rates of descent during tests with power on and idling power, accounts for only about 0·5 knots of the difference between the two curves in the 20·2° nose flap configuration. However, for the other configurations, the volume of the aircraft system was increased considerably due to the installation of pressure-plotting instrumentation. The greater difference between the corrections for 14 100 r.p.m. and engine idling shown in Fig. 6b compared with Fig. 6a is probably mainly due to the increase in lag associated with the increased system volume.

The curves for the full-span leading-edge droop configuration, Fig. 6c, are of different shape to those for the other configurations. Again a change in the position error due to lag is the probable explanation since the drag characteristics, and hence the rate of descent in a given flight condition, are appreciably different for the droop configuration compared with the other two (*see* Section 6.2). Nevertheless there are some unexplained anomalies in the curve for engine idling, the corrections at the higher speeds being rather greater than might have been expected and those at the lowest speeds being smaller than expected.

No distinction has been made in position-error determination between notch cut and notch sealed. The influence of the notch is almost certainly negligible since its effect on lift and drag was found to be small (*see* Section 6).

6. *Lift and Drag.*

The lift and drag characteristics of the aircraft were determined using the partial glide technique (*see* Appendix A). The aircraft was flown at various steady indicated airspeeds over the range from 90 knots to 260 knots, and the time measured for a given change in altitude. The mean altitude for all tests was about 5 000 ft. Results are almost inevitably subject to some scatter due to disturbances caused by atmospheric turbulence at this low altitude. In fact, in drawing curves through the experimental points each data point has been weighted according to the steadiness of the particular partial glide.

The aircraft has a low service ceiling, 10 000 ft, and this, combined with a high rate of descent during power off flight at low and high lift coefficients made testing difficult under these conditions. (About

1 000 ft of height is lost in regaining speed from 90 knots to the minimum (120 knots) for level flight with maximum continuous cruise power.) Engine power, 14 100 r.p.m., was therefore used for some of the tests to reduce the rate of descent at low speeds, thus extending the lift-coefficient range over which results could be obtained. Since no jet pipe pressure instrumentation was fitted, estimates of thrust were made using brochure figures, corrected for ambient temperature. Estimates of thrust in this manner are liable to error, inaccuracies having most effect on the drag results. But some check on the accuracy of these power-on measurements was obtained by comparison with results obtained from glides at intermediate airspeeds and engine idling.

For the tests in the 20·2° nose flap configuration the aircraft attitude was determined from readings of pitch and roll attitude gyro in the auto-observer. This was not generally satisfactory since the gyro took some time to erect to the true vertical following an acceleration. Consequently, for tests in the other configurations, a liquid bubble inclinometer was fitted.

6.1. *Lift.*

6.1.1. *Basic configuration, 4° nose flap.* Fig. 7 shows the lift curves, notch sealed and notch cut, with the nose flap deflected 4°, and with power at flight idling. With the notch sealed there is quite strong evidence for an increase in lift-curve slope commencing at an incidence of about 12° and followed, at higher incidence, by a reduction, so that above $\alpha \simeq 15°$ the slope is not much different from that at low incidence. Cutting the notch eliminates this kink. The lift-curve slopes, notch cut and notch sealed, are identical at the lower incidences with a value $dC_L/d\alpha = 2{\cdot}14$ radian^{-1}.

The results presented in Fig. 7 also suggest that sealing the notch produces, even at low incidence, an increment in C_L of approximately 0·025. This amount would appear rather difficult to accept as plausible and may be attributable to some error in the measurements, although no such error could be found in the analysis.

Fig. 8 shows the effect on the lift of deflecting the trailing-edge flaps 20°. At zero incidence lift increases by $\delta C_L \simeq 0{\cdot}17$, due to the flap deflection, but the associated lift-curve slope is surprisingly low, ($dC_L/d\alpha = 1{\cdot}73$ per radian), so that at $\alpha = 12°$ the flaps produce an increment in C_L of only 0·03. Above 12° incidence the lift curve slopes, flaps up and flaps down, are similar.

6.1.2. *20·2° nose flap configuration.* The tests in this configuration were made with power on (14 100 r.p.m.) so that, while corrections for power were made, the results are not strictly comparable with the 4° nose-flap configuration. Further, the incidence determination depended on the indication of an attitude gyro which erected slowly to the apparent, rather than the true, vertical. This could give considerable errors when the test recordings were made immediately following a change in aircraft speed. Because of these doubts the results are presented only as a broad indication of the variation of C_L with α, as shown by the dotted line in Fig. 9. No distinction is drawn between notch sealed and notch cut, and comparison with the 4° nose-flap configuration is not justified.

6.1.3. *10·7° full span drooped leading edge configuration.* Fig. 10 compares the lift curve for the drooped leading edge, with that for the nose flap deflected 4°. The curves are very similar apart from the higher incidence at which the kink occurs with the drooped leading edge. When the experimental points are weighted for the steadiness or otherwise of the particular partial glide the kink is, in fact, better defined than a simple consideration of all the points shown would indicate. The lift-curve slope below the kink has a value $dC_L/d\alpha = 2{\cdot}09$ per radian, and within the accuracy of the results this is no different from the 4° nose flap value. Measurements made with power on and power off in the drooped leading-edge configuration show reasonable agreement.

6.1.4. *Comparison with tunnels and estimates.* Wind-tunnel results are available from tests on three different models. The first tests for the 60° sweep configuration were made on a model with a high tail[3] and a low tail[4] by Short Brothers and Harland. The model differed from the aircraft in that the fuselage, from the nose to the tailplane leading edge, was wider than, and not as deep as, the aircraft fuselage, the nose and tail lines differed considerably, and the dorsal channel carrying the control cables

was omitted. There were also differences in the canopy and the tail-plane mounting and no undercarriage was fitted to the model. This model was retested[5] by the English Electric Company after modification to resemble the aircraft more closely; the differences between the original and modified models are shown in Fig. 11. An undercarriage was fitted for some of the tests. A third set of unpublished tunnel results was obtained from tests on a larger model in the R.A.E. $11\frac{1}{2}$ ft $\times$ $8\frac{1}{2}$ ft tunnel. This model was built to the dimensions of the completed aircraft rather than to drawings and ought to be expected to give the most representative results. Comparisons are presented between all of these tunnel results and the flight results, the tunnel results being reduced to trimmed lift coefficients using tunnel measurements of pitching moments. The Reynolds numbers of the tests, based on mean aerodynamic chord, were as follows:

Flight	$12{\cdot}6 \times 10^6$ to $36{\cdot}6 \times 10^6$
Shorts tunnel[4]	$1{\cdot}57 \times 10^6$
English Electric tunnel[5]	$1{\cdot}29 \times 10^6$
R.A.E. tunnel	$2{\cdot}28 \times 10^6$.

Figs. 12 to 14 show the tunnel-flight comparisons. The various tunnel results for the models with nose flaps undeflected are compared with the 4° nose-flap flight configuration in Fig. 12. All the various tunnel tests show poor agreement with flight, but it should be noted that the Shorts tests and the R.A.E. tests agree well with one another. The non-linearity in the tunnel curves first occurs at a lower angle of incidence than in flight, probably due to the lower Reynolds number[17], but the higher lift-curve slope at low incidence given by the tunnel results is opposite to the expected effect of Reynolds number.

Fig. 13 shows the effect on lift of deflecting the trailing-edge flaps. It has been prepared to show the increment in C_L produced by deflecting the trailing-edge flap 20°, as predicted in the tunnel and obtained in flight, but the results are for two different nose-flap configurations. This makes direct comparison impossible. The tunnel data shows the expected increment in C_L as a result of flap deflection. In flight the effect of the trailing-edge flap varies rather curiously with incidence, perhaps as a result of the smaller nose-flap angle, but this would not appear as adequate explanation of the flight result which suggests that the trailing-edge flap was practically useless at high C_L.

Fig. 14 shows the effect of changing leading-edge configuration on the lift curves, as obtained by the various tunnels and in flight. Shorts[4] and English Electric[5] tunnel results show no change in lift-curve slope due to changes in configuration at low incidence but a larger non-linear increment in lift-curve slope at the higher incidences with the nose flaps up than in the other configurations. The R.A.E. tunnel, however, shows little difference between the two nose-flap configurations, with, if anything, a slight increase in lift-curve slope at low incidence with the nose flaps down; it should be noted that the nose-flap deflection is less than in the other tests. The flight results also suggest an increased lift-curve slope, flaps down, and also a change in no lift angle of incidence. It is thought that neither of these changes is likely to be real, the discrepancy being due to the poor set of results with nose flaps down. The Shorts tunnel results[4] show the onset of non-linearity at a higher angle of incidence with full-span droop than with the nose flaps up, as is also shown in the flight tests, but the higher lift coefficients, flaps up, are maintained to the highest angles of incidence, unlike the flight results, where the two curves coincide again at incidences above 18°.

The estimated untrimmed lift-curve slope[6] would vary with Reynolds number as follows:

R.N.	10^6	10^7	10^8
$(dC_L/d\alpha)_{\alpha=0}$	2·12	2·24	2·28

The estimate for the flight Reynolds number of approximately 10^7 is in excellent agreement with the flight results, summarised in the Table below, which also gives the tunnel results on lift.

Lift-Curve Slope Results

Leading-edge* device		Nose flaps up		Nose flaps down	Full span droop
T.E. flaps		0°	20°	0°	0°
Trimmed $(dC_L/d\alpha)_{\alpha=0}$	Flight	2·14	1·73	2·32	2·09
	Ref. 4	2·38	2·40	2·38	2·36
	Ref. 5	2·56		2·54	
	R.A.E. tunnel	2·61		2·63	
Untrimmed $\left(\frac{dC_L}{d\alpha}\right)_{\alpha=0}$ flight		2·27		2·45	2·23

*The nose-flap/leading-edge droop deflections settings as measured in the line of flight are given below:

Nose flaps down:	Flight	20·2°
	Shorts[4]	22·9°
	English Electric[5]	22·9°
	R.A.E. tunnel	15°
Nose flaps up:	Flight	4°
	all tunnels	0°
Nose flaps, for 20° T.E. flaps:	Flight	4°
	Shorts[4]	22·9°
Full span droop:	Flight and Shorts[3]	10·7°.

6.2. *Drag.*

6.2.1. *Basic configuration and effect of leading-edge notch.* Fig. 15 shows the variation of drag coefficient with C_L^2 for the 4° nose-flap configuration and the effect of cutting the leading-edge notch. The most noticeable characteristic is a sudden increase in the slope of the curve at $C_L \simeq 0{\cdot}35$ with the notch sealed and at $C_L \simeq 0{\cdot}42$ with the notch cut. This kink corresponds to the start of the disturbed flow conditions near the wing tips. The increase in slope is rather more severe with the notch cut. Denoting the induced drag factor, $\pi A.\ dC_D/d(C_L^2)$, as k_1 at values of C_L below the kink, and as k_2 at values above the kink, the following results are obtained:

	k_1	k_2
with notch	1·7	3·4
without notch	1·4	2·8

Deflecting the trailing-edge flaps 20°, with the notch cut, Fig. 16, causes no change, within the accuracy of the results, in drag coefficient at zero lift, in k_1, or on the kink C_L, but there is an indication of a decrease in the value of $k_2(k_2 = 3{\cdot}0)$, so that there appears to be a small, but ill defined, reduction in the drag coefficient at higher values of C_L with the flaps lowered.

6.2.2. 20·2° *nose-flap configuration.* Fig. 17 gives the drag in the 20·2° nose-flap configuration. The general characteristics are similar to the basic configuration.

6.2.3. 10·7° *full-span drooped leading-edge configuration.* Fig. 18 compares results for the full-span drooped leading edge with the basic configuration. The drag curve breaks at about the same $C_L = 0{\cdot}37$ in either case but with the droop, there is only a relatively small increase in the slope up to $C_L = 0{\cdot}68$. There, a second break occurs after which k is much larger than on the basic wing, so that at about $C_L = 0{\cdot}9$ both configurations have about the same C_D.

6.2.4. *Comparison with tunnel.* Tunnel drag results are available from Shorts tests[3,4] and the unpublished data from the R.A.E. tests, and are shown in Figs. 19 to 21. The values of lift coefficient measured in the tunnel have been converted to trimmed values using tunnel pitching-moment measurements, for direct comparison with the flight measurements. However, the additional trim drag appropriate to this has not been added to the tunnel data. This additional drag would increase the overall induced drag for the tunnel results by about 5 per cent. To get an exact comparison with flight one would also have to consider the pitching moment from the momentum drag of the air entering the engine intake, which unloads the tailplane and thus reduces trim drag. An attempt to assess the drag characteristics of the wing plus fuselage, from the flight results to get a more meaningful comparison with tunnel data, is given later in this Section, but for the discussion below it should be remembered that the tunnel-drag coefficients are uncorrected for these effects and are therefore lower than they ought to be. A further allowance must be made for the absence of an undercarriage on the tunnel models, as discussed later.

Fig. 19 compares the flight and tunnel results in the basic configuration. The Shorts results[4] give a kink C_L similar to the flight value but higher values of the induced-drag factors, whereas the R.A.E. tunnel gives similar induced drag-factors but a higher kink C_L than in flight. The lower value of C_{D0} in the tunnels can be accounted for by the absence of an undercarriage.

Fig. 20 compares the effect of trailing-edge flap deflection as obtained in the tunnel and in flight. It should be noted that for the tunnel tests the nose flap is deflected 22·9°, whereas in flight it is only 4°, and that the flight results are for notch cut. Nevertheless, it is apparent that the tunnel predicts a large change in C_{D0} due to flap deflection accompanied by an increase in the kink C_L, whereas little change in either of these is evident in flight. The addition of undercarriage drag to the tunnel results would increase the drag throughout the C_L range.

Fig. 21 compares all the available results on the effect on drag of changing the leading-edge configuration.

Both the flight results and those from the R.A.E. tunnel are in agreement in showing an increase in drag over the full C_L range, when the leading edge flaps are lowered, whereas this effect is only apparent at C_L values greater than 0·7 in the Shorts results[4].

Results for the drooped leading edge are only available from flight and Ref. 4. In both cases droop reduces the drag but the variation of this effect over the C_L range differs fundamentally between these two sets of results.

All the drag results from flight and tunnels are summarised in Table 2 giving values of the induced drag factor k, the appropriate C_L range over which it applies, and the drag at $C_L = 0$.

It should be noted that, in flight, Reynolds number decreases as lift coefficient is increased. This increases the slope of the measured drag curve, at least to the kink. Estimates[6] have been made of the approximate magnitude of this effect, assuming transition at the leading edges of the wings, tailplane and fin and at the nose of the fuselage. Correcting to a constant R.N. $= 30 \times 10^6$ causes a reduction in the induced-drag factor at low C_L by about 0·04 for all configurations.

It was thought to be of interest to deduce from the flight results the induced drag of the wing plus fuselage alone by deducting the contribution of the trim drag, and to compare this then with theoretical estimates. The tailplane makes three contributions to the induced drag (*see* Appendix A):

(i) The extra wing lift required to counteract the negative tailplane lift.

(ii) The induced drag generated by the trim lift on the tailplane itself.

(iii) The drag component of the tailplane lift which acts normal to the local stream rather than to the free stream.

Calculations were carried out to estimate these quantities as relevant to the flight conditions under which the drag tests were made. Using flight data (*see* Section 8) from the longitudinal stability tests, the appropriate values of tailplane lift can be obtained. The inclination of the tailplane lift has been taken from tunnel downwash measurements[5].

The induced-drag factor for the tailplane has been taken as $k = 1{\cdot}4$. This rather high value was chosen to allow for the fact that the fuselage is relatively large in comparison with the tailplane, and to account for the additional drag of the horn balance. As it was found that the tailplane lift never exceeded 0·1, it was assumed by analogy with wing results that no vortex separation would occur. When these corrections are applied the induced-drag factor for the aircraft as obtained from trimmed flight is reduced by approximately 5 per cent at low lift. The values are shown in Table 3.

Theoretical estimates have been made for both the zero lift drag C_{D_0} and the induced-drag factor k for the wing plus fuselage contribution. The results are listed in Table 4. The estimated zero-lift drag for the complete aircraft is $C_D = 0{\cdot}037$, which is approximately 20 per cent higher than the flight data. C_{D_0} without undercarriage was estimated at a Reynolds number appropriate to the tunnel tests and gave a value of 0·019, which is in fair agreement with experiment.

A method for estimating the induced drag of sweptback wings with attached flow is given by Bagley[7]. The reference considers only cases with a uniform C_L distribution across the span, a condition which on swept wings is incompatible with design for minimum induced drag.

Consequently for this type of wing, the value of the induced-drag factor k is greater than unity by an amount δ, which depends on aspect ratio and sweep. To allow for the thickening of the boundary layer near the tips, due to spanwise drift of fluid in the 'sublayer', Bagley suggests the addition of a further increment to k which, according to the very limited data available, appears to be of the same order as the δ quoted above. On this basis we obtain a value $k = 1{\cdot}3$ for the SB 5 planform. Wind-tunnel results on wing pressure distributions on the English Electric Lightning[8] show, however, that C_L varies across the span, increasing rather erratically from the root to the tip for the 4° nose-flap configuration. But because of the rather unusual planform, in which the chord reduces gradually from the root to the trailing-edge kink, and then more rapidly to the tip, the spanwise loading distribution differs from the ideal elliptical distribution by the same order as that for the wings considered by Bagley[7].

For the 20·2° nose flap configuration, on the other hand, the C_L distribution is extremely irregular, being high, and of the same order, at the root and tips, and some 50 per cent lower between 20 and 60 per cent semispan. As a consequence, the loading on the outboard 60 per cent of the wing can be closely approximated by an ellipse, but the root of the wing is then grossly overloaded compared with the elliptic distribution. It could be concluded that $\delta = 0{\cdot}15$ is of the right order for the 4° nose-flap configuration but rather low for the 20·2° configuration.

Some trailing-edge wake experiments carried out on the aircraft with the undeflected leading edge have shown that there is no appreciable spanwise boundary-layer drift outboard of the wing trailing-edge kink. Measurements were not taken inboard of the kink, on the swept portion of the trailing edge, and some spanwise flow might well occur there*. In view of this to take an additional increment in k_1 of 0·15 for viscous affects would seem excessive. Consequently it is suggested that a value of $k_1 = 1{\cdot}15$ to $1{\cdot}20$ is reasonable for the 4° nose-flap configuration and a value somewhat higher, say $k_1 = 1{\cdot}20$ to $1{\cdot}25$, might be expected on the 20·2° nose-flap configuration.

It is of interest to note that, on the assumption of complete loss of leading-edge suction, the induced drag is given by:

$$C_{D_i} = C_L \times \tan \alpha$$

*Studies of wing tufts in flight on a Hunter show considerable outflow but none has been found on wings with unswept trailing edges (SB 5, Boulton Paul P 111, Avro 707B, Fairey Delta 2).

and that this formula gives a value of the induced drag considerably higher than that obtained in the flight measurements throughout the C_L range, so that even at values of C_L higher than the kink in the C_D *vs.* $C^2{}_L$ curves, some leading-edge suction* is maintained.

Comparing the theoretical values for the induced drag, as given in Table 4, with the corresponding corrected flight data in Table 3 shows that the estimates generally provide a much lower value for k than that obtained in flight, particularly for the nose flaps down. Obviously the flight values of C_L above the break cannot be expected to compare with the theoretical predictions which are based on attached flow.

7. *Minimum Speed.*

The behaviour of the aircraft at the lowest attainable flying speed was investigated in the configuration with the nose flap deflected 20·2° and the leading-edge notch cut. The tests were carried out with the trailing-edge flaps undeflected and at two *cg* locations, 0·363 $\bar{c}$ and 0·409 $\bar{c}$.

Great caution was exercised in approaching the lowest speeds. Speed was reduced by small increments below 120 knots, the trim curves examined at every stage for any signs of longitudinal instability or loss in elevator power. The tail setting for the first series of minimum speed tests was chosen so that at the lowest speed attained the control column was against the back stop, thus leaving maximum elevator movement for recovery.

The extract from the pilot's report quoted below adequately describes the behaviour. This test was made at the forward *cg* position, the reduction in speed being commenced at 10 000 ft.

'. . . . . Speed was reduced and the nose of the aircraft was raised by pulling on the stick until about 82 knots was registered. The directional stability seemed to deteriorate very rapidly from 83 to 80 knots, the aircraft having a tendency to yaw to starboard through approximately 6° to 7°. The ailerons were very ineffective at this stage and it was noticed that l_v had reversed sign—i.e. port rudder gave a starboard wing-down tendency. As the stick was slowly brought back nearly against the back stop the starboard yawing tendency increased and it was impossible to prevent it with quite big rudder displacements. The port wing-low tendency was counteracted by half starboard stick displacement. When at 80 knots, the aircraft suddenly yawed to starboard and dropped the *starboard wing* to approximately 60°, while the nose of the aircraft dropped about 45° to 50° from the horizontal against full back stick. The control column was pushed forward, still maintaining full port rudder, while the aircraft nosed over. A sudden reversal of roll occurred and the aircraft rolled to port while still diving in recovery. The height loss in recovery amounted to about 1 000 ft. There was no tendency to spin after the stall, but from the instant of starboard yaw and starboard wing drop when the aircraft slowly rolled and dived over—there was no control left, and the aircraft behaved as on the fall-over in a stall turn to starboard on conventional aircraft. The stick position at the entry to the stall was pro-turning or pro-spin if the spin was to commence to starboard and this may have been the reason for not entering a spin. The hinge moments in recovery were rather large as the airspeed built up quickly to approximately 150 knots . . . .'

Fig. 22 shows a typical time history of a manoeuvre of this type in which the rapid increase in sideslip, angle of bank and nose-down pitch during the recovery is clearly shown. The lack of directional stability and control rather than loss of lift evidently limits the minimum speed obtained. Therefore, an attempt was made in a further series of speed reductions, at aft *cg* position, to reach a lower speed by concentrating on keeping sideslip zero. The extract from the pilot's report below describes these tests, which were commenced at 11 000 ft.

'. . . . Control was lost on two occasions from 80 knots. The nose swung slowly but strongly to starboard and full port rudder gave no noticeable effect. Then the right wing dropped moderately slowly to 45° and the nose also drooped. The position of the ailerons is unknown but initially about one-third

*'Leading edge' is perhaps a slightly misleading term, as, when the core of the vortex originates from the root-chord leading edge, the flow is separated along the entire leading edge of the wing. However, high suction forces are induced by the vortex further aft on the chord, but still on forward facing surfaces, giving rise to a favourable component of force along the chord line.

starboard aileron was being held. But, when the wing dropped left aileron was not applied, and no explanation of the failure to use port aileron can be given. It may be that the cause of the wing drop was so obviously yaw that attention was given to this alone. When the nose dropped control was easily regained with a height loss of perhaps 500 ft . . . .'

'The pilot became convinced that the limit of control was the rudder power and if the beginning of the slightest yaw could be prevented a lower speed would be attained.'

'Accordingly, from 85 knots the aircraft was aimed at some cloud in order to keep straight and speed was reduced without referring to the instruments. Some left rudder was held on all the time and the attitude was steeply nose up. 75 knots was reached without incident and recovery was easy. No wing drop occurred on this or any of the other three occasions on which 75 knots was recorded . . . .'

Fig. 23 shows a typical time history of a speed reduction test in which control was maintained throughout. The minimum indicated airspeed attained was 75 knots though it is possible that speeds lower even than this might be reached. No position-error corrections are available at these low speeds but extrapolation of the curves in Fig. 6 gives an approximation to the correction required. On this basis an indicated airspeed of 75 knots corresponds to 82 knots equivalent airspeed and the calculated approximate value of lift coefficient allowing for a rate of descent of 40 ft/sec is $C_L = 1{\cdot}2$ at $\alpha \simeq 30°$. Considering these values in relation to the lift curve of Fig. 9 it is seen that there is still no indication of a decrease in the slope of the curve.

No deliberate minimum speed tests were carried out in the other configurations, but Fig. 24 shows an incident in which the pilot inadvertently allowed the speed to decrease while carrying out other tests in the full-span droop configuration. A complete time history is not available since a record was not taken at the time and recording was only started after the incident had developed. However, the characteristics are similar to the first series of tests with uncontrolled recovery in the 20·2° nose flap configuration. A large yaw to starboard developed followed by a starboard wing drop on which neither rudder nor aileron had any effect. The nose dropped and the aircraft recovered easily from a spiral dive after a loss of height of about 1 000 ft. It is noteworthy that the aircraft did not enter a spin in spite of the application of anti-spin aileron and, for part of the time, pro-spin rudder. The speed of 90 knots indicated is somewhat higher than might have been expected for complete loss of control.

The loss of directional control, which is the limiting factor in the tests as described in the pilots reports, is explicable from simple geometric considerations. The rudder hinge line is swept back at 44° relative to the fuselage datum so that at the lowest speed attained it is at an angle of only 18° relative to the free stream, and the fin leading edge is at an angle of only 2° to the free stream. Wing downwash and upwash round the body combined with wing and body vortices will, of course, modify the relative flow direction at the rudder from the free-stream angle quoted above but a decrease in effectiveness is to be expected. A similar argument would lead one to expect a deterioration in the fin contribution to directional stability, and the lateral stability results (Section 11.2) indicate a deterioration in directional stability as speed is reduced below about 120 knots.

8. *Longitudinal Stability.*

Longitudinal static stability, tailplane effectiveness, elevator and tab power were measured by recording steady trimmed flights mainly in the 4° and 20·2° nose-flap configurations (*see* Appendix B). The tests covered a range of centre of gravity locations and tailplane settings throughout the speed range. A limited number of further tests were made with 0° nose-flap deflection in an attempt to clarify certain anomalies in the results of the earlier tests. Most of the results were obtained with the notch cut in the 4° nose-flap configuration and with the notch sealed in the 20·2° nose-flap configuration; however, the effect on the trim curves of cutting or sealing the notch, and of deflecting the trailing-edge flaps 20°, was also briefly investigated. For the tests the stick forces were reduced to zero by use of the elevator trim tab and corrections were applied to the measured elevator angles to obtain stick-fixed trim curves at zero trim tab angle. The port elevator geared tab, however, was considered an integral part of the elevator and the results have not been corrected to zero geared tab angle; the gear ratio remained at 0·298 throughout the flight programme.

All tests were made at a constant engine speed of 14 100 r.p.m. and at approximately 5 000 ft altitude,

i.e. in the same condition in which lift and drag data were measured.

A few steady pull outs were made in the 0° flap configuration to obtain elevator angle per 'g' under the same flight conditions as for the trim tests.

8.1. *Elevator Angles to Trim.*

Fig. 25a shows the elevator angles to trim plotted against total-force coefficient C_R for various *cg* positions in the 4° nose-flap configuration. This figure also shows the very small effect of sealing the notch. The curves are linear up to $C_R = 0{\cdot}65$, thereafter showing an unstable break which, at $C_R = 0{\cdot}85$, corresponds to a shift in neutral point of $0{\cdot}08\ \bar{c}$; there is some evidence that above $C_R = 1{\cdot}0$ most of the loss in stability is recovered. As shown by the lack of scatter in the points, the aircraft can be flown accurately in the unstable region. However, pitch up occurs if 'g' is applied.

Fig. 25b gives corresponding results for the nose-flap deflected 20·2°.

Fig. 26 gives trim curves for the nose flaps down configuration as measured in the aft *cg* position for a range of tailplane settings. Comparison with Fig. 25a shows that, with the flaps deflected, the pitch up of the basic configuration is practically eliminated. This is, perhaps, more clearly shown in Fig. 27, where trim curves measured at a forward *cg* are compared for nose flaps up and down, and with the drooped leading edge*. With the drooped leading edge the trim curve appears to be completely linear over the full C_L range covered, although the scatter in the test points is too large, to have absolute confidence in this result.

Fig. 28 shows the effect of deflecting the trailing edge flaps 20° on the elevator angle to trim with the nose flaps set at 4°. There is a very slight reduction in stability with flaps down but no change in the pitch up characteristics. Fig. 29 shows corresponding results for 20·2° nose flap, and also includes, for comparison, results with the notch cut and sealed. The effect of the notch is seen to be small; the change of trim due to the trailing-edge flap deflection is $-3°$ in elevator angle, identical to that with 4° nose flap at low and moderate values of C_R, but an unstable kink occurs at about $C_R = 0{\cdot}8$ which was not observed with the trailing-edge flaps undeflected.

8.2. *Elevator Tab Angles to Trim, Stick Free.*

To determine stick-free stability and elevator-tab effectiveness, tab angles to trim were recorded for the range of configurations discussed above. As an example Fig. 30 shows the elevator tab angles required to trim, in the 4° nose flap configuration. There is a gradual loss of stick-free stability above $C_R \simeq 0{\cdot}4$ with a marked loss above $C_R = 0{\cdot}7$. However, at the forward *cg* position the loss in stability is much reduced. This can be accounted for, in part at least, by an increased value of b_2 at negative elevator angles (*see* Section 8.3), which are only used at this *cg* position.

8.3. *Longitudinal Control Effectiveness and Hinge-moment Derivatives.*

The results of the steady trimmed flight tests discussed above have been used to obtain data for the elevator and tailplane effectiveness. The analysis is based on the techniques developed by Gates and Lyons[18] and needs no detailed introduction here, but for convenience Appendix *B* gives details of the procedure used.

First the elevator effectiveness, i.e. the elevator lift slope a_2, can be obtained from the slope of the elevator angles to trim against *cg* position at a given C_L, i.e. by a crossplot of Fig. 25 for the basic configuration. The result is given for a range of C_L values in Fig. 31. Corresponding data for the nose flap down were much less well defined, giving an average value for $\underline{a_2 = 0{\cdot}882}$ for the range of C_L between 0·25 and 0·6 approximately. This would be 10 per cent more than the value obtained for the 4° nose-flap case ($\underline{a_2 = 0{\cdot}807}$). As it is difficult to find a physical basis for this difference, and in view of the fact that the nose-flap down data are rather poorly defined, they are ignored and the data given in Fig. 31 are suggested as valid for either case.

---

*Part of the reason for tests with nose flaps up was to see whether the Lightning required a nose flap (Section 4.2). The results show that the deflected nose flaps serve no useful purpose during approach and landing, which is made in the lift-coefficient range $C_L = 0{\cdot}45$ to $0{\cdot}55$; with the nose flas up about $0{\cdot}5\ g$ can then be applied before there is any danger of pitch-up.

Stick fixed and stick-free neutral points have been determined by plotting the values of the slopes of $\partial\eta/\partial C_R$ and $\partial\beta/\partial C_R$ against cg position. An example of such plots is shown in Fig. 32. Fig. 33 shows a comparison of stick-fixed neutral points, nose flaps up and down. To allow a direct comparison, the effects of engine momentum drag have been removed by correcting the results to zero mass flow. The figure shows again how the nose flap eliminates the forward movement of the aerodynamic centre at high C_L values.

To obtain the tailplane effectiveness, elevator angles to trim have to be plotted against tailplane angle at constant cg and C_L values. Such a graph is shown in Fig. 34. From the slope of these curves $\partial\eta/\partial\eta_T$ one obtains the ratio of tailplane power a_1 to elevator power a_2. This ratio is plotted against C_L in Fig. 35. Using the value for a_2 determined previously, a_1 is then determined giving the result shown in the same figure.

Plotting elevator angle against tab angle to trim at fixed tailplane angle, C_L and cg allows the determination of elevator-tab effectiveness. An example of such a graph is given in Fig. 36. The slope of these lines gives the ratio of tab effectiveness to elevator effectiveness a_3/a_2. Using the value of a_2 established previously, $a_2 = 0{\cdot}807$ and using all the available data, one gets a mean value $\underline{a_3 = 0{\cdot}083}$.

Fig. 37 shows the variation of $\partial\beta/\partial C_R$ with cg position. The slope of these points at a given C_L, $\Delta\eta/\Delta(\partial\beta/\partial C_R)$ is related to the control derivatives by

$$a_2\left(\frac{a_3}{a_2}-\frac{b_3}{b_2}\right)=\frac{1}{\bar{V}}\frac{\Delta h}{\left(\frac{\partial\beta}{\partial C_R}\right)\left(\frac{\partial C_R}{\partial C_L}\right)}.$$

Unfortunately, the points shown in Fig. 37 do not lie on straight lines which makes their interpretation somewhat difficult. The nonlinearities indicated cannot, of course, be a function of cg position, such as the range of control or tab angle used for that particular trim condition. The results for a_2 and a_3 derived earlier exclude these derivatives as likely contributors to the nonlinearity. This leaves b_2 and b_3 as suspects. In Fig. 38 elevator hinge moments are plotted against tab angle. The slope of these points at a given C_L is proportional to $b_2\left(\frac{a_3}{a_2}-\frac{b_3}{b_2}\right)$. It can be shown that the contribution of the first term in the bracket is very small, that means that $\frac{\partial C_H}{\partial\beta}\simeq b_3$. As these slopes are linear and moreover do not change with C_L, it is apparent that b_3 is constant $= -0{\cdot}121$ over the range of C_L and cg tested. This leaves b_2 as the only remaining quantity in doubt.

This is in fact confirmed in Fig. 39 where hinge moments are plotted against elevator angle and it is clearly seen that there is a well defined change in the slope of these data between elevator up and down. The slope of $\partial C_H/\partial\eta$ is related to the control derivatives by

$$\frac{\partial C_H}{\partial\eta}=b_2-b_1\frac{a_2}{a_1}.$$

As neither of the two terms in this equation is clearly small in relation to the other, this result would not by itself determine if the nonlinearity is in b_1 or in b_2 or perhaps in both. However assuming a nonlinearity in b_2 would satisfy both the trend shown in Fig. 39 and that shown earlier in Fig. 37 such an explanation is therefore suggested as highly probable.

Returning then to Fig. 37 and considering only the cg range from 0·39 $\bar{c}$ to 0·405 $\bar{c}$ confines the elevator angle to trim to positive values, and for $C_R < 0{\cdot}35$, the linear portion of the tab angle to trim curves, gives the value of $b_3/b_2 = 1{\cdot}273$. The hinge-moment measurements allow the separation of b_3 and b_2. Using the best defined test data gives a value of $\underline{b_2 = -0{\cdot}095}$ and $\underline{b_3 = -0{\cdot}121}$.

The value of b_2 derived in the previous paragraph is only applicable to positive elevator angles,

following the arguments on the nonlinearity of the curves of Fig. 37. Using this value of b_2, a value for $\underline{b_1 = -0{\cdot}0092}$ can be derived from Fig. 39. Using the same figure this leads to a value $\underline{b_2 = -0{\cdot}0475}$ for negative elevator angles. An alternative technique was used with the nose flap down configuration by trimming the aircraft, stick free, at $C_L \simeq 0{\cdot}35$ with various tailplane settings. In that case:

$$b_1 = -\frac{b_2 \Delta\eta + b_3 \Delta\beta}{\Delta\eta_T}$$

where $\Delta\eta$ and $\Delta\beta$ are the changes in elevator and tab angle resulting from a change $\Delta\eta_T$ in tailplane angle. The resulting mean value obtained of $\underline{b_1 = -0{\cdot}0101}$ which is in good agreement with that quoted above.

All of the above values of hinge-moment coefficient derivatives can be taken only as a guide since a complete explanation of the behaviour of the tab angle to trim curves has not been found.

8.4. *Manoeuvering Tests.*

Some brief tests to measure elevator angle (and stick force) per 'g' in steady pull outs were made in the 0° nose-flap configuration. The stick-force data were so erratic that no useful analysis was possible. The tests covered three *cg* positions 0·365 $\bar{c}$, 0·386 $\bar{c}$ and 0·405 $\bar{c}$, and a speed range from 260 knots to 140 knots. The pilot carefully trimmed the aircraft, stick free at the appropriate speed at about 5 000 ft altitude and 14 000 engine r.p.m. Speed was then either increased or decreased so that during the following steady pull out at between 0·5 *g* and 1 *g* excess the original trimmed speed was obtained. The pilot was asked to concentrate on keeping normal acceleration constant rather than the stick position or force. The manoeuvre was difficult to execute accurately due to the drag-thrust characteristics of the aircraft. The excess '*g*' which could be applied was limited, since at the higher speeds wing drop occurred when the appropriate lift coefficient was reached even with the notch cut. At the lower speeds 'g' was limited by the necessity to avoid pitch-up.

Fig. 40 shows a plot of elevator angle per '*g*' against trimmed force coefficient C_R. The nonlinearity of the curves is due to the loss of stability at higher values of C_R and at least some of the scatter is due to the varying amounts of excess '*g*' applied, resulting in differing excursions into the pitch-up region. The curves have been extrapolated linearly to the origin and the slopes, plotted against *cg* position, are shown in Fig. 41. The stick-fixed manoeuvre point is shown to be at 0·44 $\bar{c}$.

From the difference between the neutral point, $h_n = 0{\cdot}421\ \bar{c}$, and the manoeuvre point, $h_m = 0{\cdot}44\ \bar{c}$, stick fixed, it is possible to determine the damping in pitch derivative, m_q, since:

$$h_m = h_n - \frac{g\, m_q\, \rho\, S\, l_T^2}{W\, \bar{c}}$$

which gives $\underline{m_q = -0{\cdot}617}$.

The difference in aircraft configuration between the tests to determine the manoeuvre point (0° nose flap) and neutral point (4° nose flap) probably has a negligible effect; the neutral point in the 20·2° nose-flap configuration is at $h_n = 0{\cdot}422\ \bar{c}$, showing the small effect of flap deflection.

The usual method for estimation of the tail contribution to m_q is only applicable to aircraft with straight wings and a considerable tail arm; it neglects any possible downwash effects due to the pitching motion. Nevertheless some indication of the relative contributions of the tail and the wing plus body to m_q can be obtained from the formula which gives:

$$m_{q\,\text{tail}} = -\tfrac{1}{2}\frac{S_T}{S} a_1 = -0{\cdot}153$$

and hence,

$$m_{q(\text{wing}+\text{body})} = -0{\cdot}464\,.$$

The latter seems a rather large value of $(-m_q)$, but not excessively so.

An independent check on m_q (or, strictly, m_θ) from short-period pitching-oscillation tests was not possible since the oscillation was too heavily damped to allow sufficient accuracy in analysis.

8.5. *Comparison with Tunnel and Estimates.*

Wind-tunnel results are available from Shorts[4], English Electric[5] and the unpublished data of the R.A.E. No. 2 $11\frac{1}{2}$ ft × $8\frac{1}{2}$ ft tunnel; the nose flaps down configuration is considered in the first two references only.

A comparison of the flight and tunnel results of the variation of pitching-moment coefficient with lift coefficient is shown in Fig. 42. The flight values have been obtained from Figs. 25a and 26 using values of a_2 from Fig. 31 to find the equivalent pitching-moment coefficient. A correction has been applied for the momentum drag of the air entering the engine intake from brochure figures for air mass flow and assuming the force acts at the intake lip. Finally, the values of lift coefficient were converted to untrimmed values.

With the nose flap up there is a marked difference in pitching-moment coefficient at zero lift in Fig. 42 between the four sets of results. The model tested at English Electric[5] had been modified to correspond more closely to the aircraft shape and it also had an undercarriage fitted. At very low lift coefficients the results from these tests are in fair agreement with flight, but beyond $C_L = 0{\cdot}2$ they show nonlinearities which are not present in flight. The best agreement in the general trend with C_L is shown by the results from the R.A.E. tests, but these are displaced by a substantial constant C_m such as would be produced e.g. as an illustration by a difference in tailplane setting of about $1\frac{1}{2}$ deg. The results of the original tests on the least representative model[4] are generally in poor agreement. The same applies to corresponding results for the configuration with the nose flap down, which are shown in the lower half of Fig. 42.

Fig. 43 gives similar results for the aerodynamic centre, where again the R.A.E. model shows the best agreement, nose flaps up, except for $C_L > 0{\cdot}7$ where in flight a substantial forward movement occurs and rather the opposite in the tunnel.

Fig. 44 compares the flight and tunnel results for the tailplane lift-curve slope, a_1, and Fig. 45 gives the comparison for the elevator lift-curve slope, a_2; both figures show estimated[6,10] values. Since the elevator on the aircraft had a geared tab, the effect of which was treated as an integral part of the control effectiveness, a corresponding correction was added to the tunnel results and the theoretical estimate for a_2. There are considerable differences between the various tunnel results but they all give values for the lift-curve slopes much higher than those obtained in flight. The estimated values on the other hand are well placed in the band of tunnel results. In making the estimates account has been taken, so far as possible, of the various gaps at the tab, elevator, elevator horn and tailplane root but on the aircraft

Control Powers and Hinge-Moment Coefficient Derivatives

Derivative	Flight (mean)		Estimate	Estimate (flight a_1)	
	20·2° nose flaps	4° nose flaps		20·2° flap	4° flap
a_1	1·56	1·44	1·79		
a_2	0·882	0·807	1·03	0·89	0·82
a_3*	0·0865	0·083	0·107	0·092	0·085
b_1	−0·0101	−0·0092	+0·174		
b_2	−0·0706	−0·095	−0·080		
b_3*	−0·117	−0·121	−0·115		

*For trim tab.

there were large gaps and excressences at the tailplane-root junction for which it was not possible to make an allowance; these can be expected to reduce a_1 considerably. Lack of accurate representation of these features on the models may also account for the higher values obtained in the tunnel tests.

The Table above compares the mean values of a_1, a_2, a_3 as measured in flight with estimates over the range of lift coefficients $C_L = 0{\cdot}2$ to $C_L = 0{\cdot}6$. The estimated values of a_2 and a_3 depend on the value of a_1 and since there is already poor agreement with flight in the latter, further estimates for a_2 and a_3 were made using the flight value of a_1 as a basis. These results, shown in the last column, agree very closely with flight. The hinge moment derivatives, b_1, b_2, b_3, are also compared in the Table. Considering the unsatisfactory nature of the flight measurements, described in Section 8.3, the agreement in b_2 and b_3 is remarkably good. The uncertainty in the derivation of the flight results for b_1 plus the above mentioned difficulties of estimating tailplane derivatives, result in a discrepancy in the two values which is not surprising.

9. *Aileron Power.*

Aileron power was measured by three different techniques. The basic test consisted of measuring the aileron angles required to balance a known asymmetric load carried on one wing. Potentially a very accurate method, it does, however, require a considerable amount of flight testing and, furthermore, structural alteration to the aircraft to allow the attachment of the ballast weights. In order to find whether adequate measurements can be made of the aileron power by tests not suffering from these disadvantages two alternative dynamic methods were also tried. The first requires the pilot to apply a high-frequency oscillation to the ailerons with constant frequency and amplitude. For the second the pilot applies aileron in a step function. The aileron power is then computed from the initial acceleration in response to this control application. The analysis of the oscillatory test depends on the measurement of the amplitude of the rolling acceleration. Both these dynamic methods, therefore, depend on the measurement of rolling acceleration from which the driving force, i.e. the control power, can be calculated if the inertia of the aircraft is known. The result is in fact directly proportional to the assumed aircraft inertia and therefore dependent entirely on the accuracy with which this quantity is known. For the SB 5 in the 60° sweep configuration, only manufacturers estimates were available. Inertias derived in this way are known to be rather unreliable, and certainly not adequate for dynamic flight measurements of aircraft derivatives. However, on a later version of the aircraft, that with 69° sweep, inertias were measured on a ground rig and these gave values for the inertia in roll 15 per cent smaller than the corresponding data supplied by the manufacturer. (The inertia in yaw was found to be approximately 3 per cent larger.) It was thought that by applying the same percentage corrections to the estimated inertias for the aircraft used in the present tests there would be a good chance of arriving at more accurate values. In fact, the agreement shown later between aerodynamic data derived from dynamic tests using these corrected inertias and corresponding steady tests confirms this procedure.

Finally it should be noted that the flight tests in which aileron is rapidly applied and then held are also useful for measuring damping in roll, provided the aircraft motion following this input is not too much distorted by a superimposed Dutch-roll component.

The three rolling-power tests are now discussed in more detail.

9.1. *Asymmetric Weight Tests.*

Weights were placed in the underwing cannisters to give asymmetric loads of nominally 60 lb, 100 lb, 200 lb and 300 lb on either the port or starboard wing, the top weight being limited for safe landing. The speed range from 90 to 200 knots was covered, but the higher speeds were omitted at the lower weights as the aileron deflections required to trim the asymmetry there would have been too small to be recorded accurately. The nose flaps were deflected 20·2°.

Fig. 46 shows a plot of the rolling-moment coefficient obtained in this way against aileron angle. The data were computed according to Appendix C, making corrections for angle of bank and climb, sideslip (l_v from straight sideslip tests), rate of yaw (l_r estimated), and rudder rolling moment (l_ζ estimated from tunnel results). Within the scatter of the results there is no sign of a reduction in aileron power at the larger angles. From the slope of these lines values of l_ξ have been derived and are shown in Fig. 48, together

with results from the R.A.E. tunnel with 0° flap deflection, and a theoretical estimate[6]. For direct comparison with the flight results the tunnel results have been corrected for the estimated effect of the geared tab and for the effects of the gaps between the tab and control surface and between the control surface and wing. In addition, a correction has been applied for aileron span, the ailerons extending to the wing tips on the model and to only 93 per cent semi-span on the aircraft. This correction has been based on theoretical values of aileron power and is unlikely to be accurate under conditions of flow separation, say at $C_L > 0{\cdot}4$.

The tunnel results are in excellent agreement with flight up to C_L values of approximately 0·7, but fail to predict fully the loss of l_ξ at very high incidence. This is the region where the flow separates at the tips, progressively covering more of the wing span as C_L is increased. The estimated value of l_ξ, applicable only under conditions of attached flow, gives too low an aileron power. It is perhaps too much to hope for an accurate estimate with the very limited data available on wings of this sweepback, and particularly since the planform is rather unusual.

Fig. 47 shows a plot of yawing-moment coefficient due to aileron against aileron angle. This yawing moment is derived from the amount of rudder required to trim the aircraft, making, as above, corrections for sideslip and rate of yaw, using n_v from straight sideslips and estimated n_r. The value of n_ξ obtained is shown in Fig. 49, which also shows the values—completely uncorrected—obtained from the R.A.E. tunnel. The flight values of n_ξ are strongly dependent on the accuracy of the assumed value of n_ζ; this has not been measured in flight, and consequently tunnel data were used. In view of the rather poor agreement between flight and tunnel on n_v (Section 11.4) the tunnel value of n_ζ must be treated with some caution, but there is no reason to expect it to be grossly in error. The matter is discussed further in Sections 11.4 and 12.3. Nevertheless the agreement shown in Fig. 49 between flight and tunnel for n_ξ is not unreasonable, although there is a serious divergence at high C_L when also l_ξ was in poor agreement. The general slope of n_ξ *versus* C_L, would be expected to be greater in the tunnel than in flight due to the larger aileron span of the model, but it was not thought that any reasonable quantitative estimate to correct for this effect could be made.

9.2. *Oscillatory Tests.*

The oscillatory tests to determine aileron power were made in the 0° nose flap configuration. In general, the pilot was able to achieve a close approximation to the required steady sinusoidal input. The average variation in frequency during runs was about 5 per cent of the mean value, with a maximum in one run of 13 per cent, and the average change in amplitude during runs was about 10 per cent of the mean value, with a maximum in one run of 27 per cent. The variability of frequency showed no consistent trends either with aircraft speed or input amplitude, but amplitude variations tended to be greater at the lower aircraft speeds and at the larger amplitudes of input. The analysis of the results was made for that portion of the run at which the frequency and amplitude were most nearly constant; results from tests where the input deviated markedly from sinusoidal were discarded. A typical flight record is shown at Fig. 50.

The technique depends on the fact that when the ailerons are oscillated sinusoidally at a frequency which is substantially higher than the frequency of the short period aircraft mode (the Dutch roll) the aircraft responds in an almost pure rolling oscillation with very little yaw and sideslip being excited. The contributions from the small amount of response in these two freedoms can than be treated as small corrections, using if necessary crudely estimated data for the corresponding aerodynamic derivatives l_v and l_r without detriment to the result. In fact in practice the aileron rolling moment is almost entirely in balance with the rolling acceleration. The details of the analysis are given in Appendix D and the results are shown in Fig. 51 where they are compared with the values from the steady tests. Apart from the fact that the scatter is considerably greater than in the steady tests (Fig. 48) there is perfect agreement between the results obtained by the two methods. It would appear from these results that the oscillatory technique offers a very satisfactory alternative to the much more demanding steady flight technique.

It should be noted, however, that the success of this, or any other dynamic flight technique, depends entirely on the confidence with which the relevant aircraft inertias are known. If, for instance, the inertias supplied by the manufacturer had been used without the correction mentioned in Section 9, the l_ξ values

computed with these would have been 15 per cent larger and there would have been an apparent discrepancy between the two sets of results.

9.3. *Step Aileron Application.*

If aileron is applied in a sharp step and then held at a constant angle, the initial rolling acceleration in response to the control application can again be used to determine the rolling power of the aileron. Only the initial portion of such a manoeuvre, as shown in Figs. 52 and 53, is usable before the aircraft motion is too much contaminated by other motion parameters, rate of roll, rate of yaw, sideslip, etc. and the corresponding aerodynamic effects feeding into the rolling-moment equation.

In practice, this means, that the initial step in control application has to be very steep; that obtained in the test illustrated in Fig. 53 would for instance, not satisfy this requirement.

Ref. 11 gives an expression for the initial roll acceleration to a perfect step input as

$$\frac{\dot{p}}{\xi} = \frac{2\rho V^2 g S}{W b}\left[\frac{l_\xi\left(1+\frac{n_\xi}{l_\xi}\frac{i_E}{i_C}\right)}{i_A\left(1-\frac{i_E^2}{i_A i_C}\right)}\right].$$

This equation has been used to compute l_ξ from the available flight data for these tests, giving the results shown in Fig. 54. Not altogether surprisingly, there is now considerable scatter, but nevertheless, the mean is in very good agreement with the steady flight values of l_ξ. These results would suggest, that the step aileron technique is perhaps not a very efficient method for obtaining flight measurement of l_ξ, but certainly capable of giving the order of magnitude of this derivative. The remarks made in Section 9 about inertia data apply, of course, here also.

The principal purpose of the step aileron test is, however, the measurement of damping in roll. This will be discussed in the next section.

10. *Damping in Roll.*

Damping in roll can be measured by two distinct methods. The traditional one is to fly a steady rolling manoeuvre with a known amount of aileron applied. This method requires that (a) the aileron power is known and (b) that the aircraft responds in fact with a sensibly steady roll rate. The first of these conditions was satisfied in the present case, but as the samples shown in Figs. 52 and 53 clearly show, a steady roll rate is not obtained. Nevertheless, using a portion of the flight record where rate of change of roll rate is practically zero, l_p can be evaluated from the rolling moment equation

$$l_v\beta + l_r\frac{rb}{2V} + l_p\frac{pb}{2V} + l_\xi\xi + l_\zeta\zeta + \frac{E}{\frac{1}{2}\rho V^2 S b}\dot{r} = 0$$

assuming that all aerodynamic derivatives other than l_p are known and all the motion parameters and control angles are measured. Of course this method could be applied to any portion of an available flight record by including the inertia in roll contribution as well, but this would then introduce a rather powerful term which depends on differentiation of the roll-rate trace, an essentially inaccurate procedure.

The results obtained for l_p are plotted against C_L in Fig. 55. The scatter is quite acceptable and the data compare well with a theoretical estimate based on Ref. 6. Comparison of the number of points on Figs. 55 and 54, which are both derived from the same series of tests, shows that only a portion of these tests could be used for evaluation of l_p. In the others the motion was too unsteady.

An alternative method by which l_p (and other lateral derivatives) can be measured in flight, is to vector-analyse records of Dutch-roll oscillations. Whereas the steady roll-response technique does not require the aircraft's roll inertia to be known, the Dutch-roll analysis requires a reliable value of i_A to be available and may be more restricted for this reason. The results from the Dutch-roll tests will be

discussed separately in Section 12.3 of this Report and are shown in Fig. 75. It can be noted that there is excellent agreement between the two sets of results.

11. *Steady Sideslip Tests.*

Steady sideslips were recorded for all the configurations and covered the full speed range of the aircraft. In the configurations without leading-edge droop the aircraft developed wing drop characteristics over part of the C_L-range (*see* Appendix F.3). This phenomenon was eliminated by the leading-edge notch which was therefore also tested. With leading-edge droop this wing drop did not occur and consequently tests were only made with the notch sealed.

The tests were made in steady straight sideslips to both port and starboard at various sideslip angles up to a maximum of 8°, with an engine setting of 14 100 r.p.m. and at an altitude of approximately 5 000 ft. In order to determine the values of the derivatives l_v, n_v, y_v it is necessary to know the values of the control derivatives l_ξ, l_ζ, n_ξ, n_ζ (*see* Appendix E). The derivatives l_ξ and n_ξ were available from the aileron tests (*see* Section 9) but n_ζ and an estimate of l_ζ have been obtained from tunnel results[4]. It was considered unsafe to employ the usual method of determining n_ζ in flight by streaming a parachute from one wing tip, owing to the possibility of the parachute fouling the elevator horn balance in the event of inadvertent break-away. An error in l_ζ has only a relatively small effect on the determination of l_v but the determination of n_v is largely dependent on the value assigned to n_ζ.

Further below (Section 12.3) tests of Dutch-roll oscillation are discussed from which all the major lateral derivatives (including the sideslip derivative l_v and n_v) have been evaluated. This will allow a comparison of the results obtained by these two methods.

The results of the steady sideslip tests are first presented as obtained separately for each configuration and finally compared with tunnel data.

11.1. *Basic Configuration 4° nose flap.*

Plots of aileron angle ξ, rudder angle ζ and bank angle ϕ against sideslip β are shown in Figs. 56 to 58.

Wing drop occurred with the notch sealed at lift coefficients around $C_L = 0{\cdot}5$. Fig. 56 gives no indication of an asymmetry in lift at the appropriate lift coefficient; within the scatter of the results the curves appear to be quite straight. However, Fig. 57 shows a violent change in the slope of ζ versus β for $C_L = 0{\cdot}457$ and $C_L = 0{\cdot}527$, with the notch sealed, indicative of directional instability over a small range of sideslip. The cause can be traced to the behaviour of the leading-edge vortex. The position of the origin of the vortex on the leading edge is dependent on sideslip angle, at a given C_L, and moves steadily inboard on the trailing wing and outboard on the leading wing as sideslip is increased. The increased drag on the trailing wing causes a destabilising yawing moment; until the origin of the vortex approaches the wing root. Further movement of the vortex then has little effect on the drag and the aircraft is again directionally stable. At higher values of C_L the origin of the vortex is near the wing root at zero angle of sideslip and no unstable condition occurs. In flight in the unstable regime wing drop occurs because sideslip will suddenly increase and with it the rolling moment due to sideslip. Fig. 57 shows that cutting the notch eliminates the directional instability, thus curing the wing drop.

At the highest values of C_L investigated there is again a loss in directional stability which is not improved by cutting the notch. Extrapolation to still higher values of C_L confirms that at the minimum controllable speed (Section 7) the aircraft is directionally unstable and this causes loss of control. The tendency of both body and wing vortices to produce adverse loading on the fin at high incidence for aircraft of this general configuration is well known[12]; the low aspect ratio is detrimental because it results in wing vortices in proximity to the fin and also requires a higher incidence at a given C_L.

The sideslip derivatives, derived from these tests are shown in Fig. 59. Values of y_v were difficult to evaluate due to difficulty in measuring accurately the small angles of bank obtained in the sideslips particularly at the higher values of C_L. Otherwise there is little scatter in the results. Values of n_v have been converted to the mean quarter-chord point as a reference and, are given for both the stable and unstable region.

11.2. 20·2° *Nose-Flap Configuration.*

Plots of aileron angle, rudder angle, and angle of bank against sideslip are shown in Figs. 60, 61 and 62.

The indications of wing drop, Fig. 61, and the cure effected by cutting the notch are similar to those for the 4° nose-flap configuration.

Corresponding sideslip derivatives, are shown in Fig. 63. Again y_v is very inaccurately determined, the rapid increase of $(-y_v)$ with C_L being particularly suspect.

11.3. 10·7° *Full-Span Drooped Leading-Edge Configuration.*

Aileron angle, rudder angle, and angle of bank are plotted against sideslip angle in Figs. 64 to 66.

All the curves are quite straight to the highest C_L and β tested and there is no indication of a wing drop or severe loss in stability at high C_L. The static stability derivatives presented in Fig. 67 show no unusual features. Pilots confirm that the aircraft had good lateral characteristics in this configuration although the inadvertent loss of control at very low speed (Section 7) indicates that stability deteriorates at values of C_L higher than those tested here.

11.4. *Comparison With Tunnel and Estimates.*

Wind-tunnel results are available from Ref. 4 for the deflected nose-flap configuration and from the unpublished R.A.E. data from models with the nose flap deflected and undeflected. These are compared with the flight results (notch sealed), Figs. 68 to 70, all moment derivatives being referred to the mean quarter-chord point. The flight results have been corrected for the momentum drag of the air entering the engine intake, using engine brochure figures for air mass flow and assuming that the force acts at the intake lip. The figures also show the effect of lowering the nose flaps and incorporating full-span leading-edge droop.

In general the agreement between flight and tunnel results is poor. In Fig. 68, the tunnels give much lower values of $(-l_v)$, except at moderate C_L with the nose flaps up. A theoretical estimate[6] of l_v agrees neither with flight nor tunnel and predicts a steady increase in $(-l_v)$ with C_L, taking no account of the effects of flow separation from the wing tips. Fig. 68c shows that lowering the nose flaps, or incorporating droop, allows $(-l_v)$ to continue increasing to higher values of C_L when compared to the nose flaps up condition. The R.A.E. tunnel shows a rather erratic effect of nose flaps which is quite unrepresentative of the flight results.

The agreement between tunnel and flight is particularly poor for n_v, Fig. 69. Ignoring the area of greatly reduced n_v, corresponding to the wing drop condition in flight, the tunnels give much too large values of n_v. A theoretical estimate confirms the general level of the tunnel values, and shows a steady rise in n_v with C_L due to the effects of sweepback; again no account is taken of flow separation. Apart from some minor variations the results from the two tunnels in Fig. 69b are in good agreement. The absence of an undercarriage on the models can account for, at the most, 0·01 of the discrepancy which still leaves a difference of at least $\Delta n_v = 0{\cdot}04$ to be accounted for an it is surprising that the differences in fuselage shape between the models; and the aircraft should increase by about 60 per cent the flight values of n_v when referred to the mean quarter chord point. Referred to a realistic flight *cg* position of 0·4 $\bar{c}$, this represents an alarming overestimate by about 170 per cent of the flight value. One cause of error could be in the use of the tunnel value of rudder power, n_ζ, for the determination of n_v. n_ζ could be lower in the tunnels than in flight due to the lower Reynolds number but the discrepancy is too large to be accounted for by this means; in any event there is independent evidence from the lateral oscillation measurements (Section 12) that the flight values of n_v, and hence the assumed values of n_ζ, are about right.

Fig. 70 compares the flight and tunnel values of y_v. The poor agreement for the nose flaps down condition is almost certainly due to inaccurate determination in flight but there is also a rather large discrepancy between the two tunnels which is difficult to explain.

12. *Lateral Oscillation.*

Lateral oscillations were recorded over the speed range in the configuration with 0° nose flap. A few tests were made with the drooped leading edge. The purpose of these tests was first to obtain records

of the Dutch-roll behaviour of the aircraft and then to analyse the data to obtain values for the lateral derivatives. The tests were made by exciting the motion by a rudder kick to either port or starboard and then holding all controls fixed in the neutral position.

12.1. *Dutch Roll with 0° Nose Flap.*

The results for all the quantities measured are shown plotted against C_L in Fig. 71. The features of most interest to the pilot are the period, damping and the Dutch-roll ratio; the phase lag of roll with respect to yaw is also shown, as this is required for the later analysis. This is a quantity rather difficult to measure with the required accuracy. In fact the basic data given in Fig. 71 for values of $C_L > 0{\cdot}25$ gave quite implausible results in the vector analysis and were modified (with the benefit of hindsight) to those indicated by a dotted line. Before analysis the flight records for rate of roll and rate of yaw were converted to stability axes. The Dutch-roll ratio p/r was impossible to determine at the higher C_L values as in those cases the yaw trace on the record was too small for accurate reading. This, of course, was also responsible for the inaccuracies in the measurement of phase angle just below this range.

In the tests the aircraft tended to oscillate about the displaced position produced by the initial rudder deflection, returning only slowly to the wings level condition; if the pilot attempted to obtain a large amplitude oscillation by injecting a greater rudder input, the aircraft entered a spiral dive. The normal condition which has to be satisfied for spiral stability is:

$$l_v n_r - n_v l_r > 0$$

and with the flight values of l_v, n_v and estimated[6] values of l_r, n_r this condition is satisfied. The formula, however, depends on the assumption of small disturbances from rectilinear flight and it is likely that the estimates of l_r, n_r are inaccurate in the separated flow condition.

The period is seen to vary only slightly over the C_L range, with somewhat shorter periods at low C_L. The damping increases rapidly at $C_L > 0{\cdot}45$ and accurate measurements could not be made beyond $C_L \doteq 0{\cdot}55$. The increase in damping of the lateral oscillation on sweptback wing aircraft under conditions of separated flow has been noted previously[13] and is attributed to increased wing drag, concentrated at the wing tips, and the consequent effect on the derivative n_r.

12.2. *Full-Span Leading-Edge Droop.*

Only very limited tests were made in this configuration with the results shown in Fig. 72. The curves drawn through the few available points must be considered as tentative. In contrast to the 0° nose flap configuration damping does not appear to increase rapidly at high C_L. No flow visualisation tests were made with the drooped leading edge; however, the drag results (Fig. 18) suggest that separated flow had not occurred up to the highest C_L covered in the oscillatory tests.

12.3. *Lateral Derivatives from Lateral-Oscillation Tests.*

Time vector analysis has been used to extract derivatives from the measured lateral oscillation. The lateral equation of motion contain 9 aerodynamic derivatives: l_v, l_r, l_p, n_v, n_r, n_p, y_v, y_r, y_p. The lateral oscillation on the other hand is defined by only 6 quantities; period, damping, ratio of roll to yaw and yaw to sideslip and the corresponding 2 phase angles. The system of equation thus obtained is under-determined and can only be solved if at least three of the derivatives can be assumed as known. In fact in the present tests the ratio between the amplitudes in sideslip and yaw was ill defined, so that only four quantities, those shown in Fig. 71 were available for analysis. This increases further to 5 the number of assumptions that have to be made. These were as follows:

(i) all the sideforce derivatives were assumed, y_v as given in tunnel tests, y_r and y_p were ignored.

(ii) l_r was taken from theoretical estimates. This derivative has only a minor effect on the dutch roll so that the analysis is not greatly affected by an inaccuracy in this term.

(iii) A further term has to be postulated to be able to solve the vector polygons, the quantity normally

chosen in this type of work is either n_p or n_r. An alternative course was pursued instead; that of treating these terms as variables and solving the yawing-moment equation for all possible combinations of n_p, n_v and n_r which satisfy the flight data.

This process is illustrated in Fig. 73. The diagram in (a) gives a typical example of a yawing moment polygon. The known quantities, i.e. the inertia terms $C\ddot{\psi}$ and $E\ddot{\psi}$ are represented by full lines, whereas the unknown aerodynamic quantities are shown dotted. Only the direction (phase) of these vectors are established from the flight data; their magnitudes are not. Fig. 73 illustrates how this particular case can be satisfied by an infinite number of solutions, each establishing a combination between the three aerodynamic terms.

The results of this analysis for the flight data given in Fig. 71 (0° nose flap) are shown in Fig. 74 for four C_L values. It should be noted that rather than solving the vector polygons for each set of flight points, the smoother data represented by the curves drawn through the test points have been used. In Fig. 74 values of n_v and n_r are plotted against n_p; also shown are the combinations satisfying either the estimated value of n_r or alternatively the estimated value of n_p. The method does, of course, not uniquely define the derivative, but it allows one to speculate on the plausibility or otherwise of a certain answer. In the present case n_v is rather insensitive (especially at the higher C_L values) so that this derivative cannot be used to exclude certain solutions as improbable; however this insensitivity permits n_v itself to be determined with reasonable confidence. The exchange rate between n_r and n_p is unfortunately such that it allows in this case no clear decision either. (If n_r *versus* n_p were very flat, n_r would be fixed, similarly a very steep slope of n_r *versus* n_p would define a small range of n_p which would give plausible values of n_r.

In Fig. 75 all the results obtained from the vector analysis are summarised and compared with other flight data where available or with theoretical estimates. Values of n_v, n_r and n_p are given as ranges; these are rather arbitrarily limited by the theoretical value for n_r on the one hand and the theoretical values for n_p on the other. This band appears to be the most probable; outside it the differences from theory would become very large.

n_v compares very well with the results from steady sideslips and as it is well defined can be taken to confirm these. $(-l_v)$ values are rather lower than those obtained from the steady tests and with reference to Fig. 68a can be said to be much closer to the tunnel values.

l_p is in excellent agreement with the values evaluated from the steady roll tests.

n_r and n_p cannot be established with any confidence. If one were to accept the estimate for n_r (which is more reliable generally than that for n_p) then the corresponding flight values of n_p would be more negative than estimates suggested over the C_L range covered.

13. *General Discussion.*

A thorough investigation of wing flow characteristics has been made, the results of which will be published later in Part 2 to this Report but it is necessary here to give a brief outline of the characteristics of the flow in order to consider its influence on the present results. Of particular interest are the effects of Reynolds number and corrections on the wind-tunnel results, which have been compared with the flight results. On the whole, this comparison shows poor agreement, the tunnel results predicting the flight measurements really satisfactorily only in the aileron power tests, and even this may be fortuitous as a large and rather imprecise correction has had to be applied to account for differences in aileron span between model and flight.

Flow investigations were made in the 4° and 0° nose-flap configuration using three techniques: pressure plotting, surface tufts, and smoke discharged over the wing leading edge. While the interpretation of the results of the three techniques does not give entirely consistent indications of the precise point at which flow changes occur, it is evident that at lift coefficients below 0·4 the flow is everywhere attached and that as C_L is increased above this value a leading-edge separation occurs, forming the characteristic leading edge vortex associated particularly with highly sweptback wings with sharp leading edges. The first occurrence of the separation is, however, well outboard at about 80 per cent semispan and moves progressively inboard with increased C_L, so that at $C_L = 0{\cdot}8$ the origin of the separation has approached the wing root.

On wings with sharp leading edges there appears to be little if any effect of Reynolds number on the vortex formation or location[16]. However, wind-tunnel tests[17] on a 60° swept wing with R.A.E. 101 streamwise sections have shown both a progressive movement of the vortex core towards the leading edge and an increase in the incidence for the development of separation with increase in Reynolds number. The addition of roughness was unsuccessful in simulating higher Reynolds numbers. The effects are large for comparatively modest changes in Reynolds number. For example, at 83 per cent semispan on the wing in the tunnel[17] the vortex moved from 78 per cent local chord to 21 per cent local chord, the forward movement incidentally indicating a movement of the core outboard, for an increase in Reynolds number from $2{\cdot}2 \times 10^6$ to $3{\cdot}9 \times 10^6$, and the development of the separated flow was delayed by at least 2° of incidence. In the present Report the comparisons are between tunnel results obtained at Reynolds numbers over the range $1{\cdot}29 \times 10^6$ to $2{\cdot}28 \times 10^6$ and flight results at Reynolds number from $12{\cdot}6 \times 10^6$ to $36{\cdot}6 \times 10^6$. The expected result is therefore an earlier occurrence and more rapid inboard progression and spread of the vortex in the tunnel than in flight.

Some of the differences between the wind tunnel and flight results can now be examined in terms of the vortex formation, movement and growth. In the case of the lift characteristics, the start of the increase in lift-curve slope should occur at a lower angle of incidence in the tunnel and in fact a difference of about 4° is apparent (Fig. 12). Similarly the kink in the drag curve should occur earlier in the tunnel and, while this does not occur for the 4° nose-flap configuration (Fig. 19), it is apparent for the 20·2° nose-flap configuration (Fig. 21). There is an additional effect of Reynolds number on the value of the induced-drag factor, k. An analysis by Bagley[7] of several test series shows that there is a very rapid fall in the value of k as Reynolds number is increased from 1×10^6 to 6×10^6 for 40° and 45° sweptback wings and that this fall is still apparent on the one test series on a 60° sweptback wing up to a Reynold number of 10×10^6. Table 2 confirms the overestimate of k by the tunnels. The value of k is increased at values of C_L both below, (k_1) and above (k_2) the kink but the reasons are clearly different. k_1 is probably increased in the tunnels due to the drift of boundary-layer fluid towards the wing tips, not present in flight, whereas k_2 is increased by the greater extent of the vortex. None of the models had transition fixed on the wings and it has been shown[7] that fixing transition reduces k_1, although it does not produce values as low as in flight.

The effect on static longitudinal stability is less obvious. The vortex first occurs well outboard at the leading edge, causing an increase in lift near the wing tips and aft of the centre of gravity and hence producing a nose down change in wing pitching moment; the effect is unlikely to be large due to the weak vortex and small wing chord near the tips. As the vortex moves inboard lift is lost at the wing tips and gained near the root, forward of the centre of gravity, causing a nose up change of pitching moment. The net effect on the aircraft will depend on the contribution of the tail-plane. The low set tailplane tends to move into an area of decreasing down-wash as incidence is increased, counteracting the destabilising tendency of the inboard moving vortex. Both the wing and tailplane contributions to the pitching moment will depend on the incidence for first occurrence of the vortex, its inboard progression with increase in incidence and its extent. Tunnel results indicate that at high incidence there is a reduction in $d\varepsilon/d\alpha$, the rate of change in downwash with incidence, and that this reduction is greater when the nose flaps are deflected than on the plain wing. This probably accounts for the lack of a destabilising kink in the pitching-moment curve in flight at high C_L for the 20·2° nose-flap configuration (Fig. 42). For the nose flap up configuration the destabilising trend starts in flight at $C_L \simeq 0{\cdot}65$ when the vortex originates from about 30 per cent semispan at the leading edge. The tunnel results by Shorts[4] and English Electric[5] show a lower C_L for the kink, presumably due to a more rapid inboard progression of the vortex, producing both an earlier nose-up pitching moment change on the wing and a higher relative tailplane position, resulting in a greater, destabilising, $d\varepsilon/d\alpha$. The R.A.E. tunnel tests were made at a higher Reynolds number, which would be expected to delay the instability to a higher C_L than the other tunnel tests, but does not account for the apparent complete lack of a significant unstable break.

The other main area of disagreement between tunnels and flight is in the static lateral stability derivatives. The generally lower tunnel values of the derivative $(-l_v)$ at C_L greater than about 0·2 (Fig. 68) may again be due to earlier vortex formation, as the reason for this derivative failing to increase steadily with increasing C_L as predicted by simple estimates is due to the greater concentration of load inboard

on the wing as the vortex develops. However, the much higher tunnel values for n_v are inexplicable on this basis and, if anything, the earlier development of the vortex would lead one to expect the rapid loss of n_v to occur at a lower C_L in the tunnel than in flight; this is not apparent.

Finally, the Shorts tests[4] were of a 3 ft 10 in. span model tested in a 5 ft 3 in. diameter open jet tunnel with the consequence that the tunnel corrections were considerable. When this is combined with the absence at the time of valid blockage corrections for vortex flows, the results must be suspect. The English Electric tests[5] used the same model in a 9 ft × 7 ft tunnel and the R.A.E. tunnel tests were made with a 5 ft $6\frac{1}{2}$ in. model in an $11\frac{1}{2}$ ft × $8\frac{1}{2}$ ft tunnel so that, while the blockage corrections were again wrong, the effect is insignificant except at very high incidence.

14. *Conclusions.*

Flight tests of the Short SB 5 research aircraft have been made in the configuration with 60° sweepback and the low tailplane, with various wing inboard nose-flap deflections and full-span leading-edge droop. The effect, particularly on lateral stability, of a leading-edge notch has also been investigated and brief tests have been made with trailing-edge flaps deflected.

The lift curves are generally nonlinear, with an increase in slope occurring at moderate incidence followed by a decrease at incidences a few degrees higher. Deflection of the trailing-edge flaps causes a large decrease in lift-curve slope at low incidence so that at more moderate values of incidence little lift increment is obtained from the flap. A notch cut into the leading edge had little effect on the lift characteristics.

The drag curves show a sharp increase in slope beyond lift coefficients near 0·4 for the nose flap configurations, with a linear variation of C_D with C_L^2 above and below the kink. The induced-drag factor above the kink is more than double that below it. With the leading-edge droop a more modest change of slope occurs at $C_L \simeq 0{\cdot}4$ with the severe rise delayed to higher lift coefficients (about 0·7), but a higher induced-drag factor after the latter kink results in little difference in drag between configurations at the highest values of C_L. There is only a small effect on the drag curves of cutting the notch or deflecting the trailing-edge flaps.

The curves of elevator angle to trim with the nose flaps deflected show a small loss of longitudinal stability at moderate values of lift coefficient followed by a steady gain in stability as lift coefficient is increased further. Raising the nose flaps causes a rather larger loss in stability at moderately high lift coefficients but well above those used during landing approach. With the leading edge drooped there is no evidence of stability changes over the C_L range tested. Deflection of trailing-edge flaps with the nose flaps up causes a nose down change of trim but has little effect on stability whereas with the nose flaps down there is a large loss of stability, compared with the undeflected trailing-edge flaps, at moderately high lift coefficient, similar to that always present with the nose flaps up. The effect of the leading-edge notch on trim is small. Measurements have been made of the effectiveness and the hinge moments of the elevator and tailplane and show that the value of the elevator hinge-moment derivative b_2 changes with the sign of the elevator deflection.

Aileron power measurements using asymmetric wing weights show, with the nose flap deflected, a constant or slowly decreasing rolling power up to fairly high lift coefficient and a more rapid decrease thereafter. An oscillatory technique used with the nose flaps up confirms this result. This technique was very successful and is recommended as a simple method of determining this derivative.

The incorporation of the leading-edge notch has a pronounced effect on lateral stability, curing a wing drop otherwise present at moderate lift coefficients. This wing drop is due to a directional instability over a small sideslip range (about 4 deg total) for all configurations without leading-edge droop. The instability is not present with the leading-edge droop. The derivative $(-l_v)$ increases gradually up to moderate lift coefficient and then decreases; deflection of the nose flaps or incorporation of droop delays this decrease to higher lift coefficient. Apart from the wing drop range, n_v remains roughly constant but tends to decrease at the lowest and highest lift coefficients. y_v measurements were unsatisfactory but there is a tendency for $(-y_v)$ to decrease at high lift coefficient.

The period of the lateral oscillation increases gradually to moderate lift coefficient, thereafter gradually decreasing, whereas the damping remains constant to moderate lift coefficient and then increases quite

rapidly. Results were obtained by vector analysis of l_v, n_v, l_p, n_r and n_p. The first three agree well with flight data obtained by other techniques n_p and n_r were poorly defined.

Results from series of tests in three different wind tunnels show little agreement either with each other or the flight results. Differences in details of shape between the different models and the aircraft will account for some of this disagreement but it is suggested that there is a powerful effect of Reynolds number on the formation of the vortex at a rounded leading edge, affecting its location, strength, and extent and that this accounts for the poor correspondence in the results from moderate to high values of lift coefficient.

15. *Acknowledgements.*

The author wishes to acknowledge the skill and perseverance of all the test pilots, too numerous to mention by name, during the period of this programme, in their flying of what was, at the date of the initial tests, a most unconventional aircraft and one which at all times had unpleasant characteristics under certain flight conditions. Acknowledgement is also due to Mr. J. H. Blackmore and Mr. J. N. Cannell for considerable assistance in the conduct of the flight programme and analysis of the results.

LIST OF SYMBOLS

A		Aspect ratio
A		Rolling moment of inertia, slug ft^2
a_0		Tailplane lift coefficient at $\alpha_T = \eta = \beta = 0$
a_1	$=$	$\frac{\partial C_{L_T}}{\partial \alpha_T}$, tailplane lift-curve slope
a_2	$=$	$\frac{\partial C_{L_T}}{\partial \eta}$, tailplane lift coefficient due to elevator deflection (elevator lift-curve slope)
a_3	$=$	$\frac{\partial C_{L_T}}{\partial \beta}$, tailplane lift coefficient due to trim tab deflection (tab lift-curve slope)
b		Wing span, ft
b_0		Hinge-moment coefficient when $\alpha_T = \eta = \beta = 0$
b_1	$=$	$\frac{\partial C_H}{\partial \alpha_T}$, hinge-moment coefficient due to tailplane incidence
b_2	$=$	$\frac{\partial C_H}{\partial \eta}$, hinge-moment coefficient due to elevator deflection
b_3	$=$	$\frac{\partial C_H}{\partial \beta}$, hinge-moment coefficient due to trim-tab deflection
C		Yawing moment of inertia, slug ft^2
C_D	$=$	$\frac{D}{\rho/2\, V^2\, S}$, drag coefficient
C_{D_0}		Drag coefficient at zero lift coefficient
C_{D_i}		Induced-drag coefficient
C_{D_T}		Tailplane drag coefficient

C_{D_W} Wing drag coefficient

$C_H = \dfrac{P \times \text{gearing}}{\rho/2\, V^2\, S_F\, C_F}$, hinge-moment coefficient

$C_L = \dfrac{L}{\rho/2\, V^2\, S}$, lift coefficient

C_{L_T} Tailplane lift coefficient

C_{L_W} Wing lift coefficient

$C_R = \dfrac{W}{\rho/2\, V^2\, S}$, force coefficient

$C_l = \dfrac{L}{\rho/2\, V^2\, S\, b}$, rolling-moment coefficient

$C_m = \dfrac{M}{\rho/2\, V^2\, S\, \bar{\bar{c}}}$, pitching-moment coefficient

$C_n = \dfrac{N}{\rho/2\, V^2\, S\, b}$, yawing-moment coefficient

$C_y = \dfrac{Y}{\rho/2\, V^2\, S}$, sideforce coefficient

$\bar{c} = \dfrac{S}{b}$, geometric mean wing chord, ft

$\bar{\bar{c}} = \dfrac{2}{S}\displaystyle\int_0^{b/2} c^2\, dy$, aeordynamic mean wing chord, ft

$c_F = \dfrac{S_F}{\text{elevator span}}$, elevator mean chord aft of hinge line, ft

D Drag, lb

E Product of inertia, slug/ft^2

$e_A = \dfrac{i_E}{i_A}$, ratio of inertia coefficients, roll

$e_C = \dfrac{i_E}{i_C}$, ratio of inertia coefficients, yaw

H Pressure altitude, ft

h Position of centre of gravity as a fraction of aerodynamic mean wing chord

h_m Value of h at the manoeuvre point, stick fixed

h_n Value of h at the neutral point, stick fixed

$i_A = \dfrac{Ag}{W}\left(\dfrac{2}{b}\right)^2$, rolling moment of inertia coefficient

$i_C = \dfrac{Cg}{W}\left(\dfrac{2}{b}\right)^2$, yawing moment of inertia coefficient

$i_E = \frac{Eg}{W}\left(\frac{2}{b}\right)^2$, product of inertia coefficient

$k = \pi A \frac{\partial C_D}{\partial(C_L^2)}$, induced-drag factor

k_1 Value of k below the 'kink' lift coefficient

k_2 Value of k above the 'kink' lift coefficient

k_T Value of k for the tailplane

L Lift, lb

L Rolling moment, lb ft

l_F Fin arm, ft

$l_p = \frac{\partial C_l}{\partial\left(\frac{pb}{2V}\right)}$, rolling-moment coefficient due to rate of roll

$l_r = \frac{\partial C_l}{\partial\left(\frac{rb}{2V}\right)}$, rolling-moment coefficient due to rate of yaw

$l_v = \partial C_l/\partial\beta$, rolling-moment coefficient due to sideslip

l_T Tail arm, ft

$l_\zeta = \frac{\partial C_l}{\partial\zeta}$, rolling-moment coefficient due to rudder deflection

$l_\xi = \frac{\partial C_l}{\partial\xi}$, rolling-moment coefficient due to aileron deflection

M Pitching moment, lb ft

M_E Engine mass flow, lb sec

m Asymmetric weight, lb

$m_q = \frac{\partial C_m}{\partial\left(\frac{ql_T}{V}\right)}\frac{\bar{c}}{2l_T}$, pitching-moment coefficient due to rate of pitch

$m_\theta = \left[\frac{\partial C_m}{\partial(\alpha\, l_T/V)} + \frac{\partial C_m}{\partial(q\, l_t/V)}\right]$, full rotary damping derivative appropriate to space-fixed axes system

N Yawing moment, lb ft

n 'Excess' normal acceleration in 'g' units

$n_p = \frac{\partial C_n}{\partial(pb/2V)}$, yawing-moment coefficient due to rate of roll

$n_r = \frac{\partial C_n}{\partial(rb/2V)}$, yawing-moment coefficient due to rate of yaw

n_v = $\frac{\partial C_n}{\partial \beta}$, yawing-moment coefficient due to sideslip

n_ζ = $\frac{\partial C_n}{\partial \zeta}$, yawing-moment coefficient due to rudder deflection

n_ξ = $\frac{\partial C_n}{\partial \xi}$, yawing-moment coefficient due to aileron deflection

P Period of oscillation, sec

P Longitudinal stick force, lb

p Rate of roll, rad/sec

q Rate of pitch, rad/sec

r Rate of yaw, rad/sec

S Wing area, ft^2

S_F Elevator area aft of hinge line, ft^2

S_T Tailplane area, ft^2

t Time, sec

V True airspeed, ft/sec

V_R Rectified airspeed, ft/sec

$\bar{v}$ Effective tail-volume coefficient

W Aircraft weight, lb

$\bar{x}$ Distance of intake lip from aircraft centre of gravity, ft

Y Sideforce, lb

y_m Arm of asymmetric wing weight from *a/c* centreline, ft

y_v = $\frac{1}{2}\frac{\partial C_y}{\partial \beta}$, sideforce coefficient due to sideslip

y_ζ = $\frac{1}{2}\frac{\partial C_y}{\partial \zeta}$, sideforce coefficient due to rudder deflection

y_ξ = $\frac{1}{2}\frac{\partial C_y}{\partial \xi}$, sideforce coefficient due to aileron deflection

α Angle of incidence, rad

α_T Tailplane angle of incidence, rad

β Angle of sideslip, rad

β Trim tab angle, rad

γ Flight-path angle, rad

δ Logarithmic decrement of oscillation

ε Mean angle of downwash at tailplane, rad

ε Inclination of principal axis of inertia, deg

ε_D = $\tan^{-1}\left(\frac{\delta}{2\pi}\right)$, damping angle, deg

ζ Rudder angle, rad

η Elevator angle, rad

η_T Tailplane angle, rad

θ Aircraft attitude (fuselage datum), rad

μ_2 = $\frac{2W}{g\rho S b}$, aircraft relative density

ξ Aileron angle, rad

ρ Air density, slug/ft^3

ϕ Angle of bank, rad

Angle between wing chord and thrust lines, deg

ψ Angle of yaw, rad

ω Frequency of oscillation, rad/sec

The distance of the mean quarter chord point ($\frac{1}{4}\bar{c}$) behind a datum point is defined as $\bar{x} = \frac{2}{S}\int_0^{b/2} xc\,dy$, where x is the distance of the local quarter chord points behind the same datum point.

REFERENCES

No.	*Author(s)*	*Title, etc.*
1	K. W. Smith	The measurement of position error at high speeds and altitude by means of a trailing static head. A.R.C. C.P. 160, 1952.
2	K. W. Smith	Pressure lag in pipes with special reference to aircraft speed and height measurements. R.A.E. Report Aero 2507 (A.R.C. 17610), 1954.
3	R. F. R. Storey	Longitudinal and lateral stability investigation on the Short SB 5 (ER 100) aircraft with 60° wing sweepback. Part I—Model with high-set tailplane. Short Brothers and Harland Ltd. Wind Tunnel Report 15, 1951.
4	R. F. R. Storey	Longitudinal and lateral stability investigation on the Short SB 5 (ER 100) aircraft with sweepback. Part III—Model with low tailplane. Short Brothers and Harland Ltd. Wind Tunnel Report 17, 1952.
5	English Electric Co. Ltd. . .	Tests of an SB 5 model compared with flight test results (60° swept wing, low tailplane). Wind Tunnel Report AX135, 1954.

REFERENCES—*continued*

6	Royal Aeronautical Society	Data sheets. Aerodynamics.
7	J. A. Bagley	An aerodynamic outline of a transonic transport aeroplane. R.A.E. Technical Note Aero 2472 (A.R.C. 19205), 1956.
8	English Electric Co. Ltd. ..	P1 wing pressure distributions at low speed. Wind Tunnel Report AX109, 1953.
9	D. J. Lyons	An examination of the technique of measurement of the longitudinal manoeuvering characteristics of an aeroplane, and a proposal for a standardised method. A.R.C. R. & M. 2597, 1947.
10	D. J. Lyons and .. .. P. L. Bisgood	An analysis of the lift slope of aerofoils of small aspect ratio, including fins, with design charts for aerofoils and control surfaces. A.R.C. R. & M. 2308, 1945.
11	W. J. G. Pinsker	Aileron control of small-aspect-ratio aircraft; in particular, delta aircraft. A.R.C. R. & M. 3188, 1953.
12	R. W. Stone and .. .. E. C. Polhamus	Some effects of shed vortices on the flow fields around stabilising tail surfaces. AGARD Report 108, 1957.
13	D. H. Perry, J. C. Morrall and W. G. A. Port	Low speed flight tests on a tailless delta aircraft with wings swept back 44·5° (Avro 707B). Part 3—Lateral stability and control. R.A.E. Report Aero 2638 (A.R.C. 22242), 1960.
14	J. P. Campbell and .. .. M. O. McKinney ..	Summary of methods for calculating dynamic lateral stability and response and for estimating lateral stability derivatives. NACA Technical Note 2409, 1951.
15	H. H. B. M. Thomas and .. S. Neumark	Interim note on stability and response characteristics of supersonic aircraft (linear theory). R.A.E. Technical Note Aero 2412 (A.R.C. 18263), 1955.
16	G. H. Lee	Note on the flow around delta wings with sharp leading edges. A.R.C. R. & M. 3070, 1955.
17	H. C. Garner and .. .. D. E. Walshe	Pressure distributions and surface flow on 5 per cent and 9 per cent thick wings with curved tip and 60° sweepback. Part III—Surface flows with separation. A.R.C. R. & M. 3244, 1960.
18	S. B. Gates and H. M. Lyon	A continuation of longitudinal stability and control analysis. Part II—Interpretation of flight tests. A.R.C. R. & M. 2028, 1944.

APPENDIX A

Lift and Drag from Partial Glides

The partial glide technique was used, with the aircraft in steady rectilinear flight at constant speed. The relevant longitudinal equations of motion are:

$$L = W\cos\gamma - T\sin(\theta-\gamma)$$

$$D = -W\sin\gamma + T\cos(\theta-\gamma)$$

where L = Lift, lb

D = Drag, lb

W = Aircraft weight, lb

T = Engine thrust, lb

γ = Flight path angle (negative for glide)

θ = Aircraft attitude (fuselage datum).

The aircraft wing chord line is at 2° to the thrust line, from which the attitude is measured, so that:

$$\alpha = \theta - \gamma + 2°.$$

Measurements were made of the time, t, for a given change of altitude, ΔH, (tape measure height) so that the flight path angle is given by:

$$\sin\gamma = \frac{\Delta H}{tV}$$

where V = true airspeed.

With θ measured, W known, T from engine brochure values, L, D, α, C_L, C_D can be calculated.

For comparison with the tunnel results it was necessary to correct these to a trimmed value of lift coefficient given by:

$$C_{L_{\text{trim}}} = C_L + C_m\frac{\bar{c}}{l_T}$$

where C_L = tunnel lift coefficient

C_m = tunnel pitching-moment coefficient, corrected to the flight *cg* position

$\bar{c}$ = mean aerodynamic chord

l_T = tail arm.

For comparison with estimates an untrimmed value of the flight lift-curve slope was required, given by:

$$\frac{dC_L}{d\alpha} = \frac{dC_{L_{\text{trim}}}}{d\alpha}\left(1 - \frac{dC_m}{dC_{L_{\text{trim}}}}\cdot\frac{\bar{c}}{l_T}\right) \tag{A.1}$$

where $\frac{dC_m}{dC_{L_{trim}}}$ was obtained from flight longitudinal stability measurements.

In order to obtain the flight value of wing plus fuselage induced drag for comparison with estimates it was necessary to correct for the trim drag. Breaking the trimmed lift and drag coefficients into their component parts gives:

$$C_{L_{trim}} = C_{L_W} + C_{L_T}\frac{S_T}{S_W}\cos\varepsilon - C_{D_T}\frac{S_T}{S_W}\sin\varepsilon$$

$$C_{D_{trim}} = C_{D_W} + C_{D_T}\frac{S_T}{S_W}\cos\varepsilon + C_{L_T}\frac{S_T}{S_W}\sin\varepsilon$$

where ε = angle of downwash (from tunnel tests[5])

S = area

and the subscripts W, T refer to wing and tail values respectively.

Due to the tailplane load the wing plus fuselage induced drag differs from what it would be in the absence of a tailplane by an amount given by:

$$\left(\frac{\partial C_{D_W}}{\partial C_{L_W}}\right)\Delta C_{L_W} = \frac{2k\,C_{L_W}}{\pi A}\Delta C_{L_W} \tag{A.2}$$

where ΔC_{L_W} is the additional wing lift coefficient due to the tailplane load.

The extra tailplane induced drag is given by:

$$C_{D_{iT}}\frac{S_T}{S_W}\cos\varepsilon = \frac{K_T\,C_{L_T}^2}{\pi A_T}\frac{S_T}{S_W}\cos\varepsilon$$

and the extra drag due to the inclination of the tailplane lift by:

$$C_{L_T}\frac{S_T}{S_W}\sin\varepsilon\,.$$

Subtraction of these correction terms from $C_{D_{trim}}$ allows the determination of the variation of induced drag with lift in the absence of the tailplane and hence a value of k, the induced-drag factor, for comparison with estimates. It is necessary to reiterate for k in equation (A.2) and a value of k_T, the tailplane induced drag factor has to be estimated. This has been taken as 1·4; the tailplane lift coefficients are sufficiently small for vortex flow to be absent.

It is then necessary only to determine C_{L_T}, which can be obtained from the flight longitudinal stability measurements and tunnel downwash measurements.

APPENDIX B

Longitudinal Stability Analysis

The pitching moment and stick-force equations for an aircraft in constant speed rectilinear flight are:

$$C_m = C_L(h-h_n) - \overline{V}\,[a_0 + a_1(\alpha - \varepsilon + \eta_T - \phi) + a_2\,\eta + a_3\,\beta] = 0 \tag{B.1}$$

$$C_H = b_0 + b_1(\alpha - \varepsilon + \eta_T - \phi) + b_2\,\eta + b_3\,\beta \tag{B.2}$$

where C_m = Pitching-moment coefficient

C_L = Lift coefficient

C_H = Elevator hinge-moment coefficient

h = Position of *cg* as fraction of mean aerodynamic chord

h_n = Position of neutral point as a fraction of mean aerodynamic chord

$\overline{V}$ = Effective tail-volume coefficient

a_0 = Tailplane lift coefficient at zero tailplane incidence

a_1 = Tailplane lift-curve slope, $dC_{L_T}/d\alpha_T$

a_2 = Tailplane lift coefficient due to elevator angle, $dC_{L_T}/d\eta$

a_3 = Tailplane lift coefficient due to tab angle, $dC_{L_T}/d\beta$

b_0 = Hinge-moment coefficient at zero tailplane incidence, elevator angle and tab angle

b_1 = Hinge-moment coefficient due to tailplane incidence, $dC_H/d\alpha_T$

b_2 = Hinge-moment coefficient due to elevator deflection, $dC_H/d\eta$

b_3 = Hinge-moment coefficient due to tab deflection, $dC_H/d\beta$

α = Wing incidence

ε = Angle of downwash at tailplane

η_T = Tailplane setting relative to fuselage datum

ϕ = Wing chord setting relative to fuselage datum = 2°

η = Elevator angle

β = Tab angle.

Then from (B.1):

at constant $(h-h_n)$, η_T, C_L and hence constant α and ε

$$a_2\,\Delta\eta + a_3\,\Delta\beta = 0$$

i.e.
$$\frac{a_3}{a_2} = -\frac{\Delta\eta}{\Delta\beta}$$

and also
$$\Delta\eta = -\frac{a_3}{a_2}\beta$$

gives the correction to η for determination of elevator angle at zero tab angle.

at constant $(h-h_n)$, C_L and hence constant α and ε, and with $\beta = 0$ (i.e. elevator angle corrected to zero tab angle).

$$a_1\,\Delta\eta_T + a_2\,\Delta\eta = 0$$

i.e.
$$\frac{a_1}{a_2} = -\frac{\Delta\eta}{\Delta\eta_T}$$

at constant η_T, C_L and hence constant α, ε, and with $\beta = 0$

$$C_L \Delta h - \overline{\overline{V}}\, a_2 \Delta\eta = 0$$

i.e.
$$a_2 = \frac{\Delta h\, C_L}{\Delta\eta\, \overline{\overline{V}}}$$

since
$$\Delta\eta = C_L \Delta\left(\frac{\partial\eta}{\partial C_L}\right)$$

$$a_2 = \frac{\Delta h}{\overline{\overline{V}}\, \Delta(\partial\eta/\partial C_L)}.$$

Hence a_1, a_2, a_3 can be obtained.

With the aircraft trimmed by the elevator tab and the stick free:

from equation (B.1) at constant η_T, C_L and hence constant α, ε

$$C_L \Delta h - \overline{\overline{V}}\,(a_2 \Delta\eta + a_3 \Delta\beta) = 0$$

therefore
$$C_L \Delta h = \overline{\overline{V}}\, a_2 \Delta\beta \left(\frac{\Delta\eta}{\Delta\beta} + \frac{a_3}{a_2}\right)$$

and from (B.2), since $C_H = 0$

$$b_2 \Delta\eta + b_3 \Delta\beta = 0$$

therefore
$$\frac{\Delta\eta}{\Delta\beta} = -\frac{b_3}{b_2}$$

and since also
$$\Delta\beta = C_L \Delta\left(\frac{d\beta}{dC_L}\right)$$

we have
$$a_2\left(\frac{a_3}{a_2} - \frac{b_3}{b_2}\right) = \frac{\Delta\eta}{\overline{\overline{V}} \cdot \Delta\left(\frac{d\beta}{dC_L}\right)}.$$

With finite stick forces, i.e. $C_H \neq 0$ and at constant η_T, C_L and hence α and ε

$$\frac{dC_H}{d\beta} = b_2 \frac{d\eta}{d\beta} + b_3 = -b_2 \frac{a_3}{a_2} + b_3.$$

Also at constant β, C_L and hence α and ε

$$\frac{dC_H}{d\eta} = b_1 \frac{d\eta_T}{d\eta} + b_2 = -b_1 \frac{a_2}{a_1} + b_2.$$

Hence b_1, b_2, b_3 can be obtained.

Hinge-moment coefficient was determined from stick force giving:

$$C_H = \frac{P \times \text{gearing}}{\frac{1}{2}\rho V^2 S_F C_F}$$

when P = stick force

S_F = elevator area aft of hinge line

C_F = mean elevator chord aft of hinge line

and the 'gearing' is the distance the control colume moves (at the pilot's grip) per unit elevator deflection.

For the determination of the manoeuvre point, stick fixed, the elevator movement per 'g' is determined with the following assumptions:

(a) The manoeuvre is performed as a portion of a vertical circle.

(b) The forward speed is constant.

(c) The angular pitching velocity is constant, giving

(d) A constant radial normal acceleration, approximately.

Then the rate of pitch is given by:

$$q = \frac{ng}{V}$$

and the lift coefficient by:

$$C_L = \frac{(n+1)W}{\frac{1}{2}\rho V^2 S}$$

where q = Rate of pitch

n = Excess normal acceleration.

In the steady state the total pitching moment is zero and therefore:

$$\frac{\partial C_m}{\partial n} = \frac{\partial C_m}{\partial C_L} \cdot \frac{\partial C_L}{\partial n} + \frac{\partial C_m}{\partial \eta} \cdot \frac{\partial \eta}{\partial n} + \frac{m_q l_T^2}{\frac{1}{2} V \bar{c}} \frac{\partial q}{\partial n} = 0 \tag{B.3}$$

where the term in m_q accounts for the additional pitching moment due to the rate of pitch.

Also

$$\frac{\partial C_m}{\partial C_L} = h - h_n$$

$$\frac{\partial C_m}{\partial \eta} = -\bar{V} a_2$$

and thus substituting in (B.3):

$$\bar{V} a_2 \frac{\partial \eta}{\partial n} = (h - h_n)\frac{\partial C_L}{\partial n} + \frac{m_q l_T^2}{\frac{1}{2} V \bar{c}} \cdot \frac{\partial q}{\partial n} = C_{L_0}\left(h - h_n + \frac{g\, m_q \rho S l_T^2}{W \bar{c}}\right)$$

where C_{L_0} = lift coefficient in rectilinear flight at speed V.

At the stick fixed manoeuvre point, $h = h_m$, and by definition $\frac{\partial \eta}{\partial n} = 0$, so that:

$$h_m = h_n - \frac{g\, m_q\, \rho\, S\, l_T^2}{W\, \bar{c}}.$$

For comparison with tunnel results it was necessary to apply a correction to the flight pitching-moment results for the engine mass flow.

The momentum drag due to engine mass flow is given by:

$$\text{Momentum drag} = \frac{M_E\, V}{g}$$

and, assuming the force acts at the intake lip, gives an incremental pitching moment:

$$\Delta C_m = \frac{M_E V}{g} \cdot \frac{\bar{x} \sin(\alpha - \phi)}{\frac{1}{2}\rho\, V^2\, S\, \bar{c}}$$

where M_E = Engine mass flow

V = True airspeed

$\bar{x}$ = Distance of aircraft *cg* aft of intake nose

α = Angle of incidence

ϕ = Angle of wing chord line above engine thrust line = 2°.

In addition, correction to an untrimmed lift coefficient was made using the formula given in Appendix A.

APPENDIX C

Aileron Power from Asymmetric Ballast Tests

The equation of the equilibrium of rolling moments of the aircraft with asymmetric weights on the wings and with rate and acceleration in roll zero, and acceleration in yaw zero, is:

$$l_\xi \xi + l_\zeta \zeta + l_v \beta + l_r \frac{rb}{2V} + \frac{m y_m \cos\phi \cos\gamma}{\frac{1}{2}\rho V^2 S b} = 0$$

where l_ξ = Aileron rolling-power derivative

l_ζ = Rudder rolling-power derivative

l_v = Rolling moment due to sideslip derivative

l_r = Rolling moment due to rate of yaw derivative

m = Asymmetric wing weights

y_m = Moment arm of wing weights

ξ = Aileron angle

ζ = Rudder angle

β = Sideslip angle

r = Rate of yaw

ϕ = Bank angle

γ = Climb angle.

If the balancing rolling moment is defined as the sum of all terms except $l_\xi \xi$ then the slope of the plot of the balancing rolling moment against aileron angle, ξ, gives the aileron power, l_ξ.

Under the same conditions the yawing moment equation is:

$$n_\xi \xi + n_\zeta \zeta + n_v \beta + n_r \frac{rb}{2V} + \frac{m y_m \cos\phi \sin\gamma}{\frac{1}{2}\rho V^2 S b} = 0$$

where n_ξ = Aileron yawing-power derivative

n_ζ = Rudder yawing-power derivative

n_v = Yawing moment due to sideslip derivative

n_r = Yawing moment due to rate of yaw derivative

and the slope of the plot of balancing yawing moment against aileron angle, ξ, gives the aileron yawing derivative n_ξ.

APPENDIX D

Aileron Power from Oscillatory Aileron Tests

If the lateral control performs a sinusoidal oscillation

$$\xi = \bar{\xi} \sin(\omega t)$$

with amplitude $\bar{\xi}$ and frequency ω, the aircraft will respond in an oscillation at the same frequency. Consequently all the contributions to the rolling moments acting on the aircraft vary in an oscillatory manner and can be described by the equation

$$C_l(t) = l_\xi \bar{\xi} \sin(\omega t) + l_v \bar{\beta} \sin(\omega t + \varepsilon_\beta) + l_p \frac{b}{2V} \bar{p} \sin(\omega t + \varepsilon_p) +$$

$$+ l_r \frac{b}{2V} \bar{r} \sin(\omega t + \varepsilon_r)$$

$$= \frac{1}{\frac{1}{2}\rho V^2 S b} \left[\bar{A}\, \bar{p}\, \omega \sin\left(\omega t + \varepsilon_p + \frac{\pi}{2}\right) - E \bar{r}\, \omega \sin\left(\omega t + \varepsilon_r + \frac{\pi}{2}\right) \right]. \tag{D.1}$$

In this expression all phase angles ε are defined with respect to aileron and use is made of the relationship that if

$$\begin{aligned} x &= \bar{x} \sin(\omega t) \\ \dot{x} &= \bar{x}\, \omega \sin\left(\omega t + \frac{\pi}{2}\right). \end{aligned} \tag{D.2}$$

If the amplitudes of the motion of the aircraft in the three degrees of freedom p, r and β are measured in addition to that of the aileron excitation and if the phase relationship between the quantities is also known, the rolling-moment equation can be solved for any of the unknowns, if all the remaining quantities are either known or can be shown to be negligible. We have to solve the equations for an instant of time, at which the quantity required is not zero. So to obtain $l_\xi \bar{\xi}$ we choose $\left(\omega t = \frac{\pi}{2}\right)$. This gives

$$\begin{aligned} &l_\xi \bar{\xi} + l_v \bar{\beta} \cos \varepsilon_\beta + l_p \frac{b}{2V} \bar{p} \cos \varepsilon_p + l_r \frac{b}{2V} \bar{r} \cos \varepsilon_r \\ &= -\frac{2}{\rho V^2 S b} \left[A\, \bar{p}\, \omega \sin \varepsilon_p - E \bar{r}\, \omega \sin \varepsilon_r \right]. \end{aligned} \tag{D.3}$$

Combining terms in $\bar{p}$ and $\bar{r}$ this can be written:

$$l_\xi \bar{\xi} = -l_v \beta \cos \varepsilon_\beta - \frac{\omega}{2} \frac{W b}{\rho g V^2 S} \left[i_A \bar{p} \sqrt{\left(\frac{1}{\omega} \frac{l_p}{i_a} \frac{\rho g V S}{W}\right)^2 + 1} \sin(\varepsilon_p + \Delta\varepsilon_p) - \right.$$

$$\left. - i_E \bar{r} \sqrt{1 + \left(\frac{1}{\omega} \frac{l_r}{i_E} \frac{\rho g V S}{W}\right)^2} \times \sin(\varepsilon_r + \Delta\varepsilon_r) \right], \tag{D.4}$$

where

$$\Delta\varepsilon_p = -\sin^{-1}\left(\frac{1}{\omega}\frac{l_p}{i_a}\frac{\rho g V S}{W}\right)$$

$$\Delta\varepsilon_r = -\sin^{-1}\left(\frac{1}{\omega}\frac{l_r}{i_E}\frac{\rho g V S}{W}\right).$$

Provided ω is sufficiently large the second term in each of the roots and $\Delta\varepsilon_p$ and $\Delta\varepsilon_r$ become very small and can be ignored. (This applies even for the terms in $\bar{r}$ when i_E vanishes, because then the whole $\bar{r}$ term also vanishes.) In fact the success of the oscillatory aileron response technique depends in the first place on the achievement of a sufficiently large frequency, to minimise the effect of as many terms as possible in the analysis. It can be shown that in fact the contribution of l_p and l_r in the present tests are completely insignificant and we can simplify to:

$$l_\xi \bar{\xi} = -l_v \bar{\beta}\cos\varepsilon_\beta + \frac{\omega}{2}\frac{W b}{\rho g V^2 S}[-i_a \bar{p}\sin\varepsilon_p - i_E \bar{r}\sin\varepsilon_r]. \tag{D.5}$$

It should be noted that in these tests ε_p is virtually 90° so that small errors in reading this phase angle from the records and for the same reason $\Delta\varepsilon_p$ make no practical difference to the corresponding values of $\sin\varepsilon_p$.

The sideslip amplitude β was also small in relation to the other quantities. In fact it could not be read reliably from the available flight records and instead it was assumed that the lateral translatory response of the aircraft can be neglected so that $\bar{\beta} = -\bar{\psi}$.

With the relationship $(D-2)\,\bar{\psi} = \dfrac{\bar{r}}{\omega}$ and we get

$$l_\xi \bar{\xi} = -l_v \frac{\bar{r}}{\omega}\cos\varepsilon_r + \frac{\omega}{2}\frac{W b}{\rho g V^2 S}[-i_a \bar{p} - i_E \bar{r}\sin\varepsilon_r] \tag{D.6}$$

from which l_ξ can be readily evaluated if the inertias i_a and i_E are known and an estimate for l_v is available. Again at large frequencies, the l_v term will be small in relation to the other terms and inaccuracies in the assumed value of l_v will have no great effect on the result.

APPENDIX E

Static Lateral Stability

The equilibrium equations defining the forces acting on the aircraft in a straight sideslip are:

$$l_v \beta + l_\xi \xi + l_\zeta \zeta = 0$$

$$n_v \beta + n_\xi \xi + n_\zeta \zeta = 0$$

$$y_v \beta + y_\xi \xi + y_\zeta \zeta + \tfrac{1}{2} C_L \phi = 0 .$$

Rearranging:

$$l_v = -l_\xi \frac{\xi}{\beta} - l_\zeta \frac{\zeta}{\beta}$$

$$n_v = -n_\xi \frac{\xi}{\beta} - n_\zeta \frac{\zeta}{\beta}$$

$$y_v = -y_\xi \frac{\xi}{\beta} - y_\zeta \frac{\zeta}{\beta} - \tfrac{1}{2} C_L \frac{\phi}{\beta} .$$

Neglecting y_ξ and writing $-y_\zeta = \tfrac{1}{2} n_\zeta \dfrac{b}{l_F}$ we get:

$$y_v = \tfrac{1}{2} n_\zeta \frac{\zeta}{\beta} \frac{b}{l_F} - \tfrac{1}{2} C_L \frac{\phi}{\beta}$$

where y_v = Sideforce due to sideslip derivative

y_ξ = Sideforce due to aileron angle derivative

y_ζ = Sideforce due to rudder angle derivative

l_F = Fin moment arm.

The slopes ξ/β, ζ/β, ϕ/β were obtained from the straight sideslip tests, the aileron derivatives, l_ξ, n_ξ from flight measurements and the rudder derivatives l_ζ, n_ζ from wind tunnel tests.

For comparison with tunnel results it was necessary to apply corrections for the engine mass flow, as in Appendix A.

This gives:

$$\Delta l_v = \frac{M_E V}{g} \cdot \frac{\bar{x} \sin(\alpha - \phi)}{\tfrac{1}{2} \rho V^2 S b}$$

$$\Delta n_v = \frac{M_E V}{g} \cdot \frac{\bar{x} \cos(\alpha - \phi)}{\tfrac{1}{2} \rho V^2 S b}$$

$$\Delta y_v = \frac{M_E V}{g} \cdot \frac{1}{\rho V^2 S} .$$

APPENDIX F

Pilot's Comments on General Handling

The following remarks on the general handling of the aircraft are based on pilots' reports. The speeds quoted are those read by the pilot, i.e. indicated airspeed.

F.1. *Taxying and Take-off.*

Taxying of the aircraft was satisfactory with the only slight difficulty arising in turning from rest when a somewhat higher speed than desirable was required before the nosewheel would castor.

The take-off was similar for all configurations. The tailplane was set at $-5°$ with zero tab and zero trailing-edge flap deflection. (Up to 15° of trailing-edge flap could be used for take-off but little if any advantage was gained by the use of flap. Larger angles caused excessive drag and prolonged the take-off and also caused buffet, increasing in severity with increased flap angle.) Considerable vibration was transmitted by the nosewheel on the ground run and became excessive at speeds above 80 knots. At this speed a light pull force lifted the wheel. The minimum safe unstick speed of 130 knots was achieved after about 1 800 yards when the aircraft flew itself off. However, the aircraft was very underpowered, and unstick was generally delayed until 135 knots to 140 knots was obtained in order to improve the climb away, which was still very laborious.

F.2. *Longitudinal Stability and Control.*

Longitudinal control was satisfactory and the elevator was moderately effective. Tailplane actuation and effectiveness were quite normal and the trim tab was very powerful. There were symptons of elevator over balance at extreme tailplane settings but these occurred only at large tailplane angles and not at large elevator angles. Slight tremors could be felt on the control column at all times but these were of no consequence even at the highest speeds obtained.

In the 20·2° nose flap and full span leading edge droop configurations the aircraft was longitudinally stable throughout the speed range. With the nose flap raised to 4° the aircraft became unstable, with reduction of control column pull force below about 125 knots. There was a recovery in stability below about 110 knots.

F.3. *Lateral Stability and Control.*

In the three configurations without full-span droop and with the notch sealed, a disturbance, characterised by a wing drop and aileron snatch occurred between 130 and 142 knots in level flight and at higher speed pro rata with application of normal acceleration. Either wing could drop depending on the direction of the sideslip. Correction was by use of ailerons, which were heavy and only moderately effective, about half travel being required. The use of rudder to remove the sideslip caused a wing drop in the opposite direction and the resultant oscillation of wing drop from side to side could not be controlled by the pilot. At 132 knots to 130 knots this characteristic had largely disappeared and the aircraft was in lateral trim but with some slight control buffet. Below about 130 knots the lateral stability again deteriorated until ultimately the minimum speed obtainable on the aircraft was determined by the lateral stability and control (*see* Section 7 of main text). This wing dropping characteristic was not present with the full-span leading-edge droop incorporated.

Initial attempts to cure the wing drop were made by adding leading-edge spoilers $1\frac{3}{8}$ in. wide and 101 in. long at the extreme outboard position (*see* Fig. 5). The spoilers were fitted in sections, 26 in., 26 in., 26 in., 23 in., starting with the tip section. The tests were carried out in the 20·2° nose flap configuration. Each of the first two outer sections of the spoiler reduced by about two knots the upper and lower limits of the speed range for wing drop, which was also less violent, but the corrective aileron force was still about the same (15 lb). The addition of the third section of spoiler caused a marked reduction in aileron force (2 to 4 lb) but did not alter the speed for the onset of the wing drop, which was very gradual. The fourth and last section of spoiler eliminated the wing drop entirely. The spanwise extent of the spoiler was then reduced in stages, removal of the outboard two sections having no effect on the now satisfactory behaviour. With the inboard section detached, leaving only the third portion from the tip in position, a very gentle wing drop occurred, requiring 2 to 4 lb aileron force to correct. This was clearly the most effective section of spoiler and further tests would have revealed the best position, span and chord of the strip. However, further investigation of the spoiler was abandoned since it was thought that a notch cut in the leading edge would achieve the same results and be a more acceptable solution for application to the English Electric P 1. Cutting the notch was completely effective in eliminating the wing drop and a more detailed description is given in Section 11.1 of the main text.

In all configurations the lateral oscillation was damped but the aircraft tended to fly in a constant dutch roll in rough conditions. The aircraft was spirally unstable, but less markedly so with the full span leading edge droop.

Stick-force characteristics with rate of roll and sideslip were satisfactory apart from the conditions under which the wing drop was apparent.

F.4. *Trailing-edge Flap.*

Lowering the flap caused a nose down change of trim, slight up to 10° deflection, moderate at 20° and very strong at 30° deflection. Buffet was moderate up to 30° but became progressively more severe as the flap angle was increased. With full flap, 60°, the aircraft would not maintain level flight at any speed.

The upper and lower limits of the wing-drop speed range, where applicable, were reduced about 5 knots on use of 15° flap deflection.

F.5. *Maximum Speed.*

At 5 000 ft and with engine setting 14 000 r.p.m. the aircraft descended at speeds below about 120 knots and above 190 knots. Speed has been increased to 310 knots which was an adequate upper limit as regards attitude and rate of descent especially since the aircraft was limited to 10 000 ft maximum altitude. At this speed there was no abnormal vibration or buffeting and the controls behaved normally. There was no reduction in control column longitudinal forces.

F.6. *Approach and Landing.*

The approach was normally made at about 145 knots. On landings at Bedford Airfield, with its long runway, flap was not generally used on the approach, but up to 20° could be used, the chief gain being that a somewhat lower approach speed could be chosen whilst still avoiding the wing drop region for those cases in which the notch was sealed. Normal touchdown speed was 130 knots to 125 knots though the aircraft could be held off the runway down to 120 knots. At lower speeds there was a danger of bumping the tail on the ground. Selection of full flap immediately after touchdown produced a considerable deceleration. Care had to be taken to avoid applying the toe operated Maxaret brakes prior to and at touchdown as the wheels then remained locked after touchdown. Otherwise, the braking system was very effective.

Figs. 76 and 77 give time histories of typical approaches and landings in mild and moderate turbulence respectively.

TABLE 1

General Aerodynamic Data

(60° sweepback, low tailplane configuration)

Wing

Gross area, sq ft	351·0
Span, ft	30·5
Standard mean chord, ft	11·52
Aerodynamic mean chord, ft	13·415
Aspect ratio	2·64
Distance from aircraft centreline to trailing-edge kink, ft	8·26
Sweepback (leading edge)	60°
Sweepback ($\frac{1}{4}$ chord line to trailing-edge kink)	58°
Sweepback (trailing edge to kink)	51·5°
Chord at aircraft centreline, ft	17·03
Chord at wing root, ft	16·22
Chord at trailing edge kink, ft	13·27
Chord at tip, ft	1·17
Aerofoil section, type	symmetrical
Thickness chord ratio (root)	5·26%
Thickness chord ratio (slant chord)	7·735%
Anhedral	3°
Chord line setting to fuselage datum	2°
Washout	0°
Distance of $\frac{1}{4}\bar{c}$ aft of centreline chord leading edge, ft	13·6

Flaps

Type	leading-edge droop
Span, % wing semi-span (perpendicular to centreline)	85·3%
Maximum deflection, in line of flight	17·2°
Hinge line sweep	58·5°
Chord at root, % wing root chord	12·4%

Type	leading edge
Area, sq ft (each)	6·77
Span, % wing semi-span (perpendicular to centreline)	24·4%
Maximum deflection, in line of flight	20·2°
Hinge line sweep	42·2°
Chord at root, % wing root chord	21·2%

Type	Trailing-edge split cum Zap
Area, sq ft (each)	18·44
Span, % wing semi-span (perpendicular to centreline), up	22·9%
Span, % wing semi-span (perpendicular to centreline), fully down	39%
Maximum deflection, in line of flight	54°
Hinge-line sweep, up	51·5°
Hinge-line sweep, fully down	27°

TABLE 1—*continued*

Ailerons	
Type	set back hinge
Area, aft of hinge line, sq ft (each)	8·65
Balance, % area aft of hinge line	29%
Chord, aft of hinge line, ft	1·5
Span, % wing semi-span	38·5%
Maximum deflection	±12°
Hinge line sweep	0°
Aileron tabs	
Type	geared balance
Area, % control surface aft of hinge line	13·7%
Span, % aileron span	41%
Chord, ft	0·5
Maximum deflection	±20°
Horizontal tailplane	
Gross area, sq ft	74·5
Nett area, sq ft	43·85
Span, ft	11·62
Mean chord, ft	6·41
Aspect ratio	1·81
Chord at aircraft centreline, ft	11·44
Chord at fuselage side, ft	8·24
Chord at tip, ft	1·375
Thickness/chord ratio	6%
Sweepback (leading edge)	60°
Sweepback ($\frac{1}{4}$ chord line)	52°
Movement, relative to fuselage datum	±10°
Volume coefficient (*cg* at 0·42 $\bar{c}$)	0·218
Elevators	
Type	set back hinge
Area, aft of hinge line, sq ft (each)	7·81
Chord, aft of hinge line, ft	1·75
Balance, % area aft of hinge line	29·5%
Maximum deflection	±20°
Hinge-line sweep	0°
Stick gearing, ft/radian	1·19
Elevator tabs	
Type	Geared balance—port trim—starboard
Area, % control surface aft of hinge line	12·64%
Span, ft	1·975
Chord, ft	0·5
Maximum deflection (geared)	±20°
Maximum deflection (trim)	±17·5°

TABLE 1 – *continued*

Fin	
Net area, sq ft	51·98
Mean chord, ft	8·85
Aspect ratio	0·66
Root chord, ft	11·0
Tip chord, ft	5·0
Thickness/chord ratio	8%
Sweepback (leading edge)	60°
Sweepback ($\frac{1}{4}$ chord line)	56°
Sweepback (trailing edge)	37°
Volume coefficient (cg at 0·42 $\bar{c}$)	0·0611
Rudder	
Type	set back hinge
Area, aft of hinge line, sq ft	13·69
Chord, aft of hinge line, % fin chord	25%
Balance, % area aft of hinge line	34·3%
Maximum deflection	±25°
Hinge line sweep	44·5°
Rudder tab	
Type	geared balance
Area, % control surface aft of hinge line	17·22%
Span, ft	3·771
Chord, ft	0·625
Maximum deflection	±20°
Miscellaneous	
Notch—location, % wing semi-span	70%
Notch—width, % wing semi-span	1·64%
Notch—depth, % local chord	4·84%
Tip cannisters—location, % wing semi-span	89·3%
Tip cannisters—maximum load (each), lb	420
Engine type	Derwent Mk. 8
Maximum fuel capacity, Imp gallons	300
Maximum permissible speed, knots	350
Maximum normal acceleration, g	4·5
Maximum permissible AUW at take-off	13 000 lb
Centre of gravity limits, % aerodynamic mean chord	34·1% – 43·5%

TABLE 2

Summary of Drag Measurements

Leading edge conf.		Nose flap down						Nose flap up						Droop
Trailing edge flap		0°			20°			0°			20°			0°
Source of data	Parameter	Nose flap angle	Notch		Nose flap angle	Notch		Nose flap angle	Notch		Nose flap angle	Notch		Notch sealed
			Sealed	Cut		Sealed	Cut		Sealed	Cut		Sealed	Cut	
Flight	k (C_L-range)	20·2°	1·7 (0–0·39) 3·0 (0·39–0·95)	1·7 (0–0·43) 3·3 (0·43–1·05)				4°	1·4 (0–0·35) 3·0 (0·35–0·77)	1·7 (0–0·42) 3·5 (0·42–0·77)	4°		1·6 (0–0·43) 3·0 (0·43–0·70)	1·3 (0–0·38) 1·9 (0·38–0·69) 4·3 (0·69–0·90)
	C_{D_0}		0·031	0·031					0·030	0·030			0·031	0·029
Tunnel Ref. 4	k (C_L-range)	22·9°	1·9 (0–0·28) 3·1 (0·28–0·70)		22·9°	1·95 (0–0·48) 3·1 (0·48–0·70)		0°	2·35 (0–0·36) 3·17 (0·36–0·77)					1·56 (0–0·46) 2·76 (0·46–0·70)
	C_{D_0}		0·019			0·034			0·016					0·019
RAE tunnel	k (C_L-range)	15°	1·8 (0–0·37) 3·21 (0·37–0·80)					0°	1·83 (0–0·39) 2·97 (0·39–0·77)					
	C_{D_0}		0·017						0·013					

TABLE 3

Flight Values of Induced-drag Factors Reduced to Wing and Fuselage alone (Trailing-Edge Flap Up)

Leading-edge configuration	Nose flap 20°		Nose flap 4°		Drooped
Notch	Sealed	Cut	Sealed	Cut	Sealed
k for C_L below kink	1·62	1·62	1·31	1·61	1·23
k for C_L above kink	2·95	3·25	2·94	3·45	1·85 ($0.38 < C_L < 0{\cdot}69$) 4·26 ($0{\cdot}69 < C_L$)

TABLE 4

Induced-Drag Factor k

Leading-edge configuration	Nose flap down	Nose flap up
k wing only	1·20 – 1·25	1·15 – 1·20

Zero-Lift Drag C_{D_0}

Configuration	Reynolds number	C_{D_0}
Without undercarriage	2×10^6	0·019
	∞	0·010
Undercarriage	∞	$\Delta C_{D_0} = 0{\cdot}027$
Complete aircraft	∞	0·037

TABLE 5

Inertia Data and l_r Used in the Analysis of Dynamic Lateral Tests

C_L	0·15	0·2	0·3	0·4
i_a	0·077	0·077	0·081	0·087
i_C	0·553	0·553	0·550	0·543
i_E	−0·007	−0·017	−0·038	−0·060
l_r	0·05	0·055	0·067	0·080

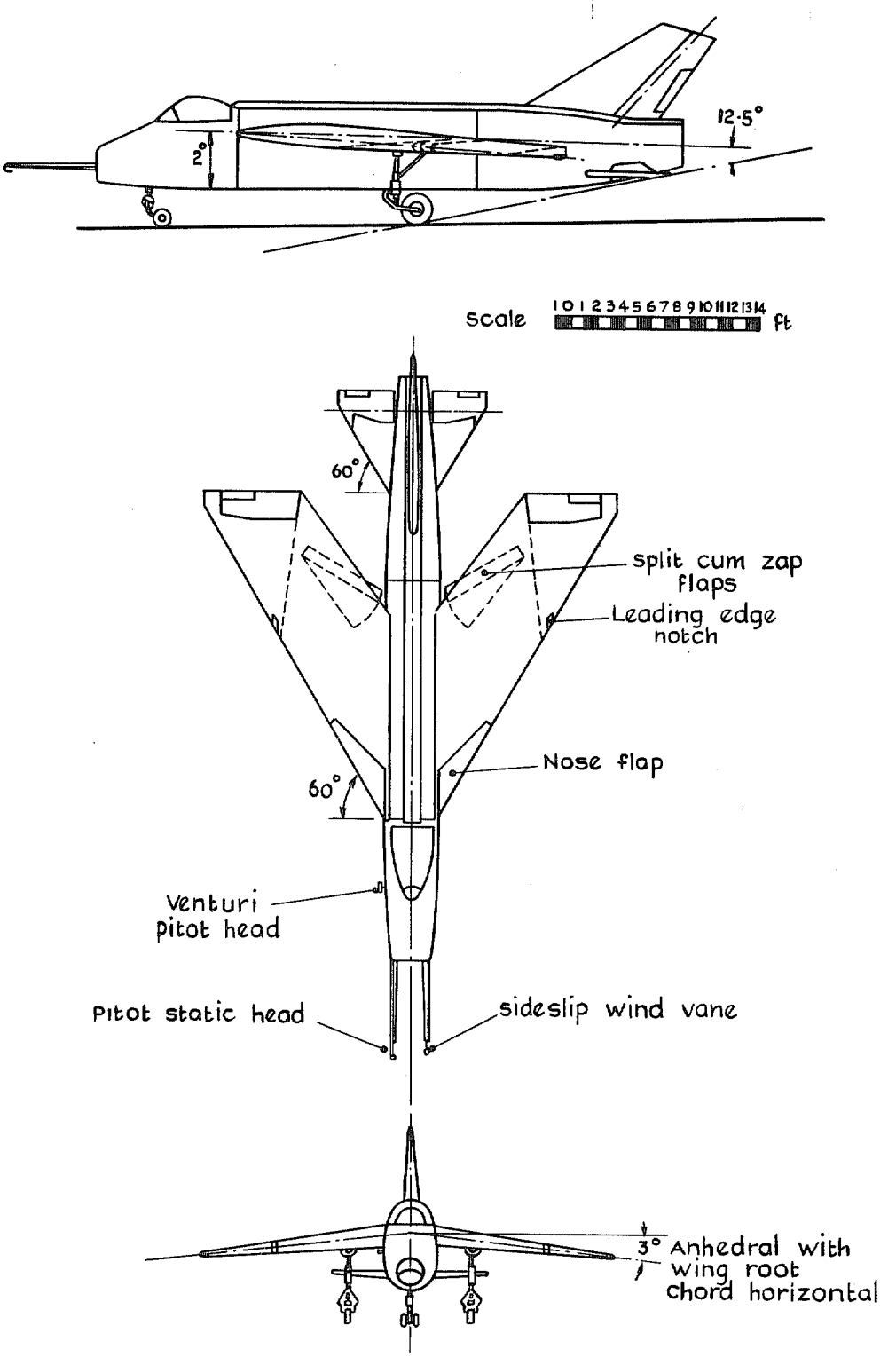

FIG. 1. G.A. of Short S.B.5 WG–768.

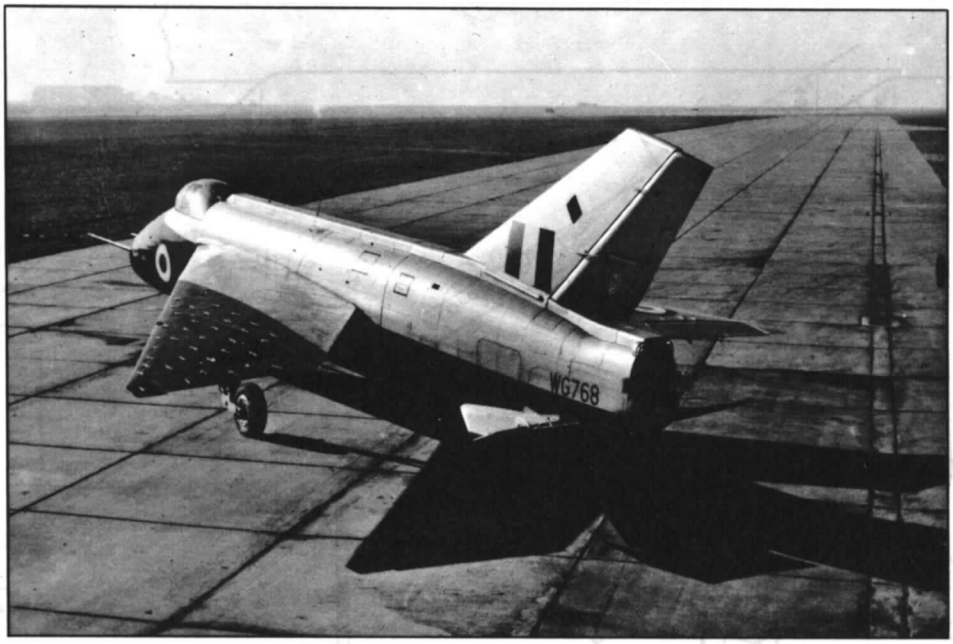

(a) 4° nose flap configuration with notch.

(b) 10·7° full span leading edge droop configuration.

FIG. 2. Short S.B. 5, 60° sweepback.

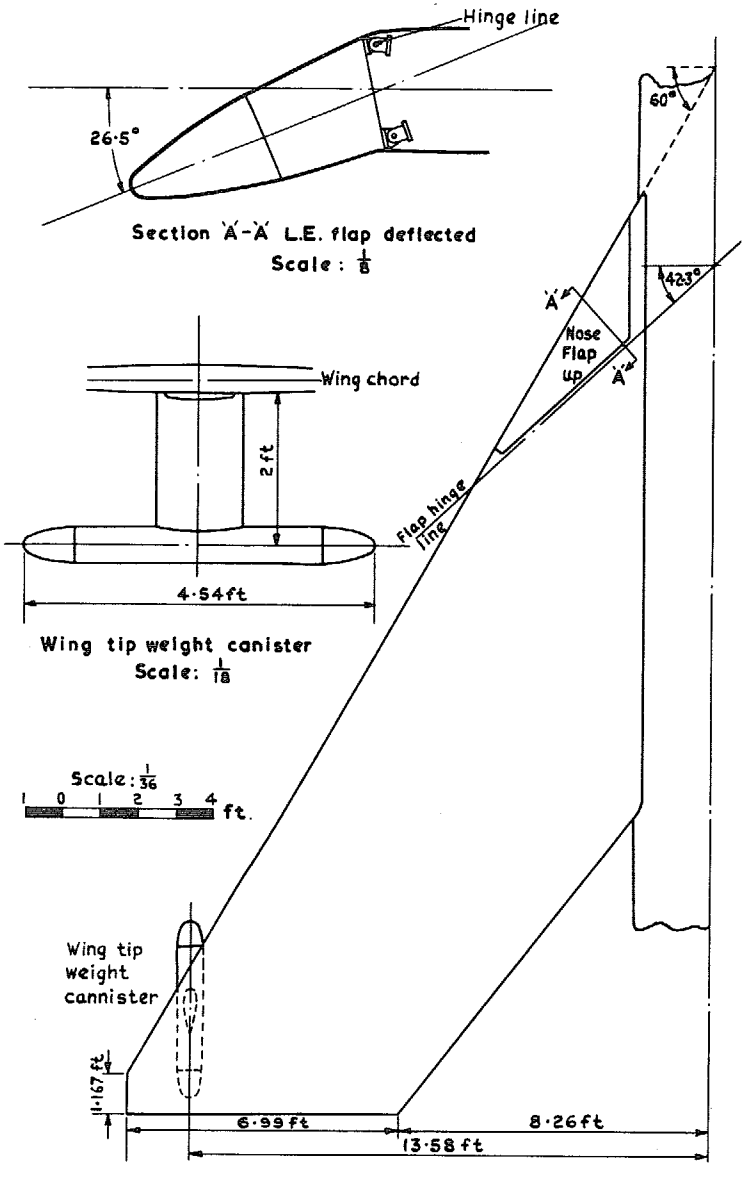

FIG. 3. Details of leading edge flaps and wing tip canisters.

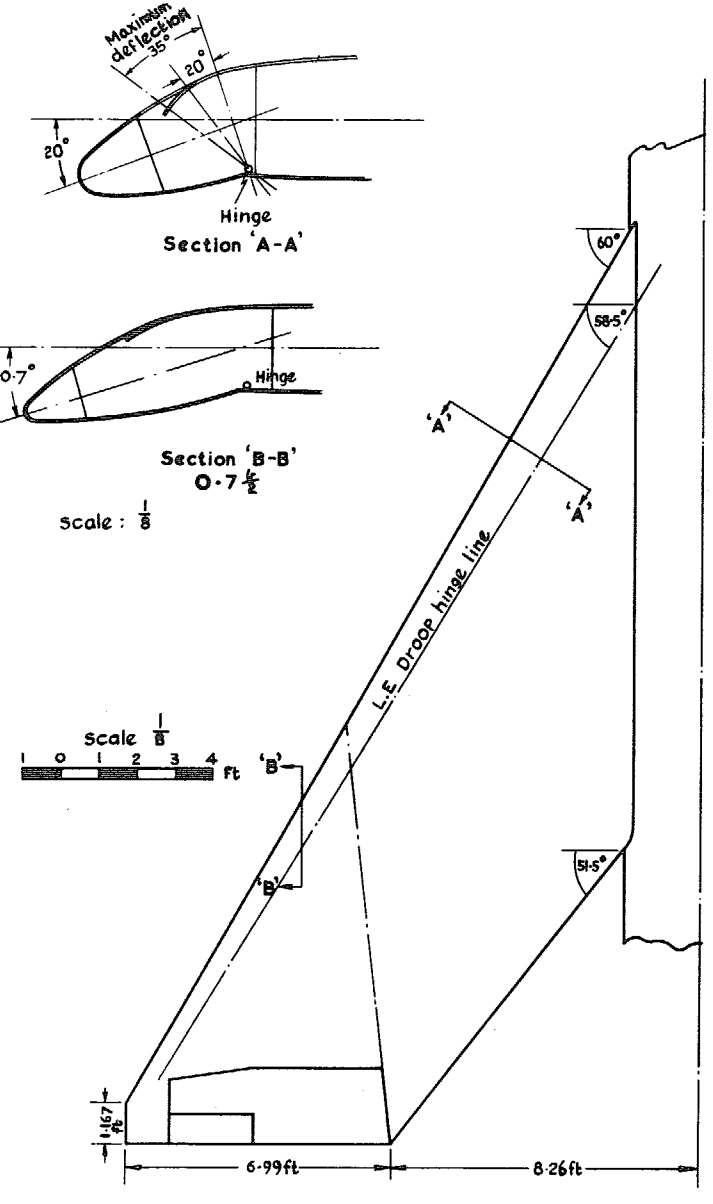

FIG. 4. Details of full span leading edge droop.

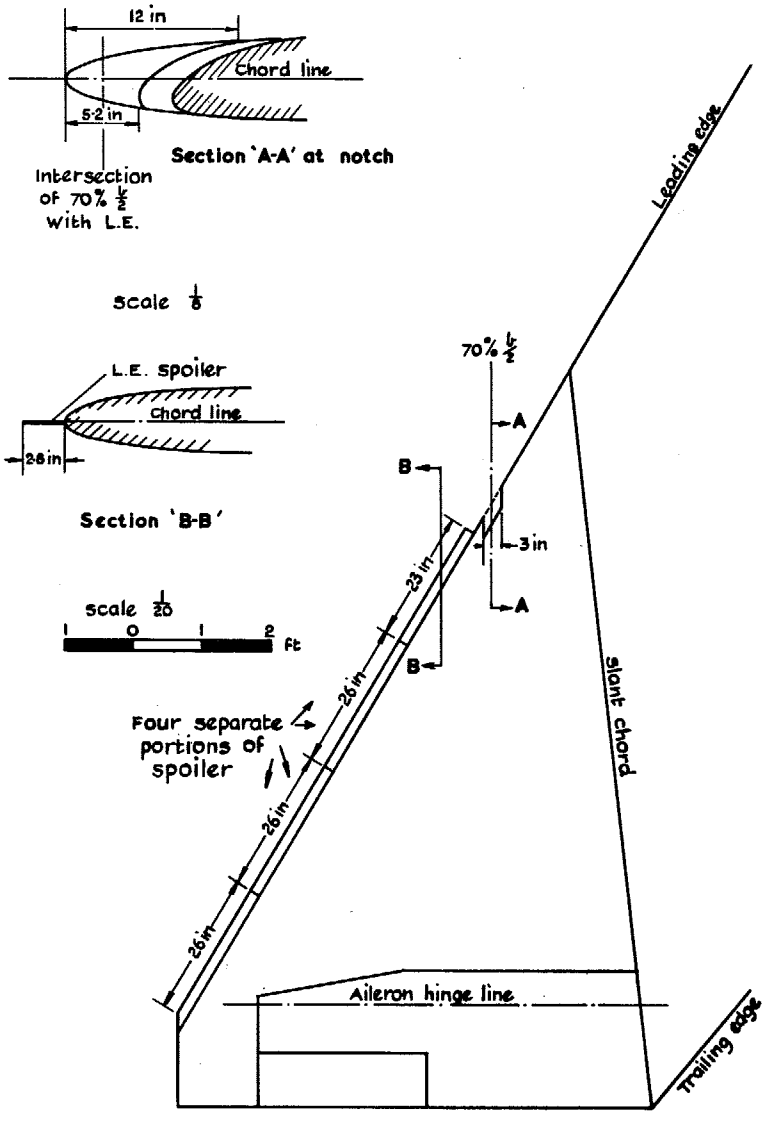

FIG. 5. Details of wing leading edge notch and knife spoiler (Appendix F).

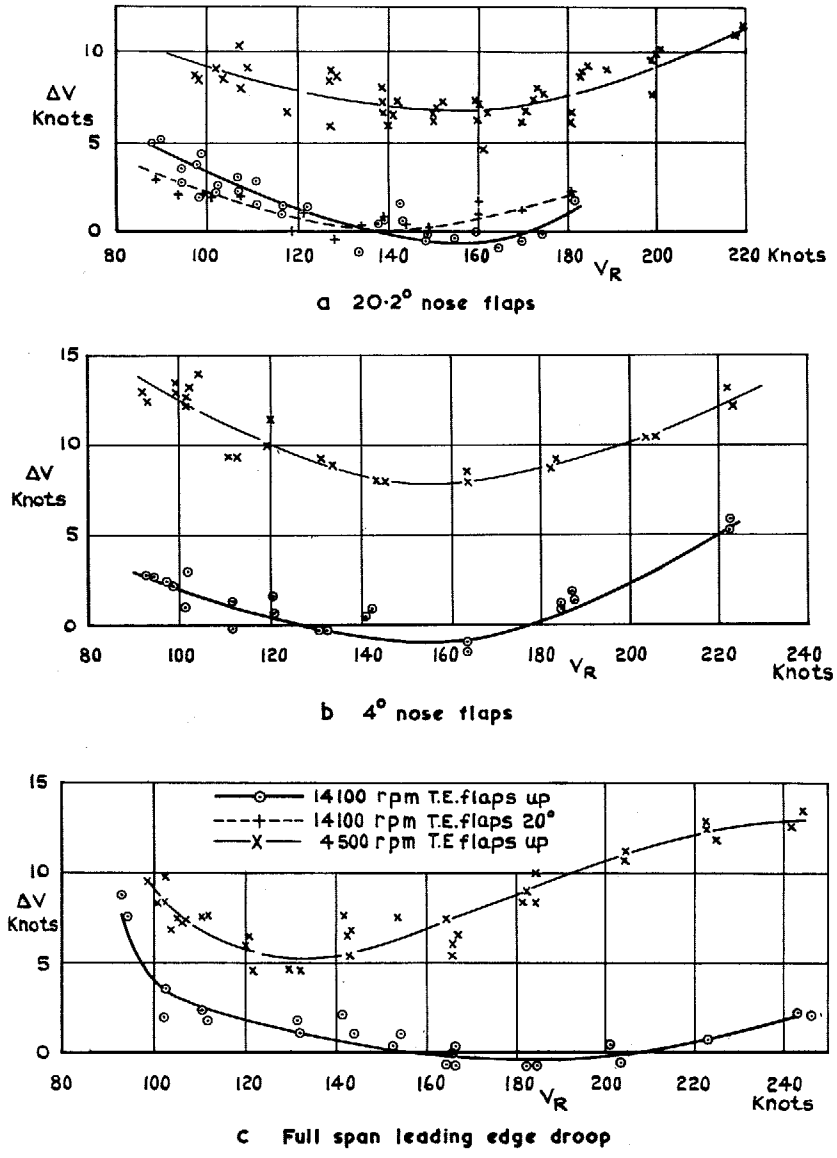

FIG. 6a–c. Flight calibration of airspeed position error corrections.

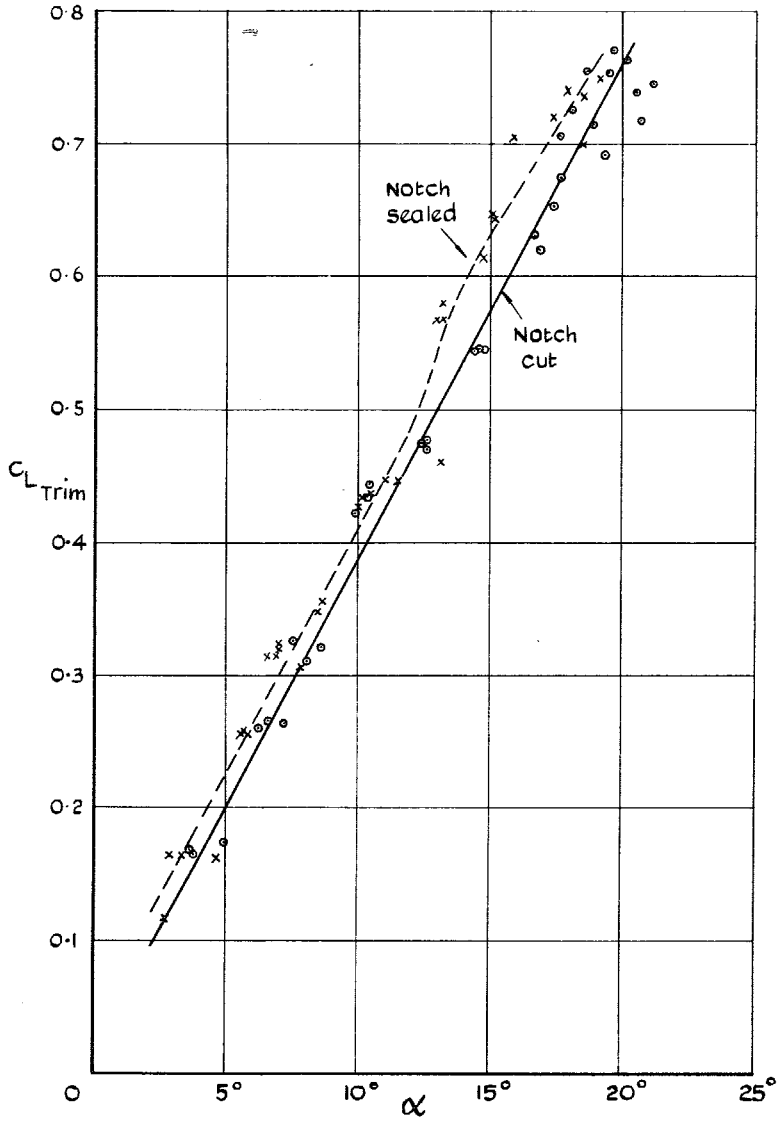

FIG. 7. Effect of notch on lift coefficient of basic configuration (nose flap 4°, trailing edge flaps up) power off, c.g. at 0·363 $\bar{c}$.

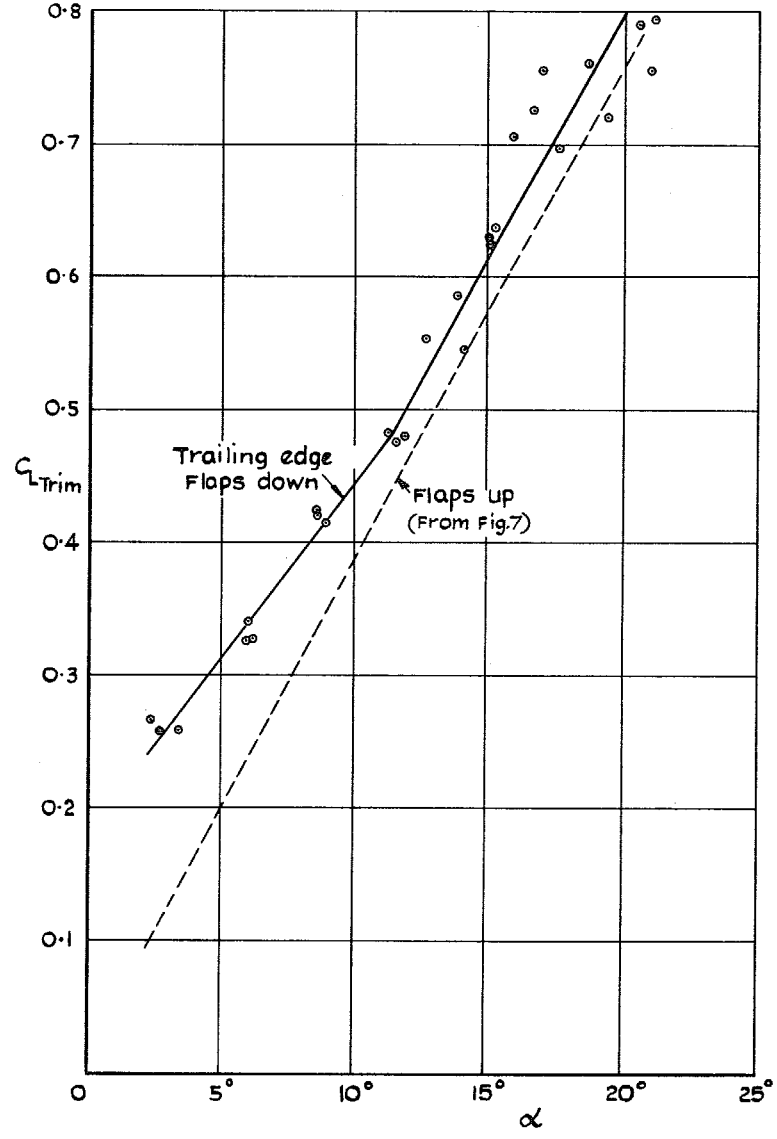

FIG. 8. Effect of trailing edge flaps on lift coefficient of basic configuration, notch cut, power off, c.g. at 0·363 $\bar{c}$.

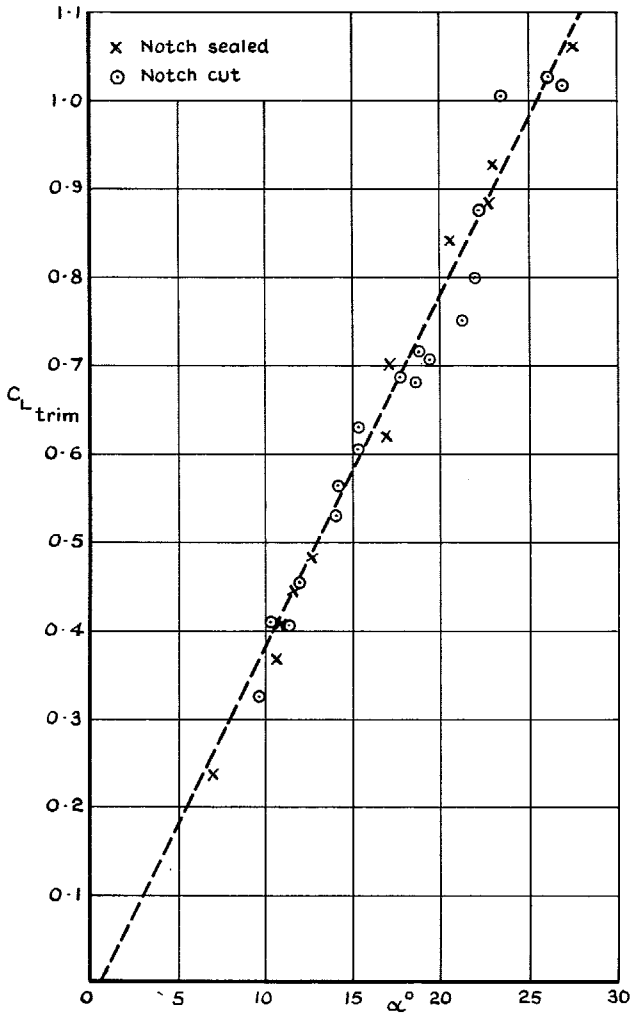

FIG. 9. Lift for 20·2° nose flap configuration, trailing edge flap up, power on, c.g. at 0·363 $\bar{c}$.

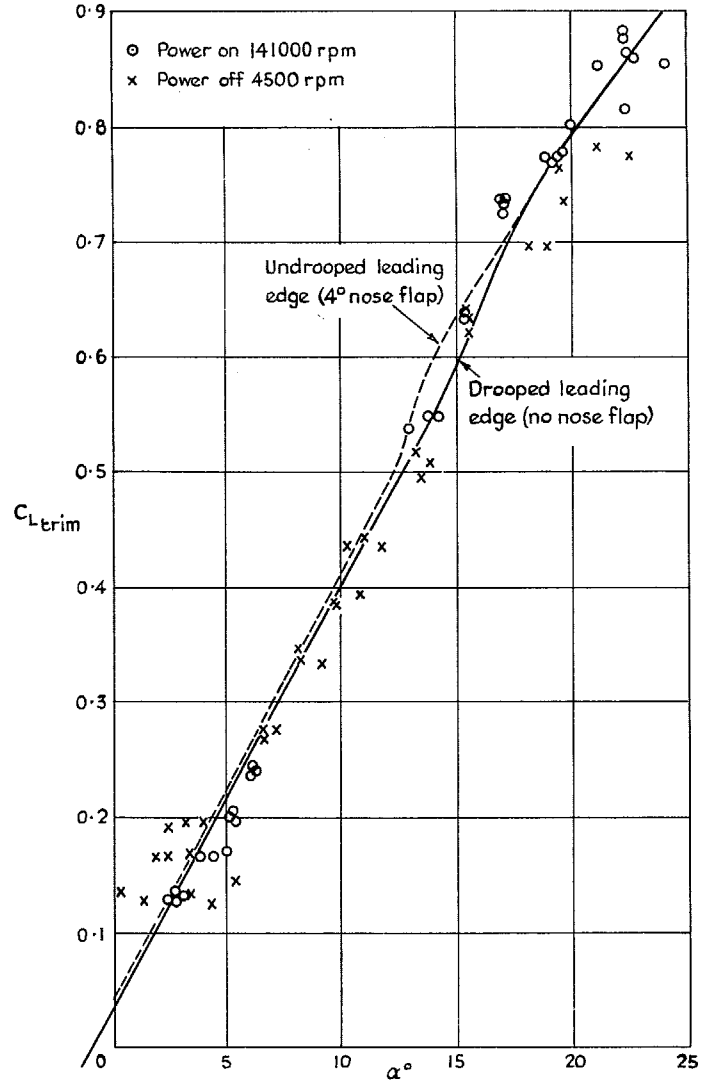

FIG. 10. Effect of 10·7° full span leading edge droop on lift coefficient of basic configuration, notch sealed, c.g. on 0·363 $\bar{c}$.

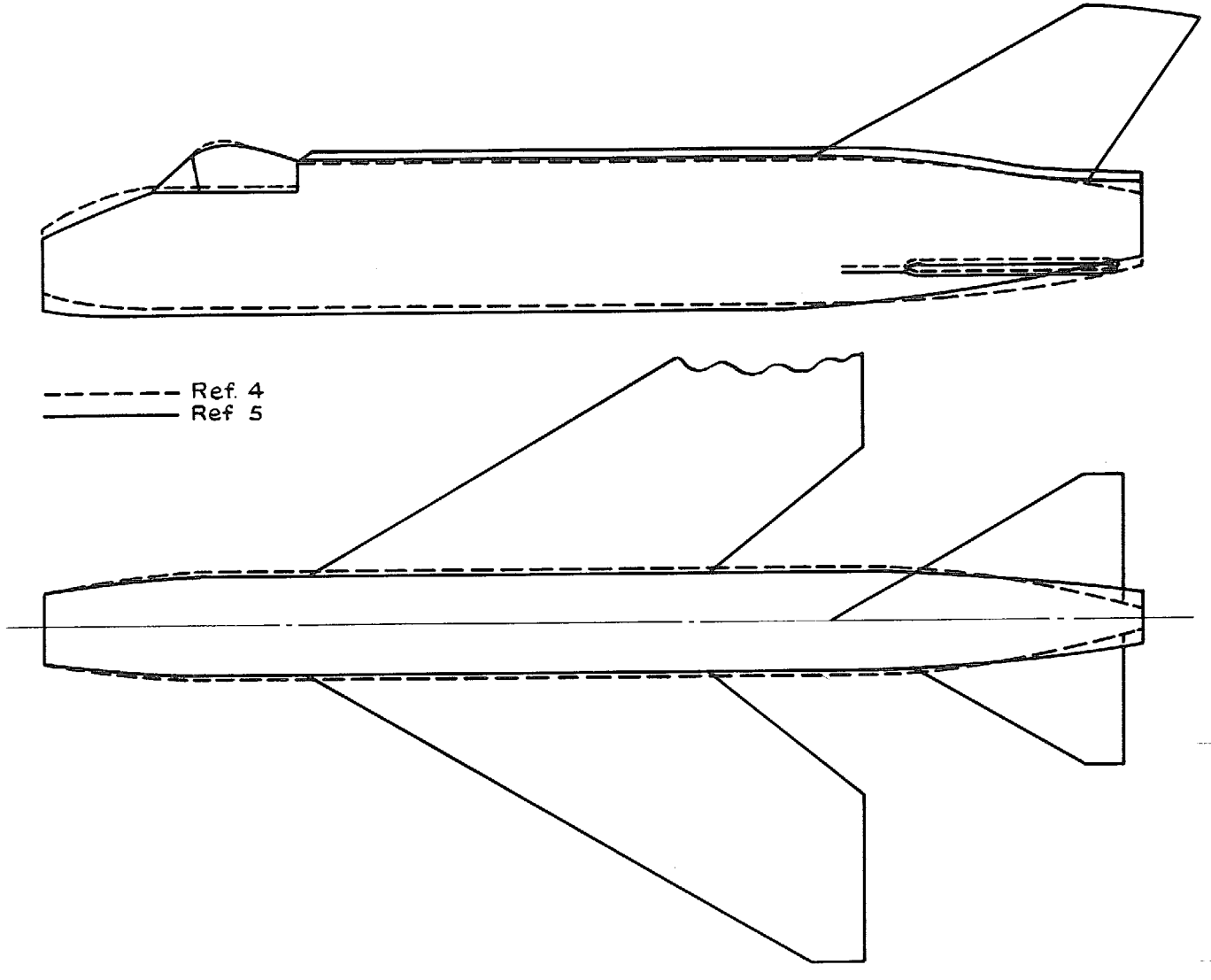

FIG. 11. Comparison of geometry of wind tunnel models of Ref. 4 and 5.

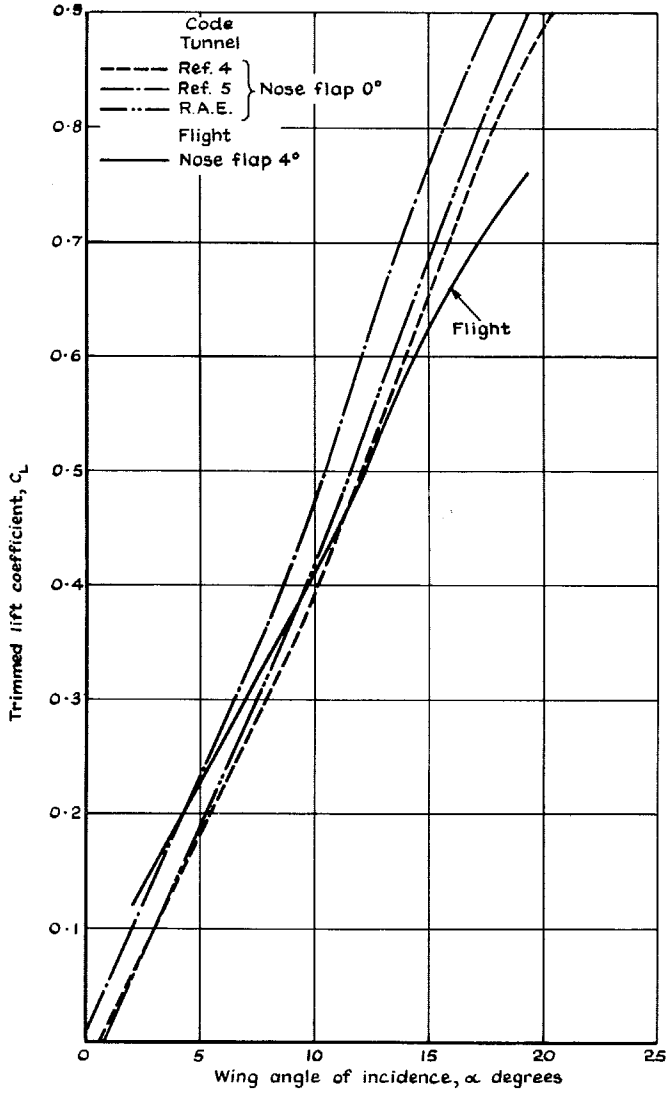

FIG. 12. Comparison of flight and tunnel lift curves for basic configuration, notch sealed.

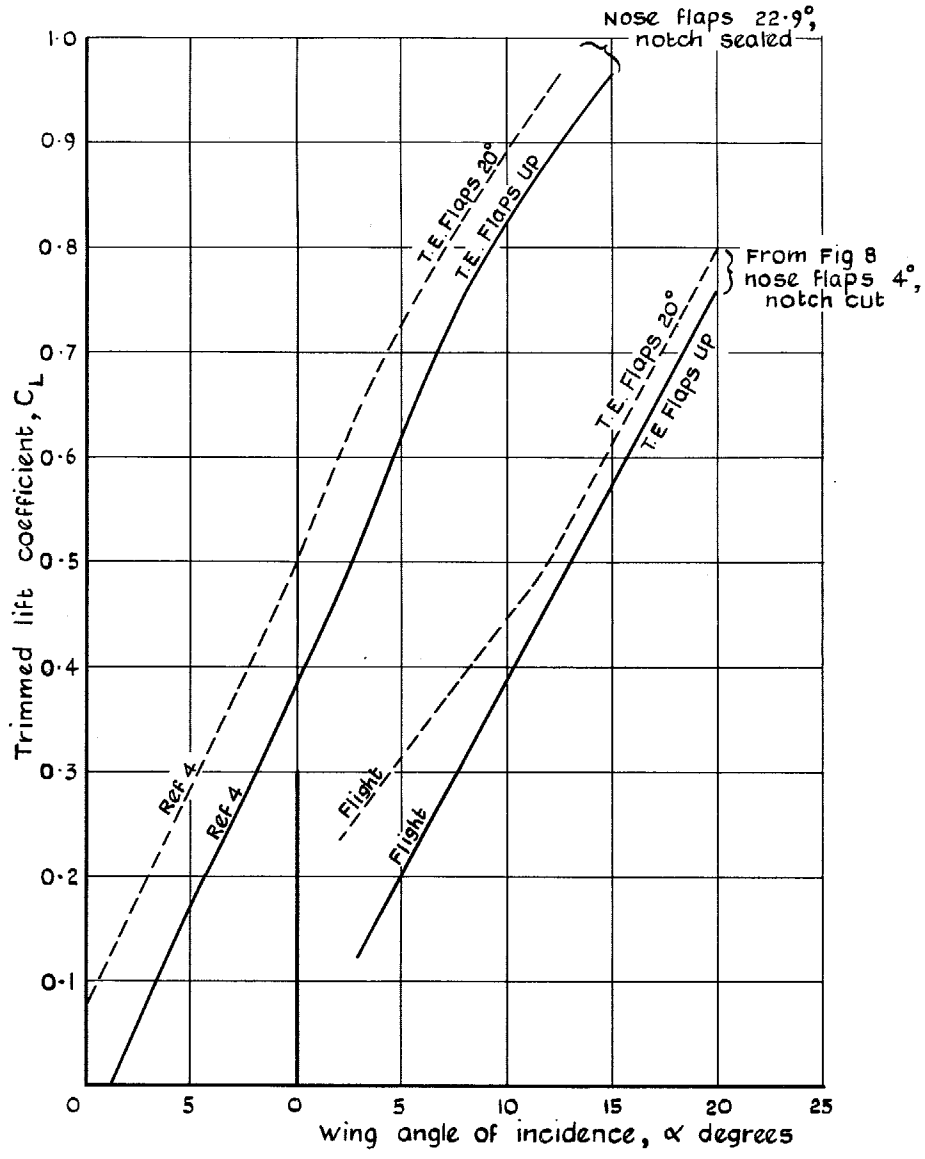

FIG. 13. Effect of trailing edge flap on lift coefficient of basic configuration, flight and tunnel.

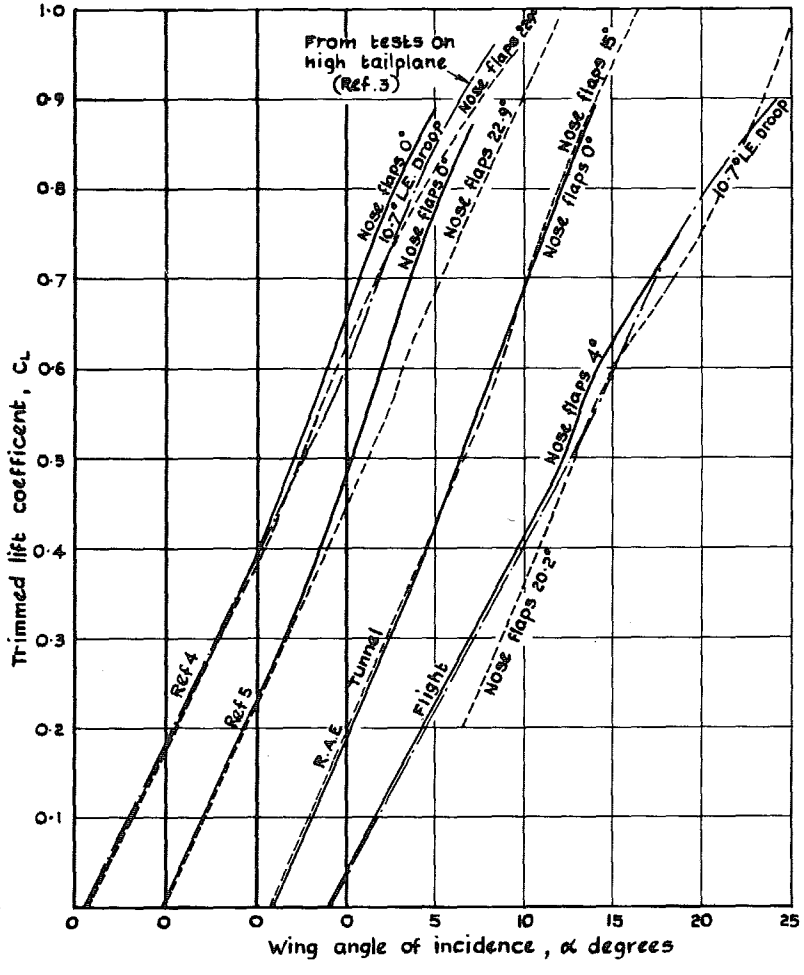

FIG. 14. Effect of nose flap and of leading-edge droop, flight and tunnel, notch sealed.

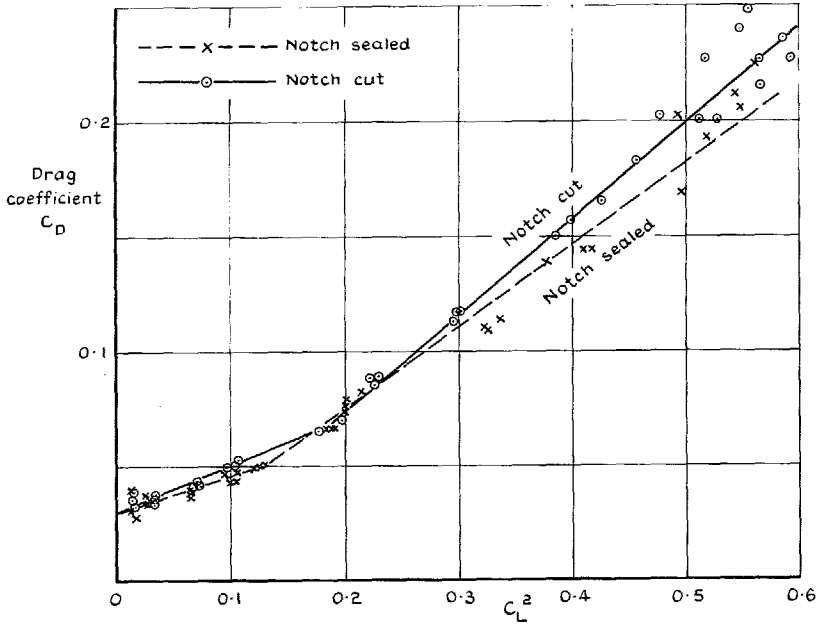

FIG. 15. Effect of leading edge notch on drag of basic configuration (nose flap 4°, T.E. flaps up, power off).

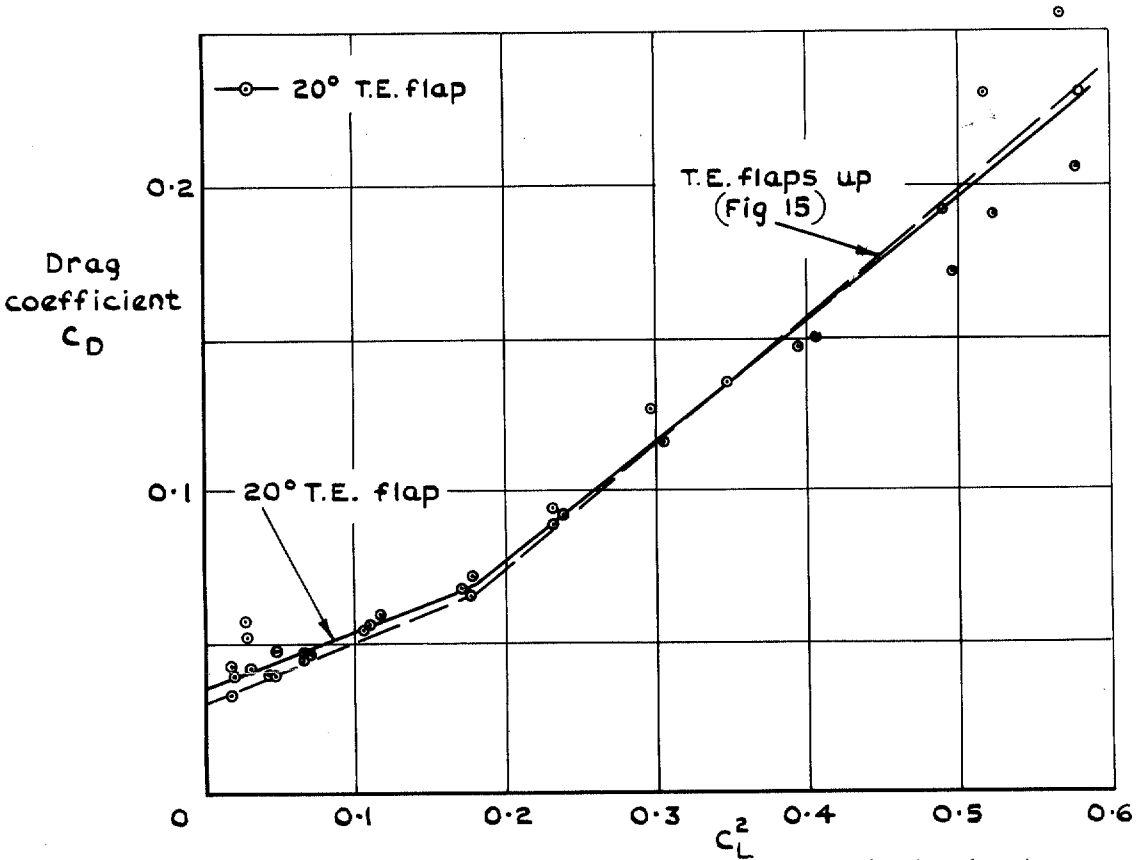

FIG. 16. Effect of trailing edge flap on drag of basic configuration (notch cut), power off.

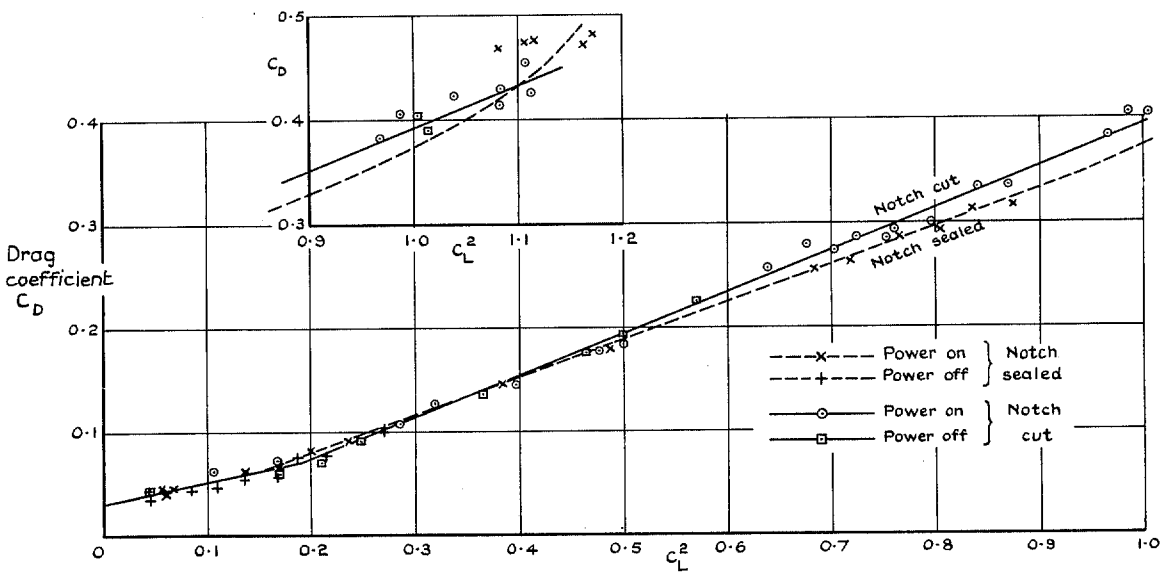

FIG. 17. Effect of leading-edge notch on drag, nose flap 20·2°, trailing edge flap up.

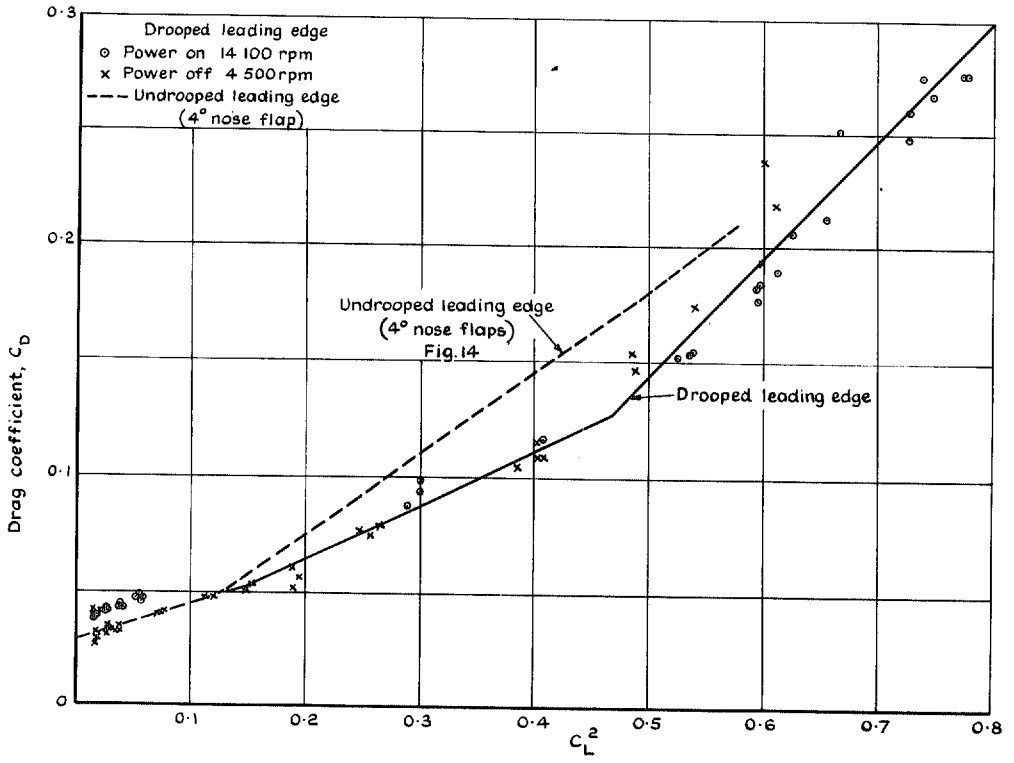

FIG. 18. Effect of 10·7 degrees full-span leading-edge droop on basic configuration, notch sealed, trailing-edge flaps up.

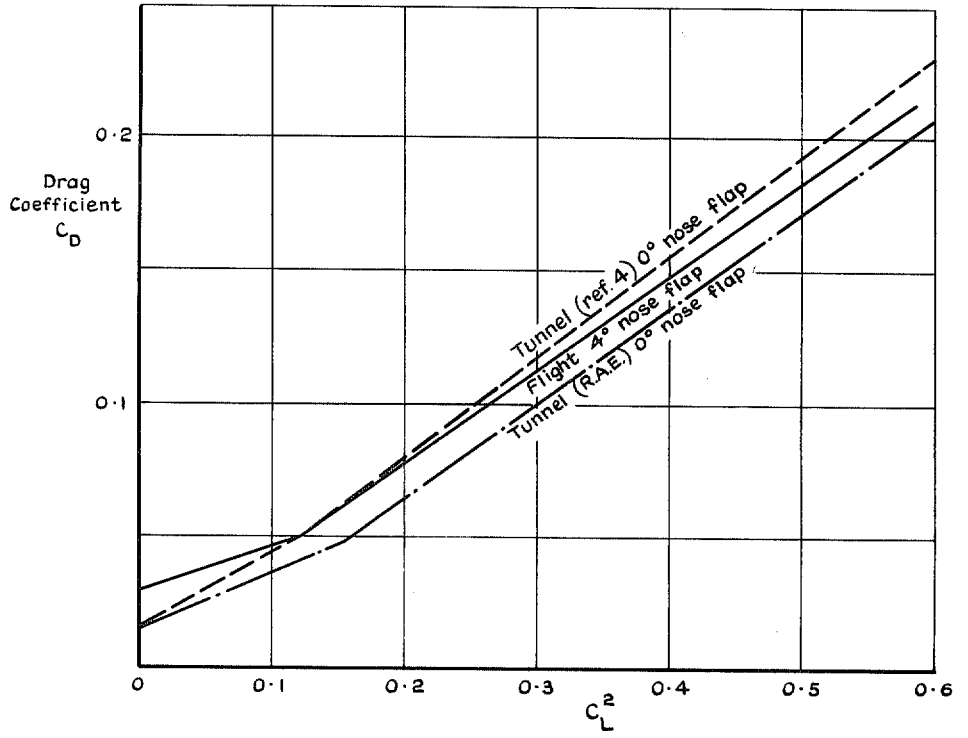

FIG. 19. Comparison between flight and tunnels of drag for basic configuration (notch sealed).

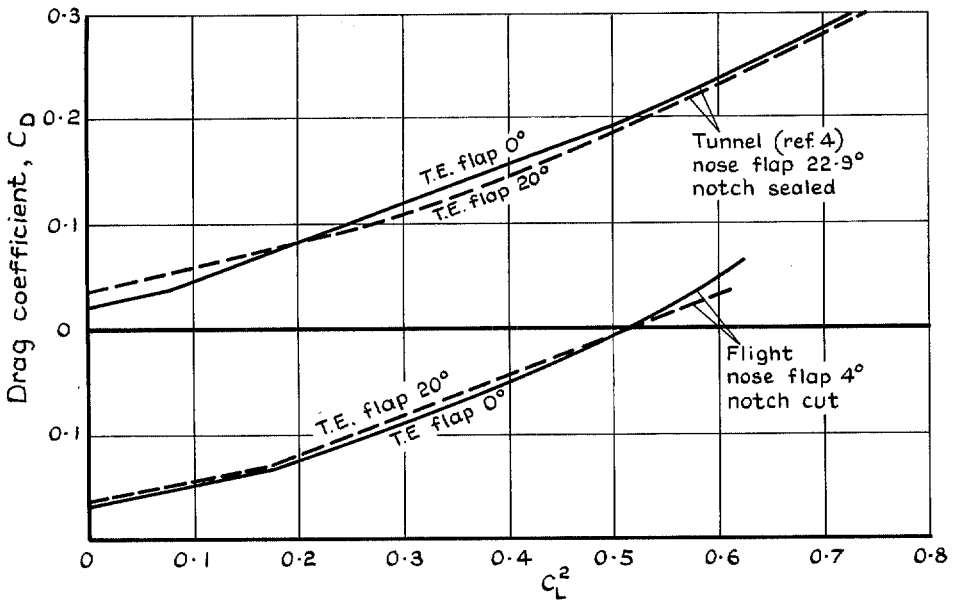

FIG. 20. Comparison between flight and tunnel of effect of trailing edge flap on drag.

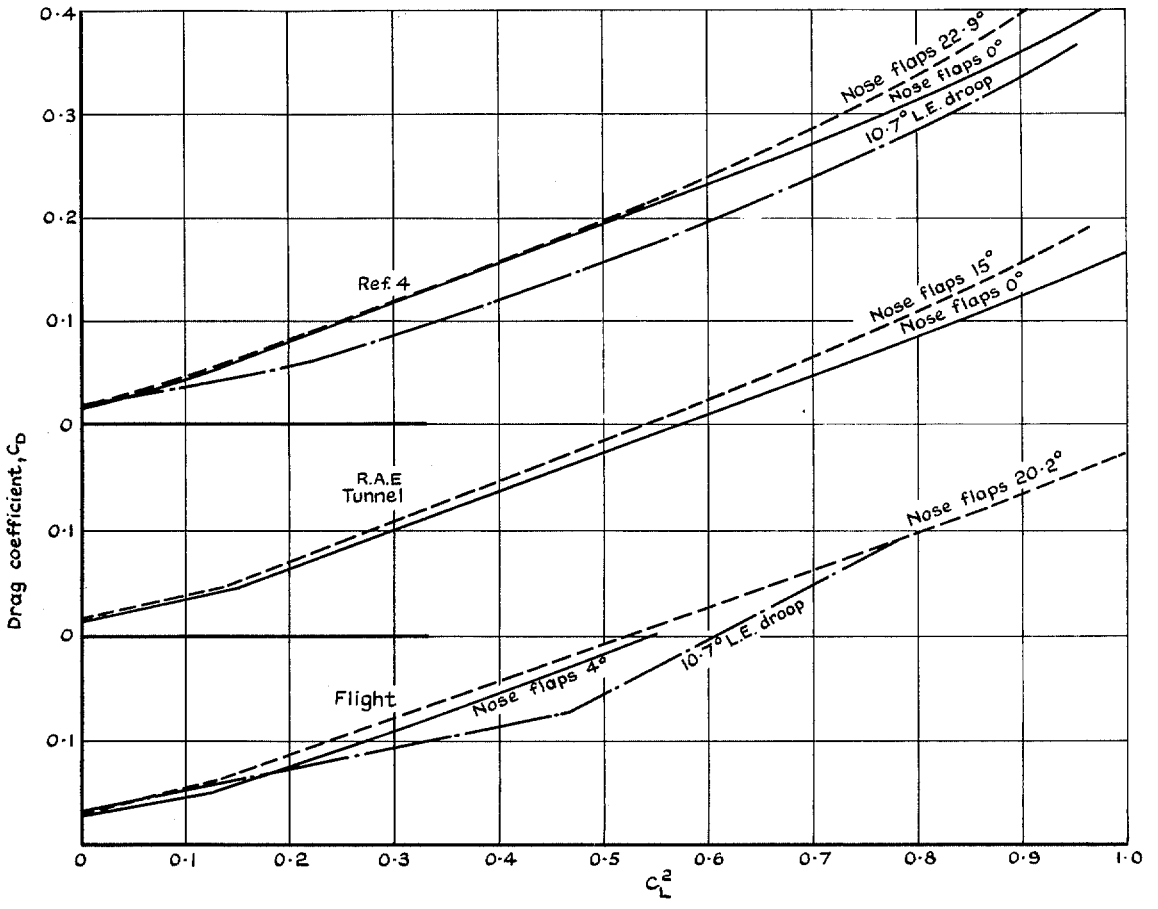

FIG. 21. Effect of nose flap and of leading edge droop, flight and tunnel, notch sealed.

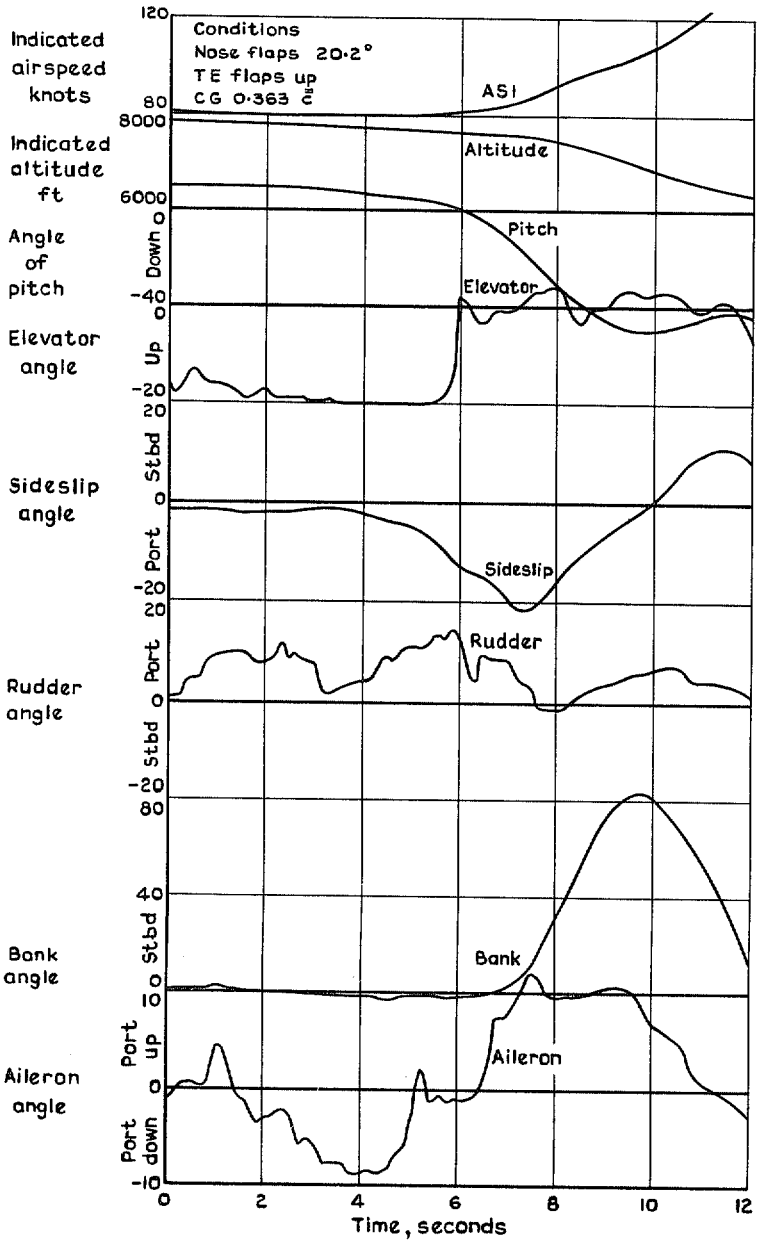

FIG. 22. Slow down to minimum speed, loss of control and recovery nose flaps down.

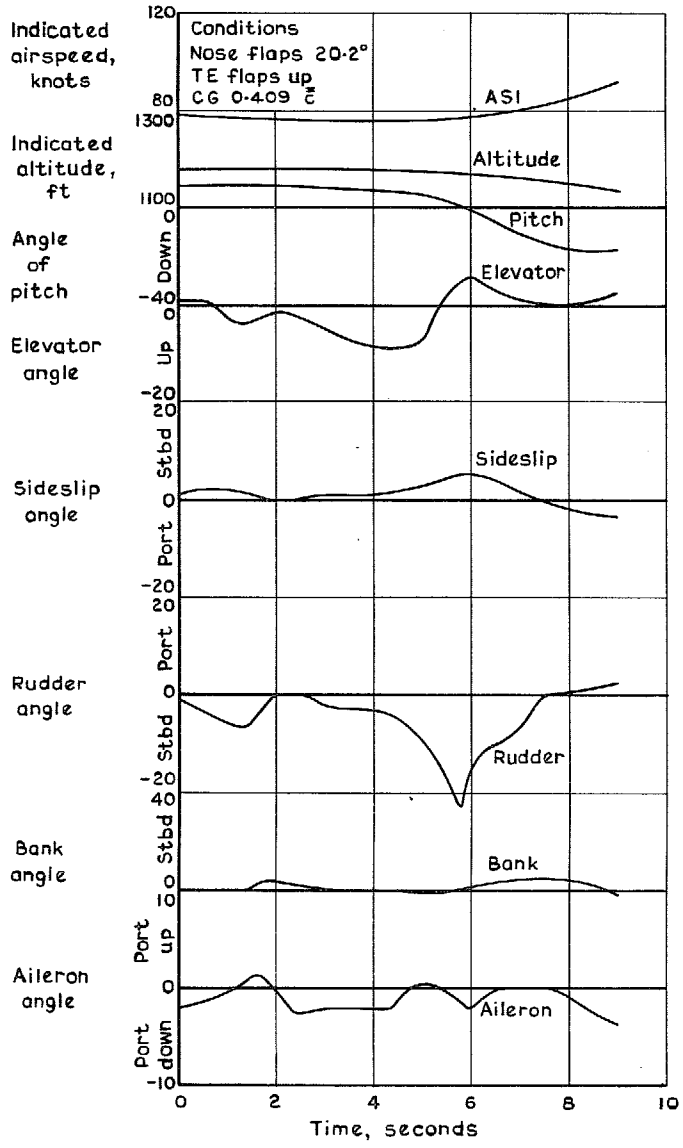

FIG. 23. Slow down to low speed, no loss of control nose flaps down.

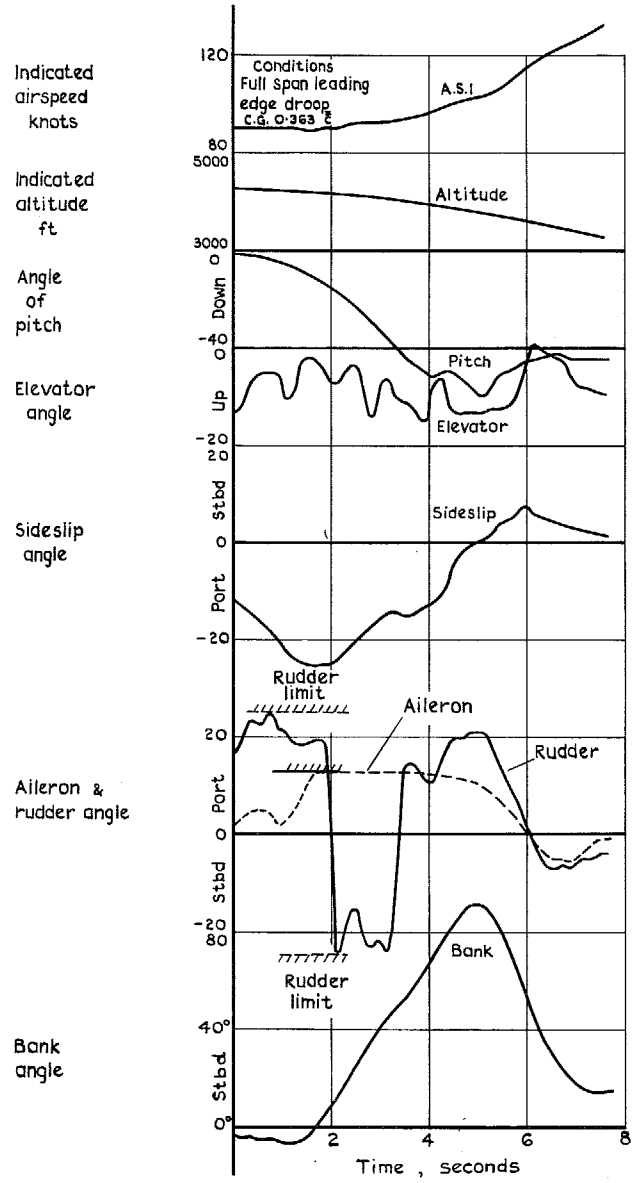

FIG. 24. Loss of control at low speed and recovery leading edge droop.

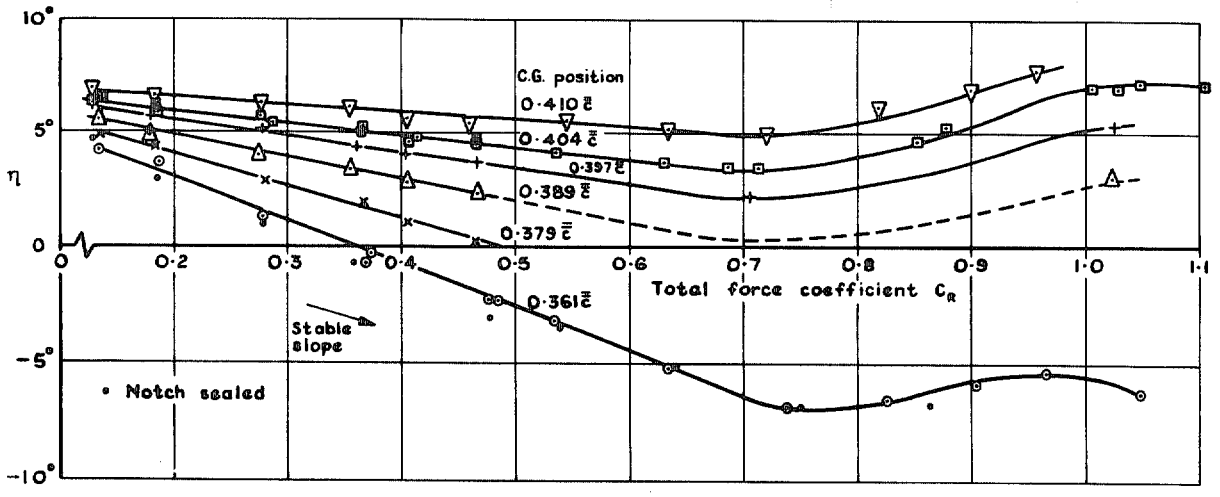

FIG. 25a. Elevator angles to trim, η, at various c.g. positions for basic configuration (nose flaps 4°, T.E. flaps up, notch cut), power on, tail set at −3·6°.

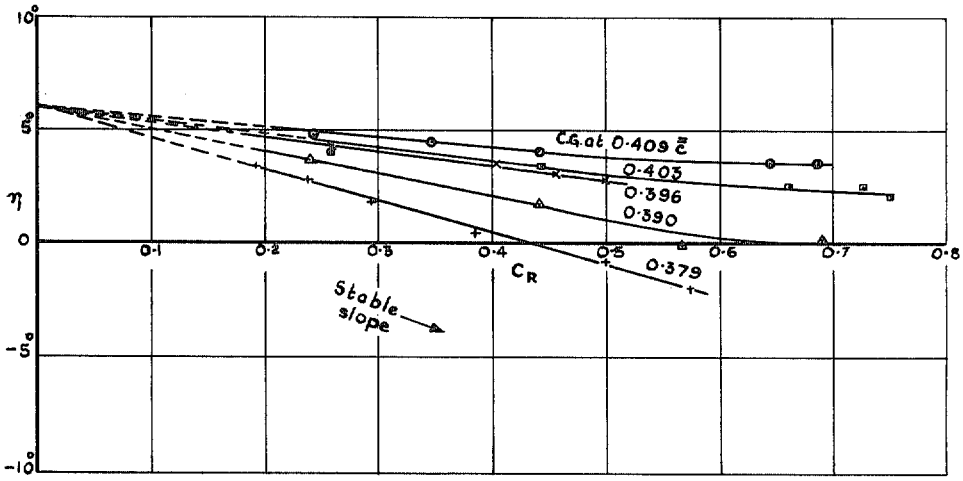

FIG. 25b. Elevator angles to trim, η, at various c.g. positions, nose flaps 20·2°, T.E. flaps up, notch sealed, power on, tail set at −4·8°.

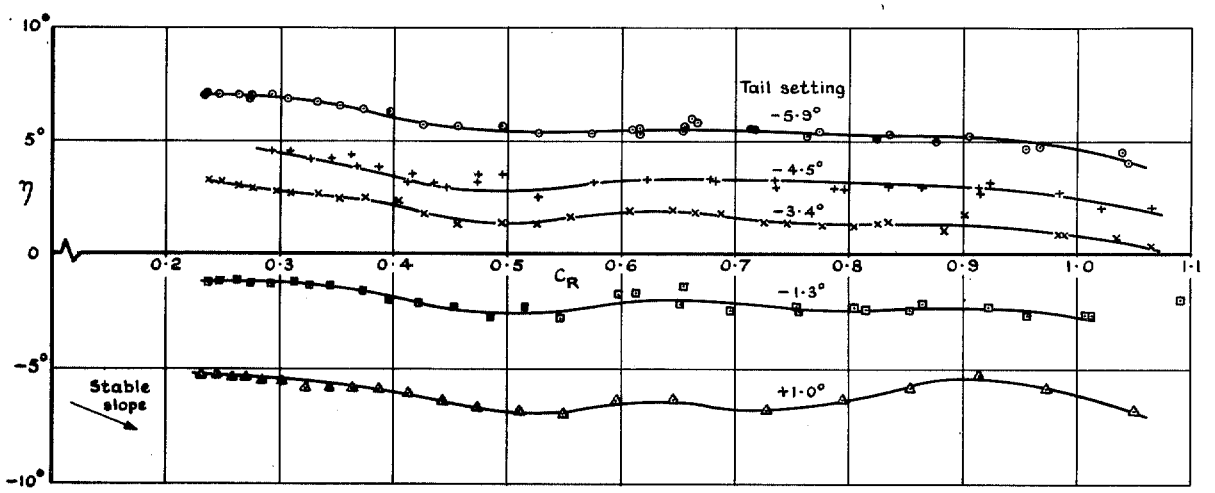

FIG. 26. Elevator angle to trim η at various tail settings, nose flaps 20·2°, notch sealed, 14 100 r.p.m., aft c.g. (0·409 $\bar{c}$).

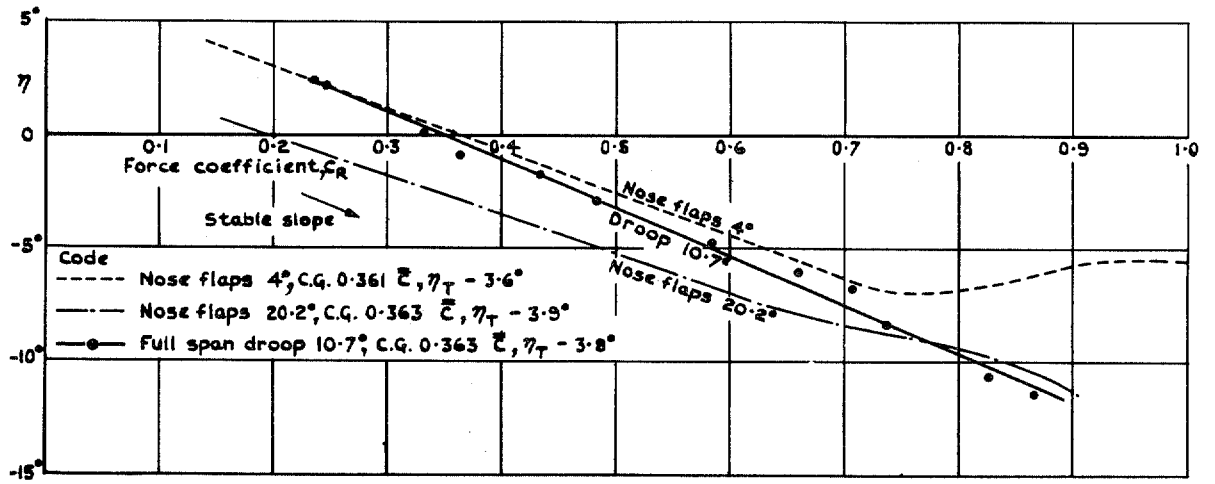

FIG. 27. Elevator angles to trim η; effect of leading-edge devices. T.E. flaps up, 14 100 r.p.m.

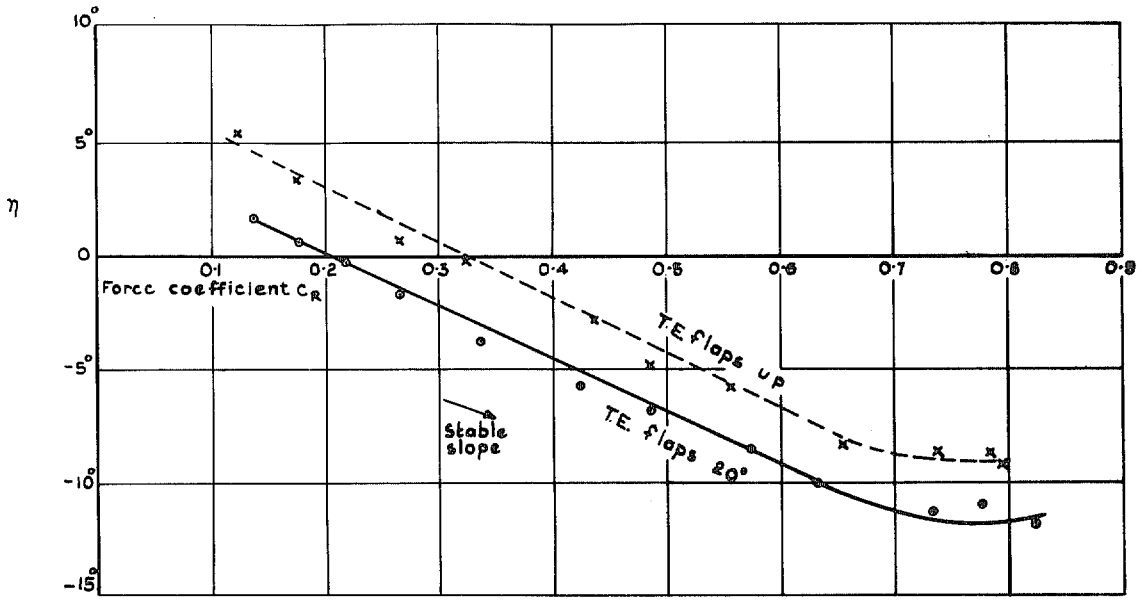

FIG. 28. Elevator angle to trim η; effect of trailing edge flaps. Nose flaps 4°, notch cut, power off c.g. at 0·361 $\bar{c}$, tail setting −3·4°.

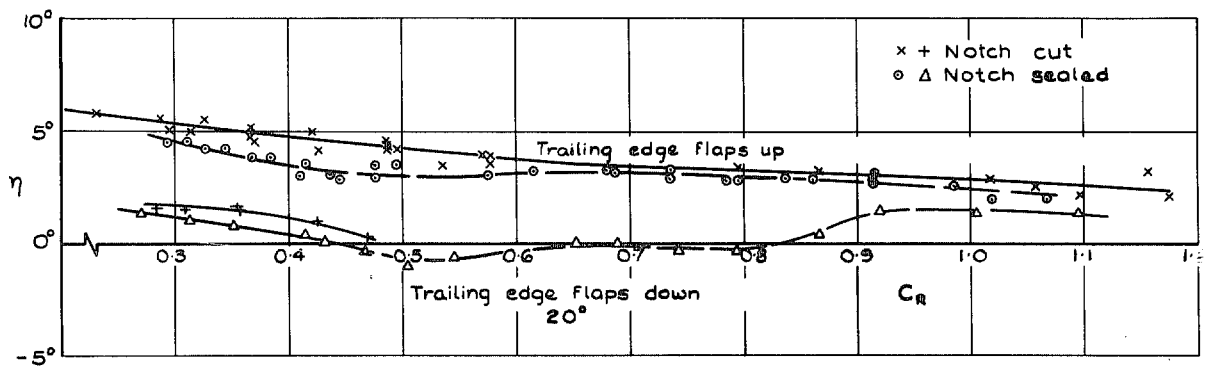

FIG. 29. Effect of trailing edge flaps and leading edge notch on elevator angle to trim, tail setting −4·5°, nose flap 20·2°, c.g. at 0·409 $\bar{c}$, power on.

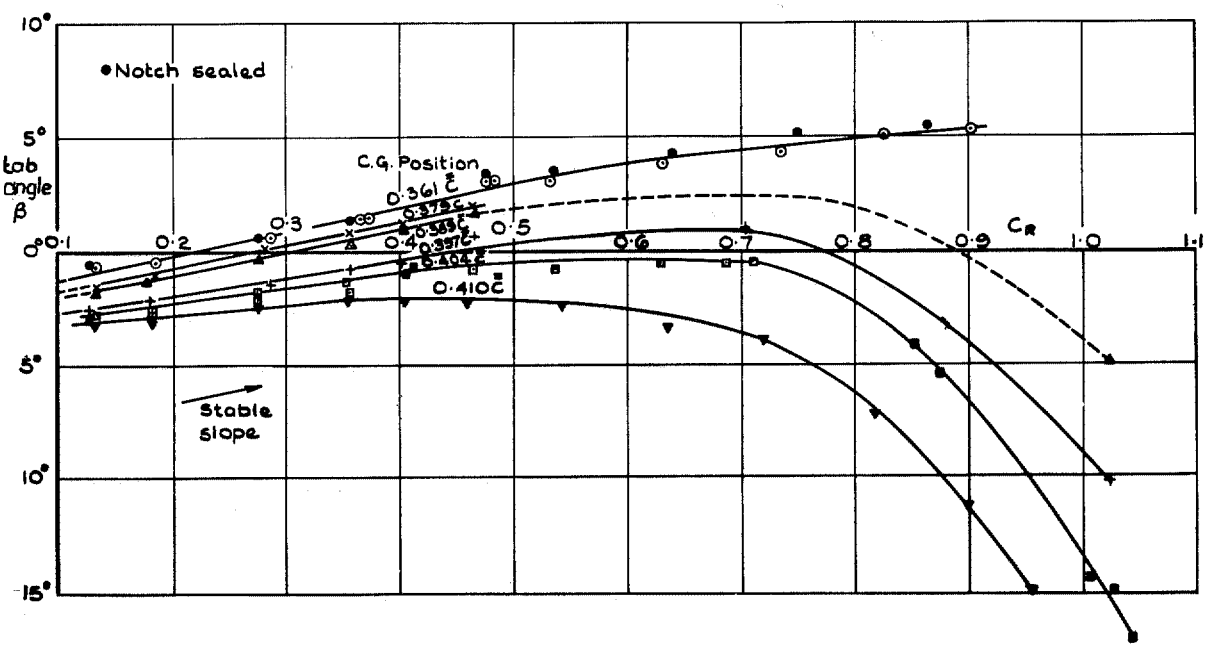

FIG. 30. Elevator tab angles to trim, β stick free, at various c.g. positions in basic configuration. Tail setting $-3{\cdot}6°$, nose flaps 4°, T.E. flaps up, notch cut, 14 100 r.p.m.

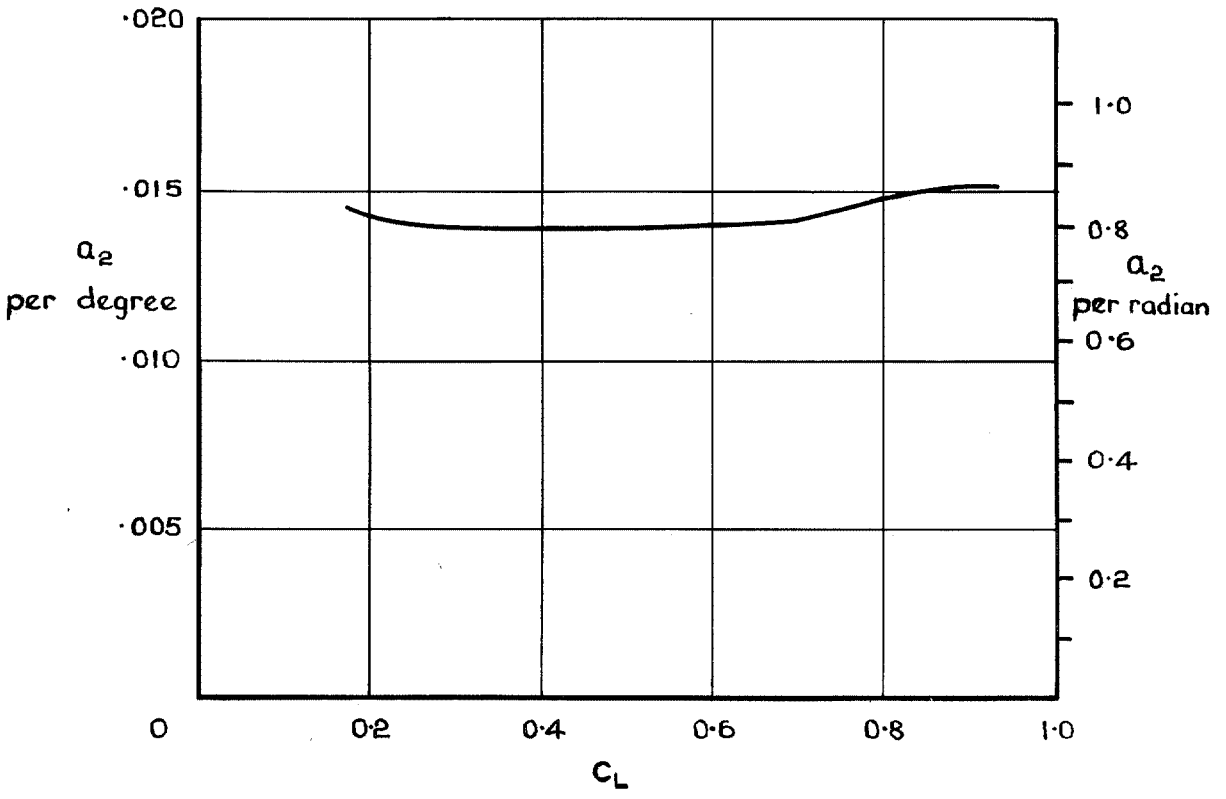

FIG. 31. Elevator lift slope a_2 for basic configuration.

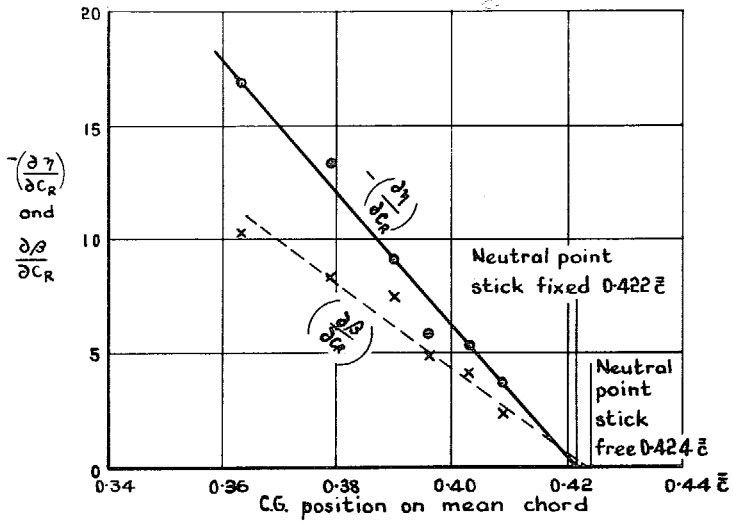

FIG. 32. Example of plot to determine stick fixed and stick free neutral points, nose flaps down.

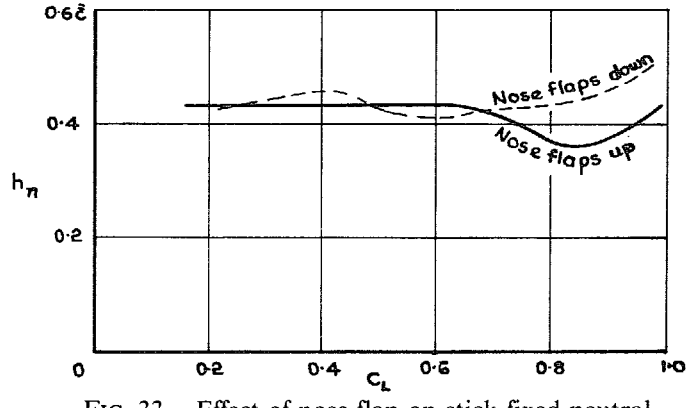

FIG. 33. Effect of nose flap on stick fixed neutral point in flight.

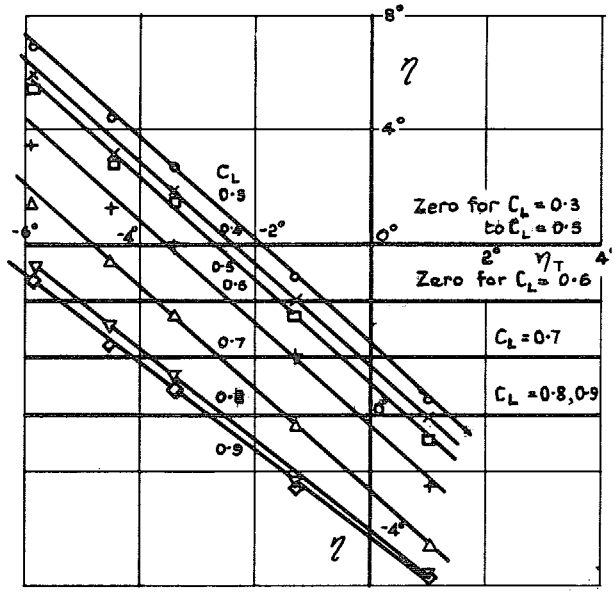

FIG. 34. Elevator angle versus tailplane setting, c.g. at 0·409 $\bar{c}$, nose flaps 20·2°, T.E. flaps up, notch sealed, power on (from Fig. 26).

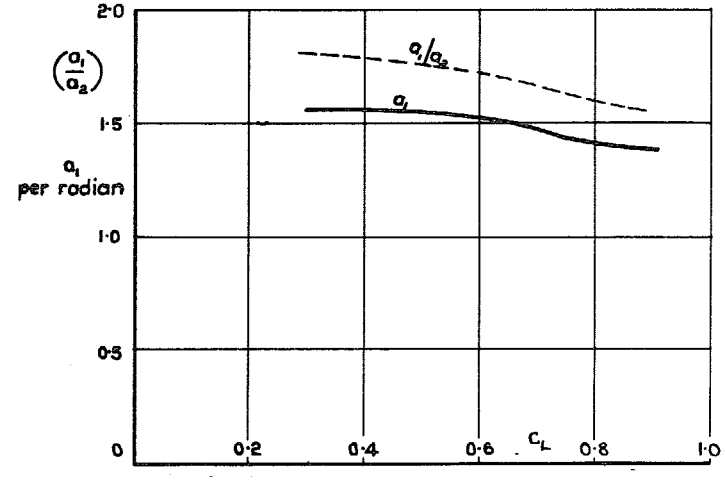

FIG. 35. Tail plane power a_1, nose flaps 20·2° T.E. flaps up, notch sealed.

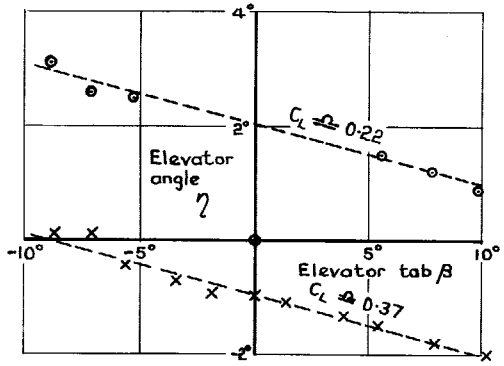

FIG. 36. Plot for the determination of elevator tab lift slope a_3.

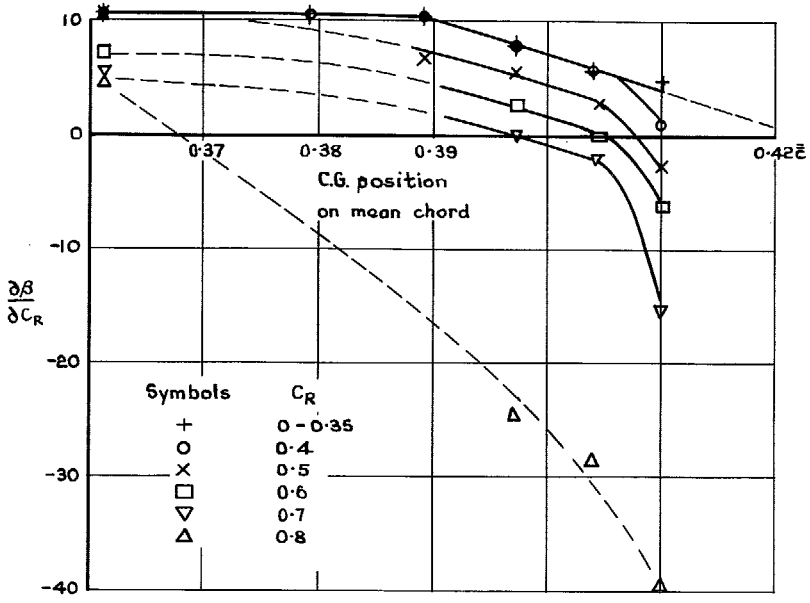

FIG. 37. Determination of stick free neutral points, nose flap 4°, trailing edge flap up, tail setting −3·6°, notch cut, 14 100 r.p.m.

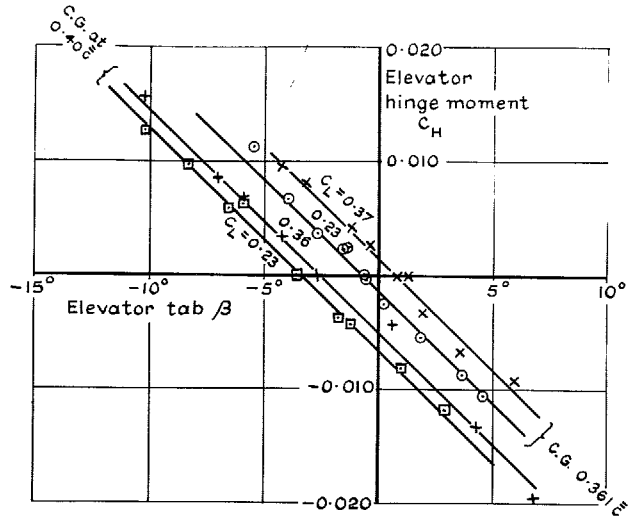

FIG. 38. Determination of elevator hinge moment coefficient b_2 and tab effectiveness b_3. Nose flap up, notch sealed, T.E. flaps up, 14 100 r.p.m.

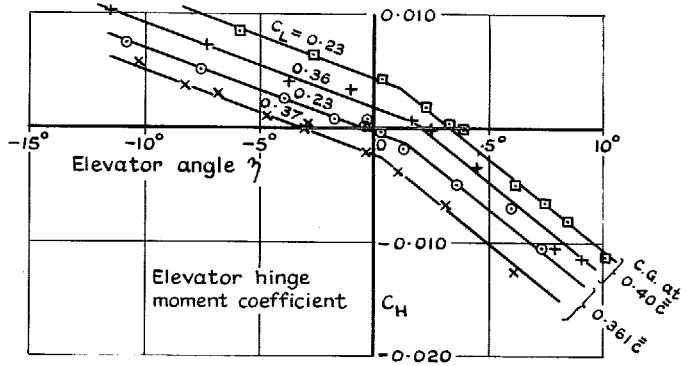

FIG. 39. Determination of tailplane hinge moment derivative b_1, nose flap up, notch sealed, T.E. flaps up, 14 100 r.p.m.

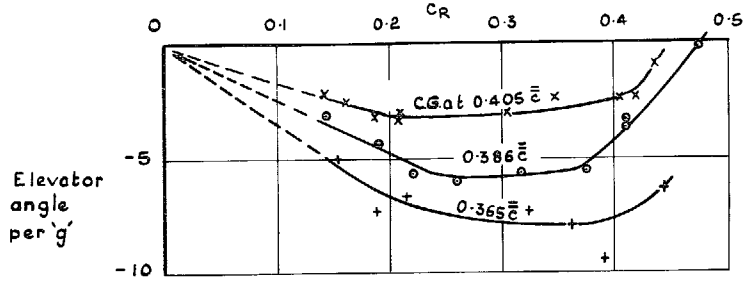

FIG. 40. Elevator angle per 'g' in pull outs, nose flap 0°, T.E. flaps up, notch cut 14 100 r.p.m., tail setting $-3{\cdot}5°$.

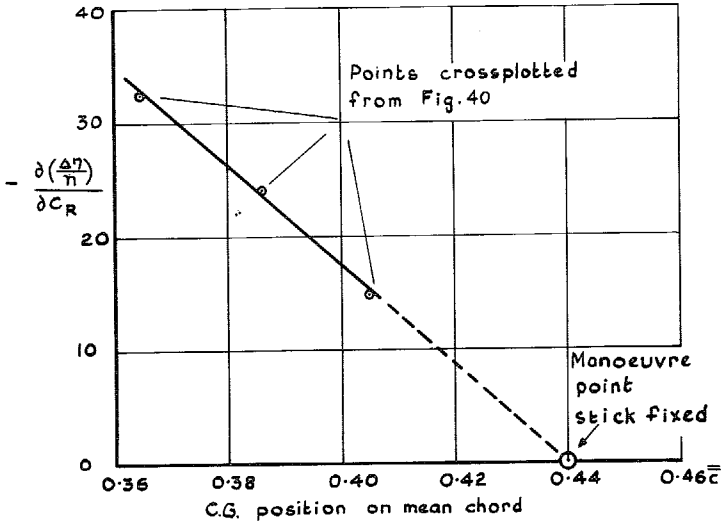

FIG. 41. Determination of stick fixed manoeuvre point, nose flap 0°, T.E. flap up, notch cut, 14 100 r.p.m., $0 < C_T < 0{\cdot}2$.

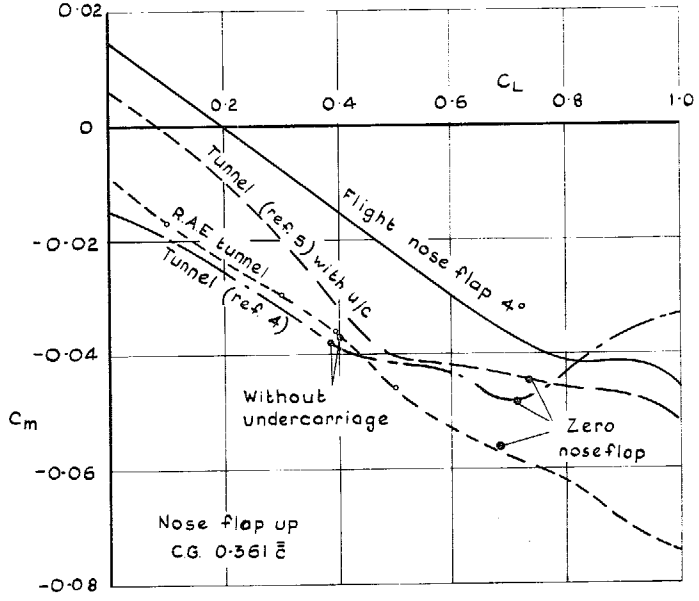

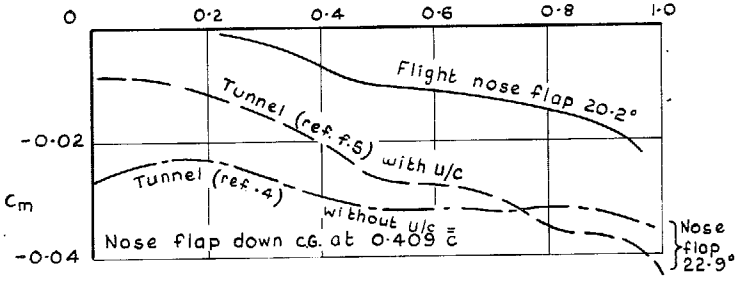

FIG. 42. Comparison between flight and tunnels of pitching moments, nose flap up and down. Trailing edge flap up, $\eta_T = -2°$, $\eta = 0°$.

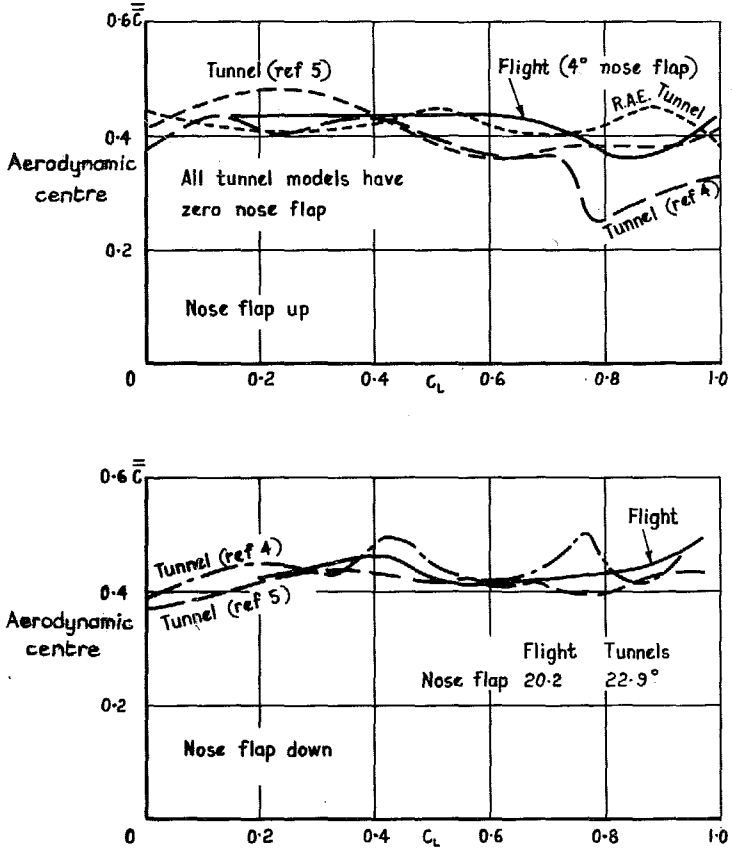

FIG. 43. Comparison between aerodynamic centre determined by tunnel test and corresponding flight-measured stick-fixed neutral point for two nose-flap configurations corresponding to Fig. 42.

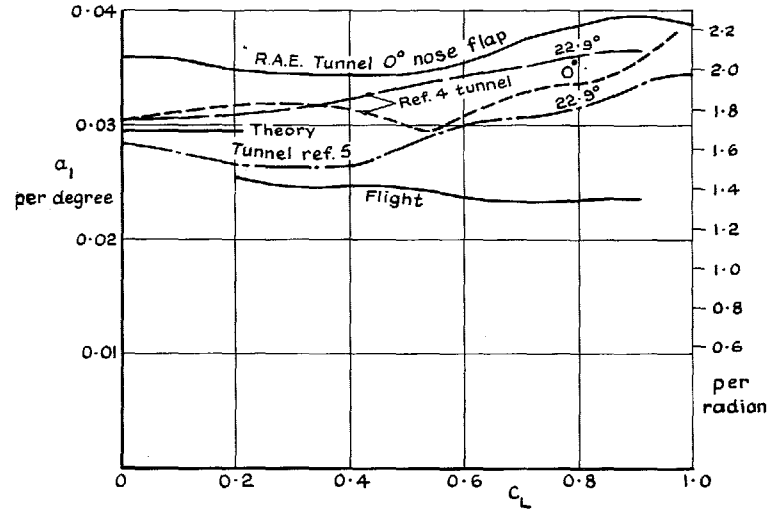

FIG. 44. Comparison between flight and tunnels of tailplane lift slope a_1.

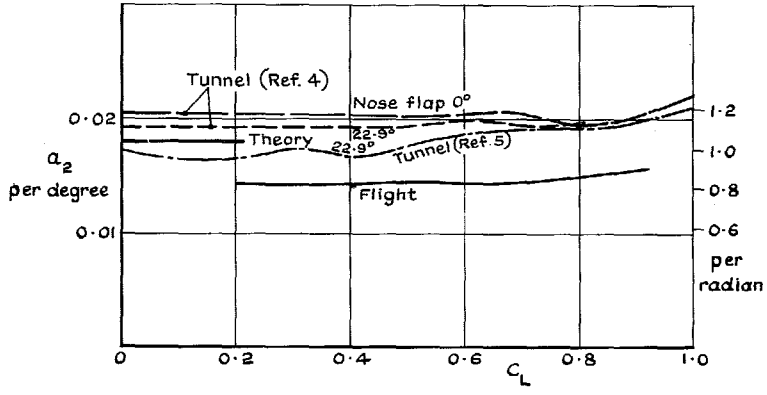

FIG. 45. Comparison between flight and tunnels of elevator lift slope a_2.

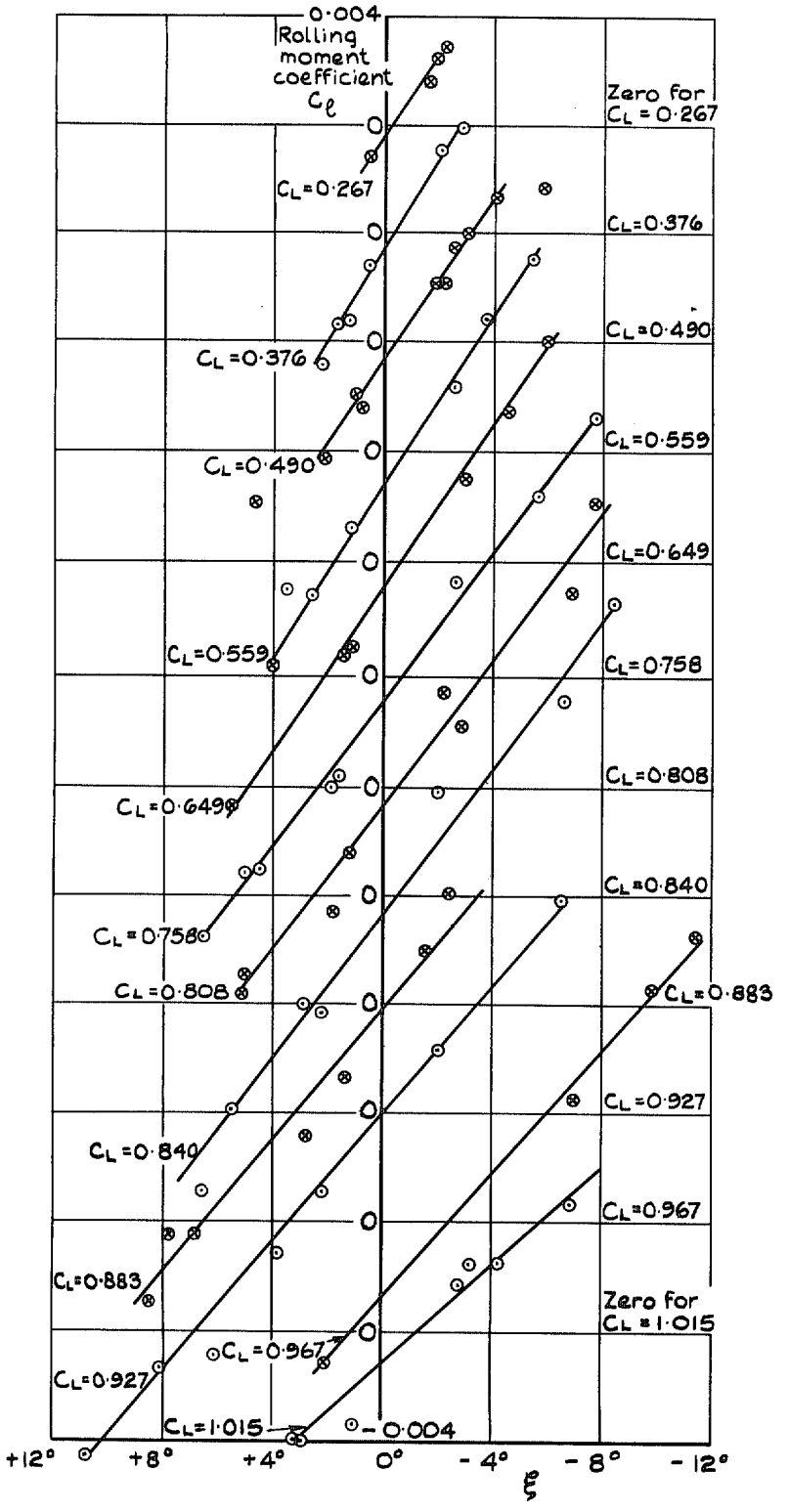

FIG. 46. Aileron angles to trim asymmetric wing weights, nose flaps 20·2°.

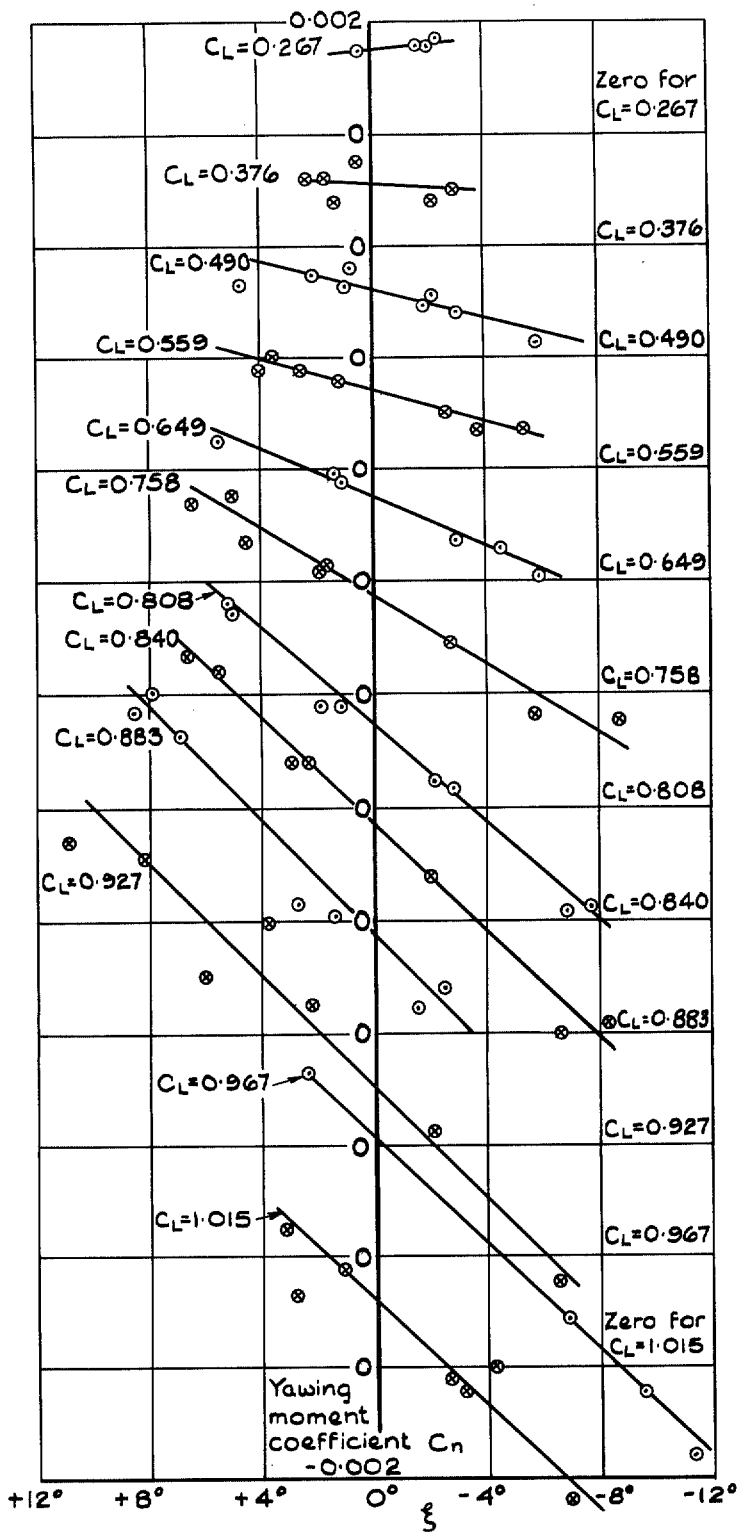

FIG. 47. Aileron yawing-moment coefficient in trimming asymmetric wing weights, nose flaps 20·2°.

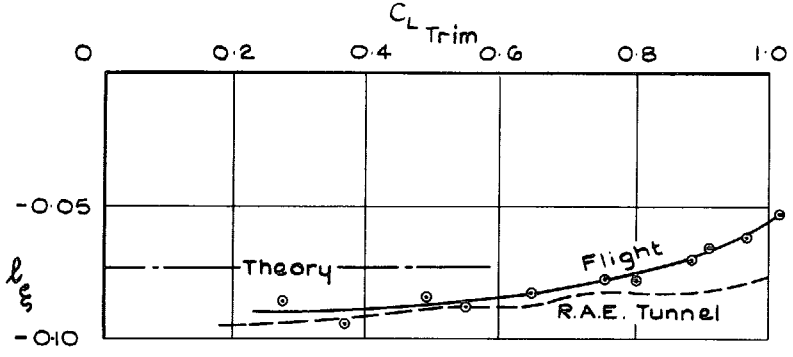

FIG. 48. Aileron rolling moment l_ξ from steady flight tests with asymmetric wing weights; comparison with tunnel results and theory.

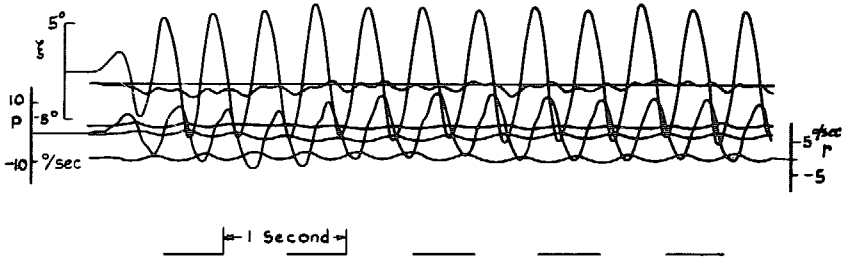

FIG. 50. Flight record of oscillatory aileron application.

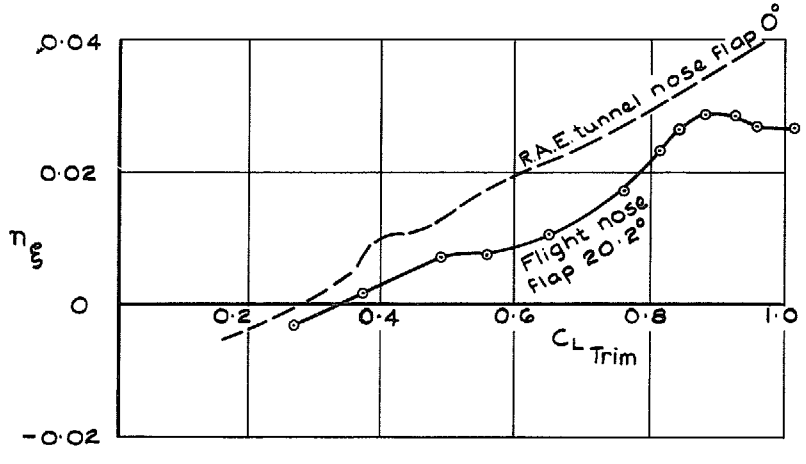

FIG. 49. Aileron yawing moment η_ξ from steady flight tests; comparison with tunnel.

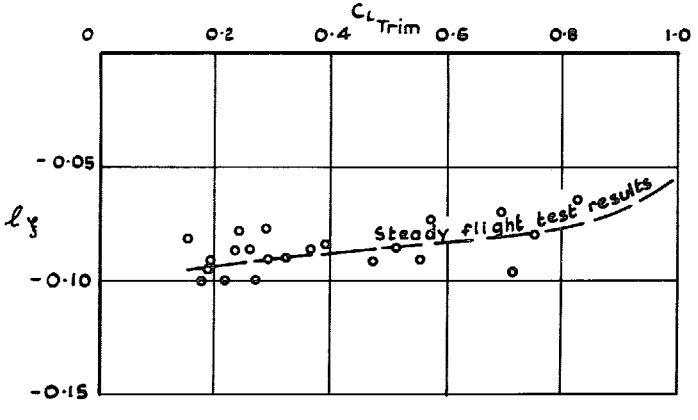

FIG. 51. Aileron rolling power l_ξ from oscillatory aileron tests.

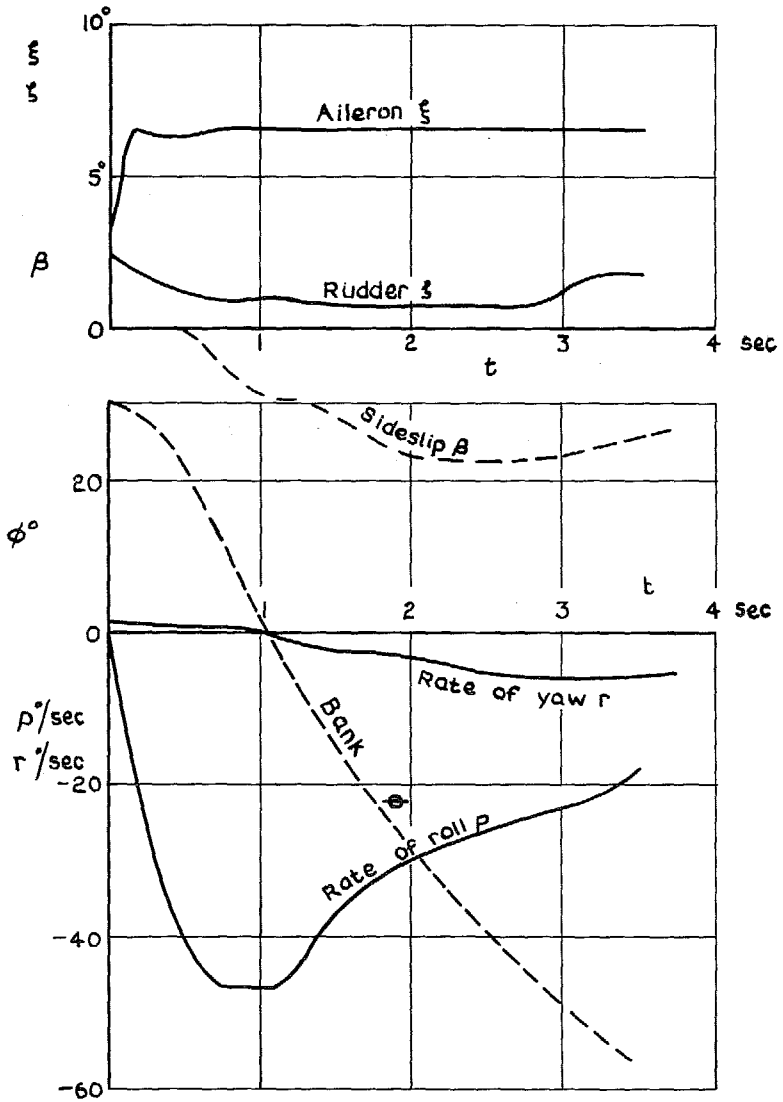

FIG. 52. Time history of an aileron step response at 190 knots.

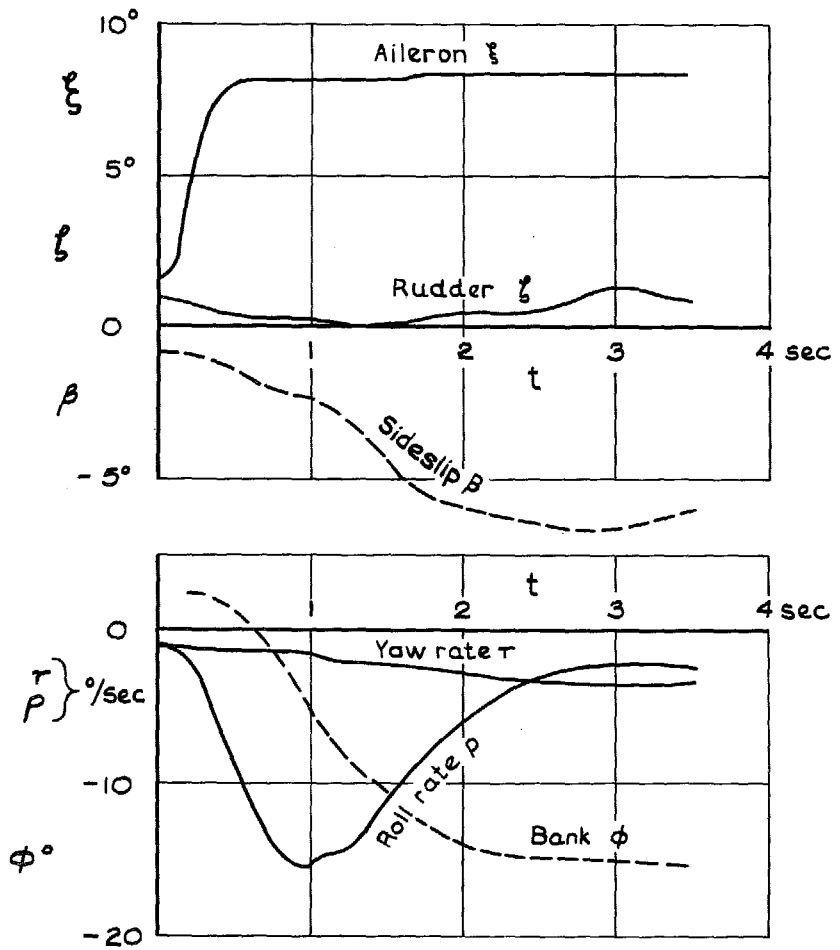

FIG. 53. Time history of an aileron step response at 110 Snots.

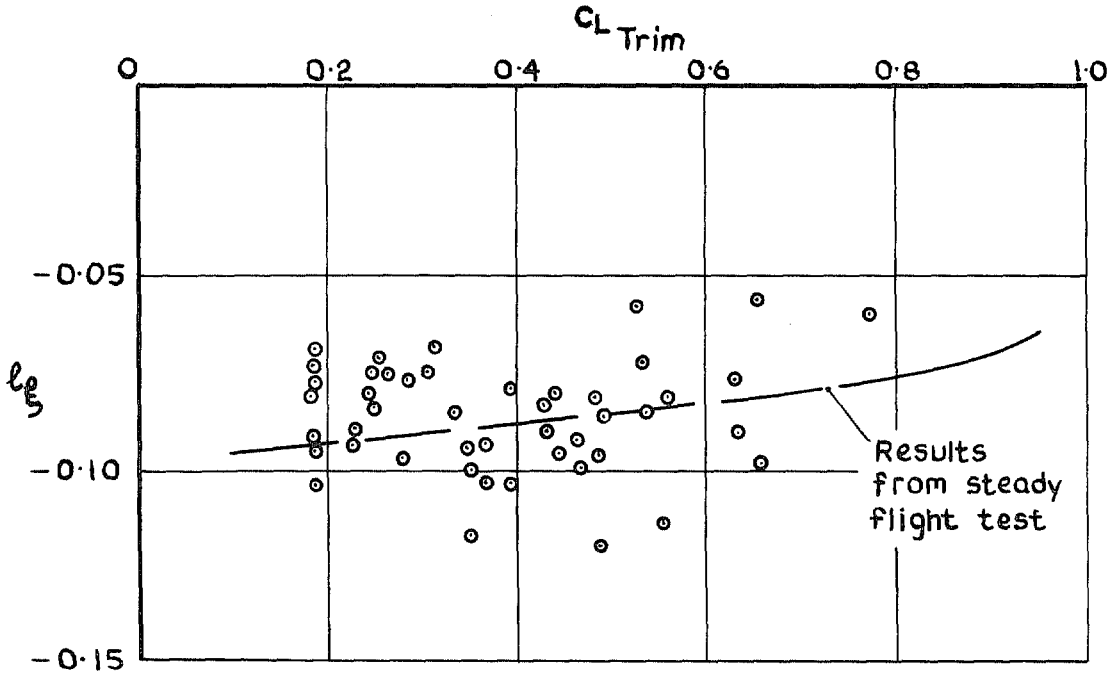

FIG. 54. Aileron power l_ξ from initial roll acceleration in aileron step responses.

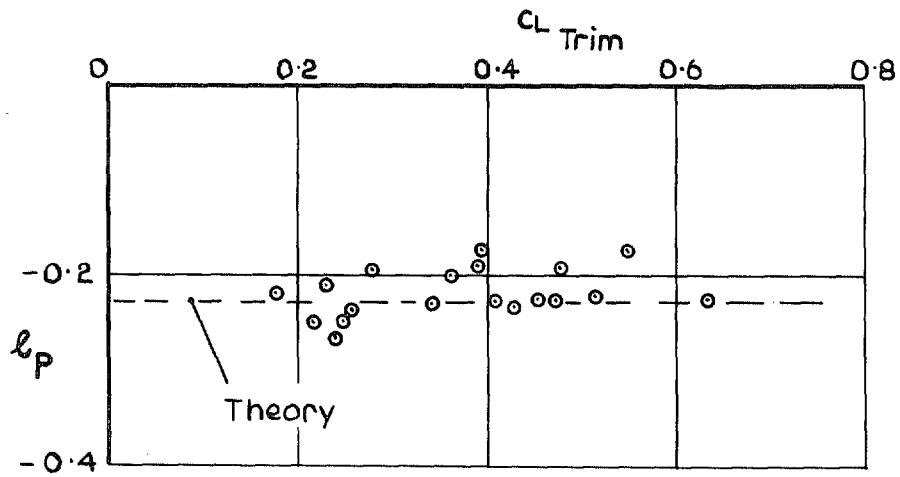

FIG. 55. Damping in roll derivative l_p from steady aileron rolls, nose flap 20·2°.

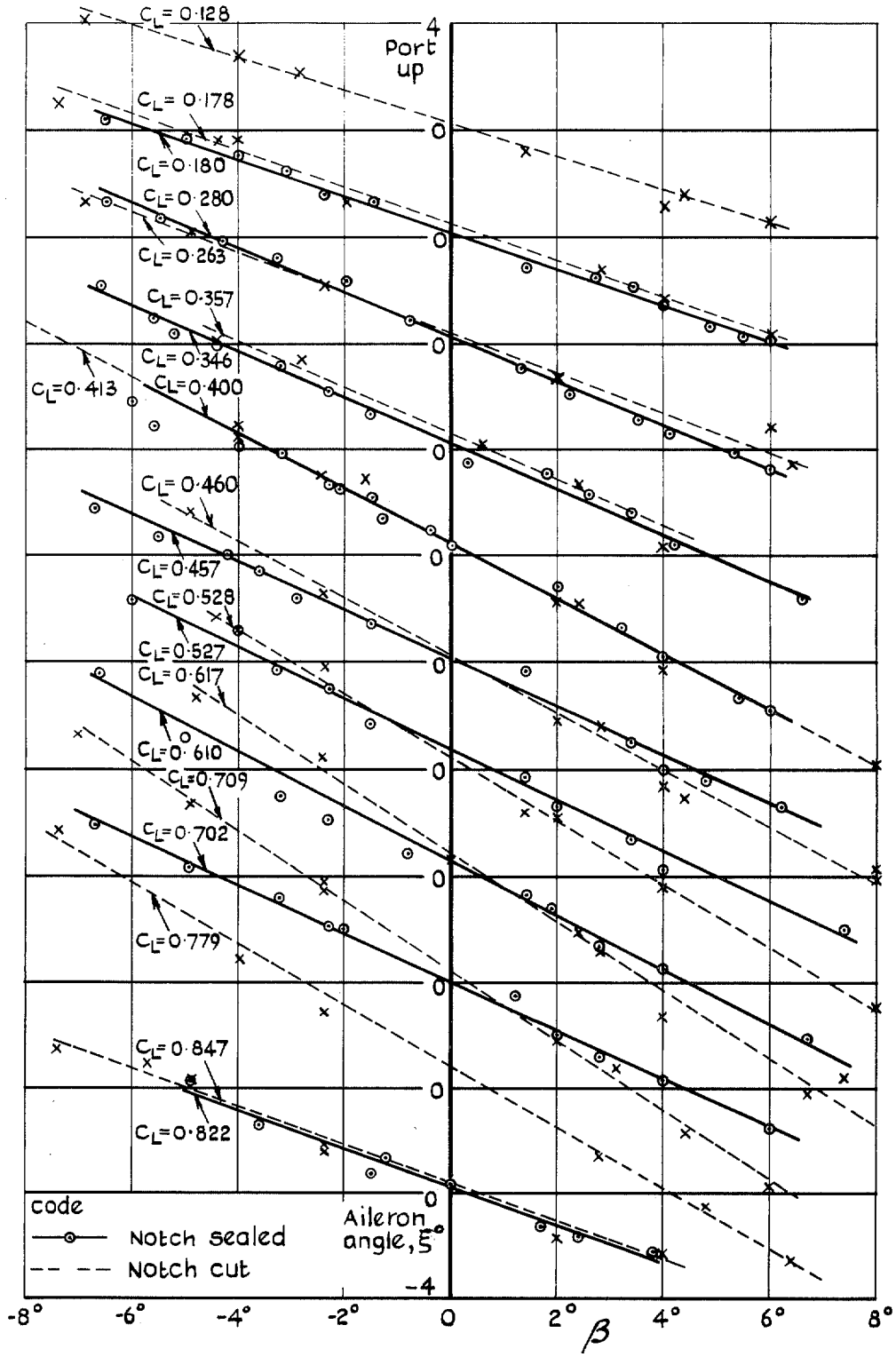

FIG. 56. Aileron angles to trim straight sideslips, nose flaps 4°, T.E. flaps up.

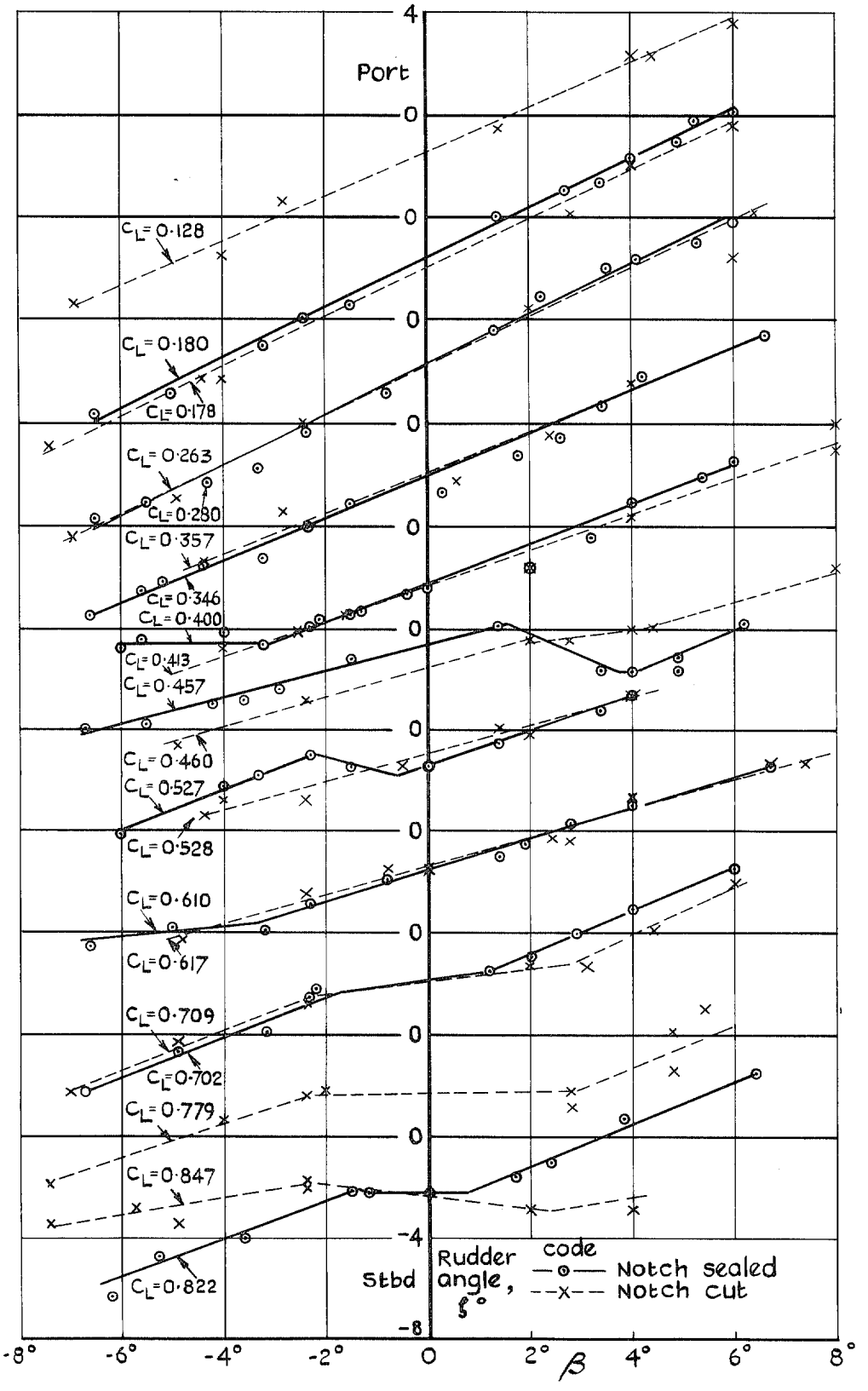

FIG. 57. Rudder angles to trim straight sideslips, nose flaps 4°, T.E. flaps up.

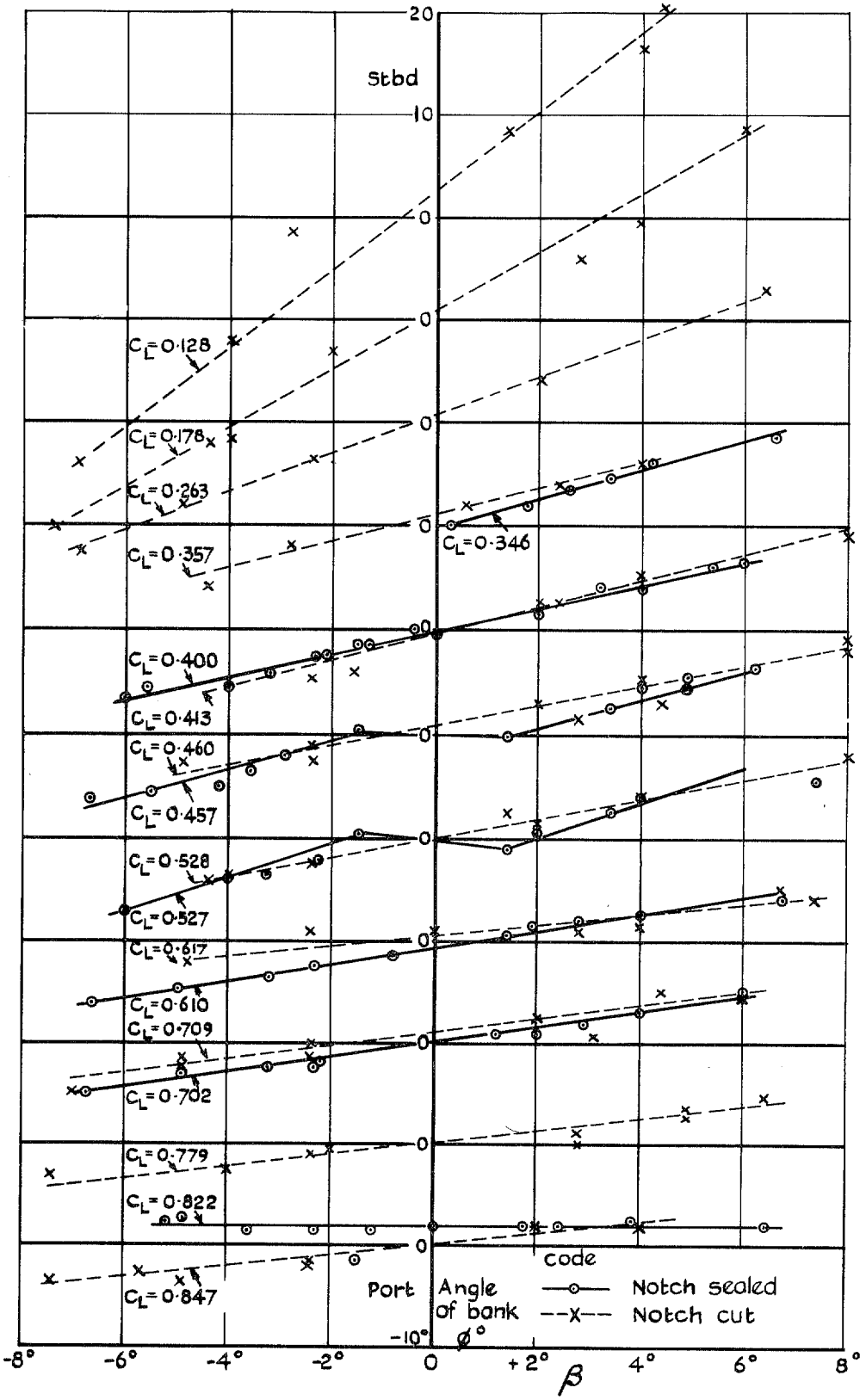

FIG. 58. Angles of bank in straight sideslips, nose flaps 4°.

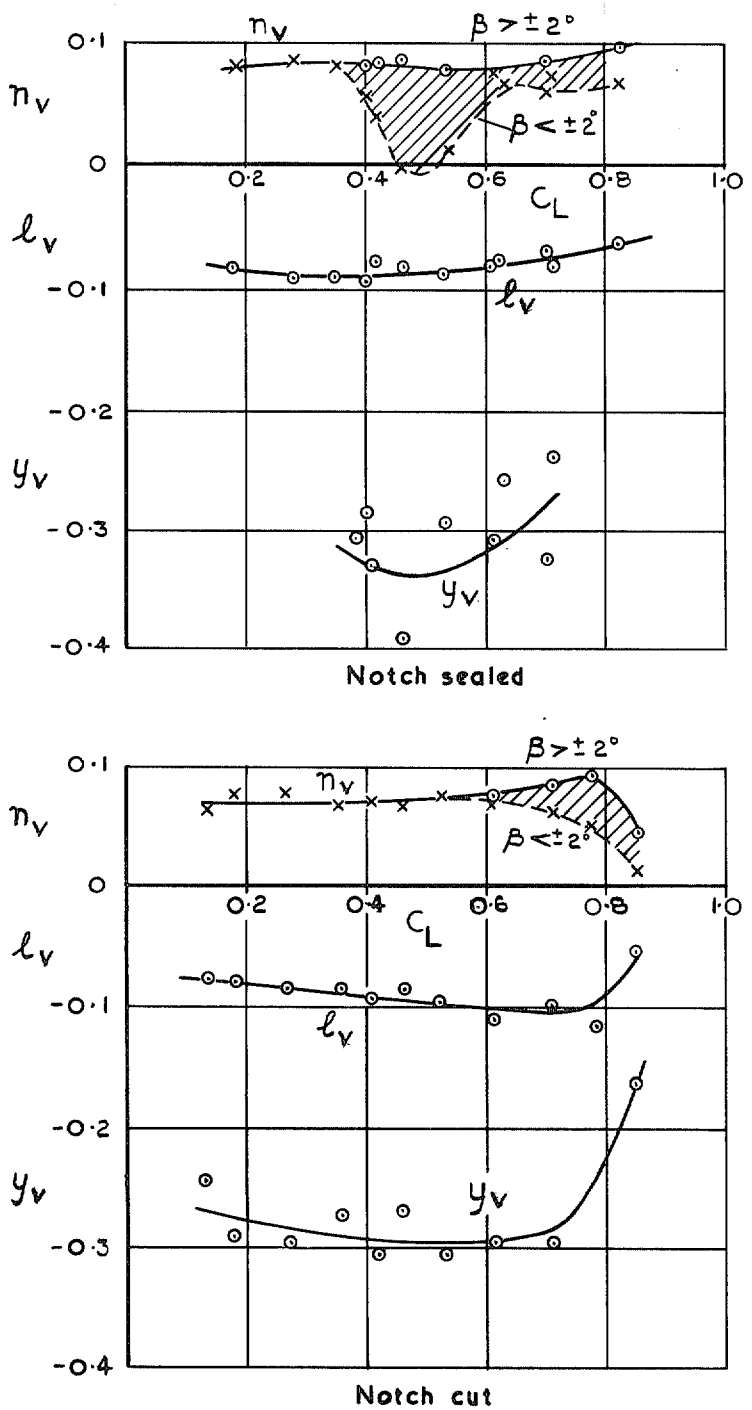

FIG. 59. Sideslip derivatives from steady flight tests (4° nose flap), moments corrected to 0·25 $\bar{c}$.

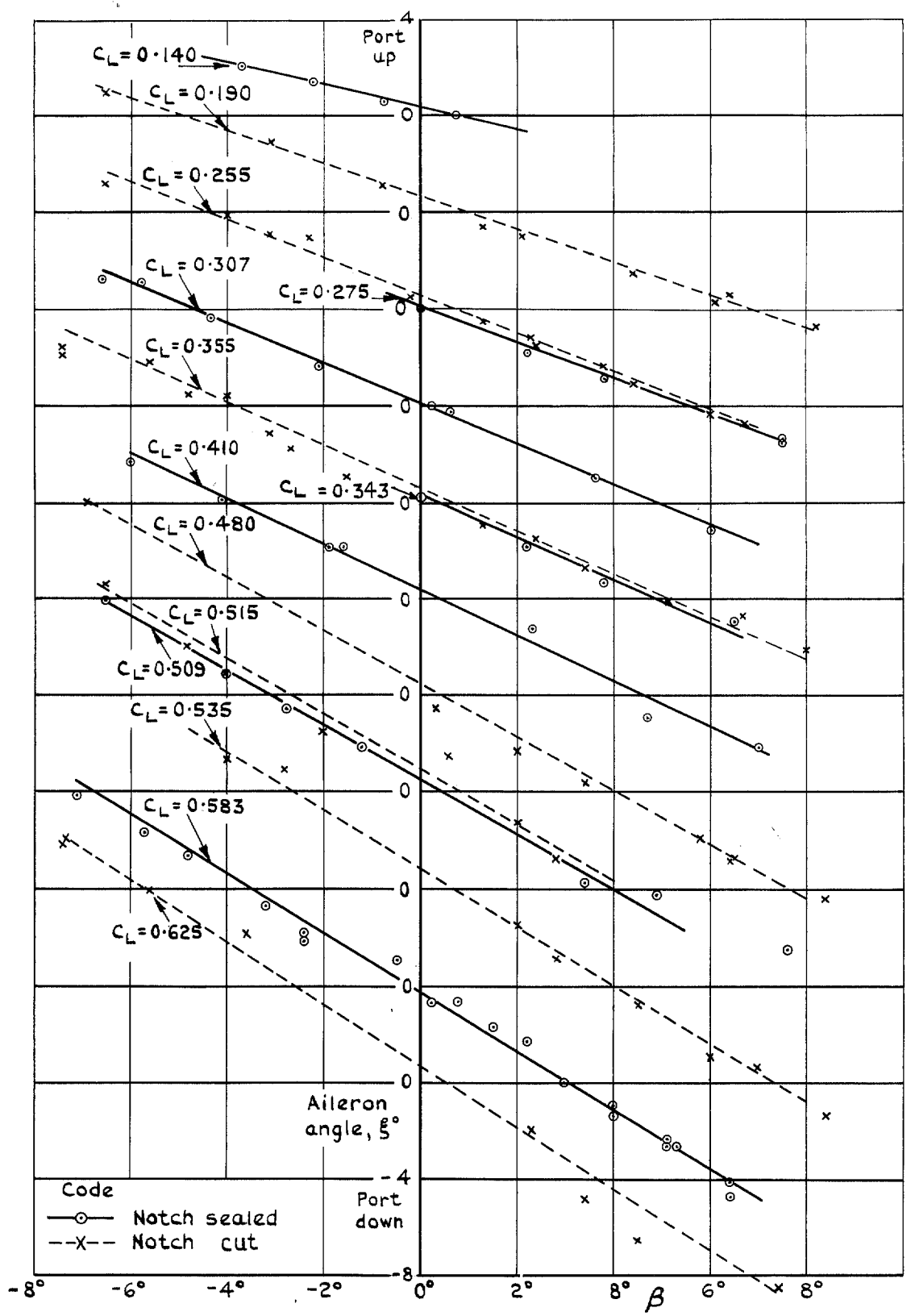

FIG. 60. Aileron angles to trim straight sideslips, nose flaps 20·2°.

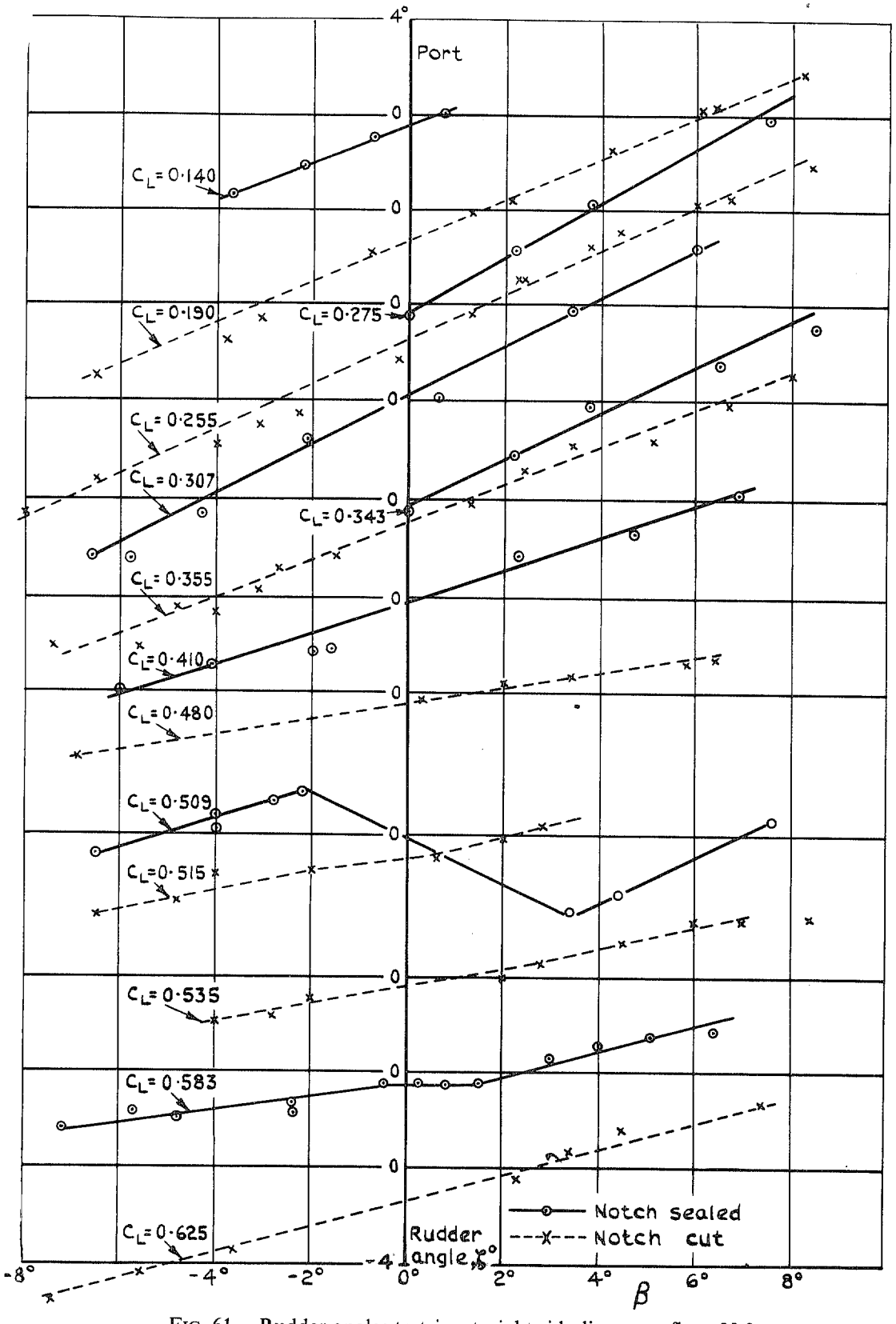

FIG. 61. Rudder angles to trim straight sideslips, nose flaps 20·2.

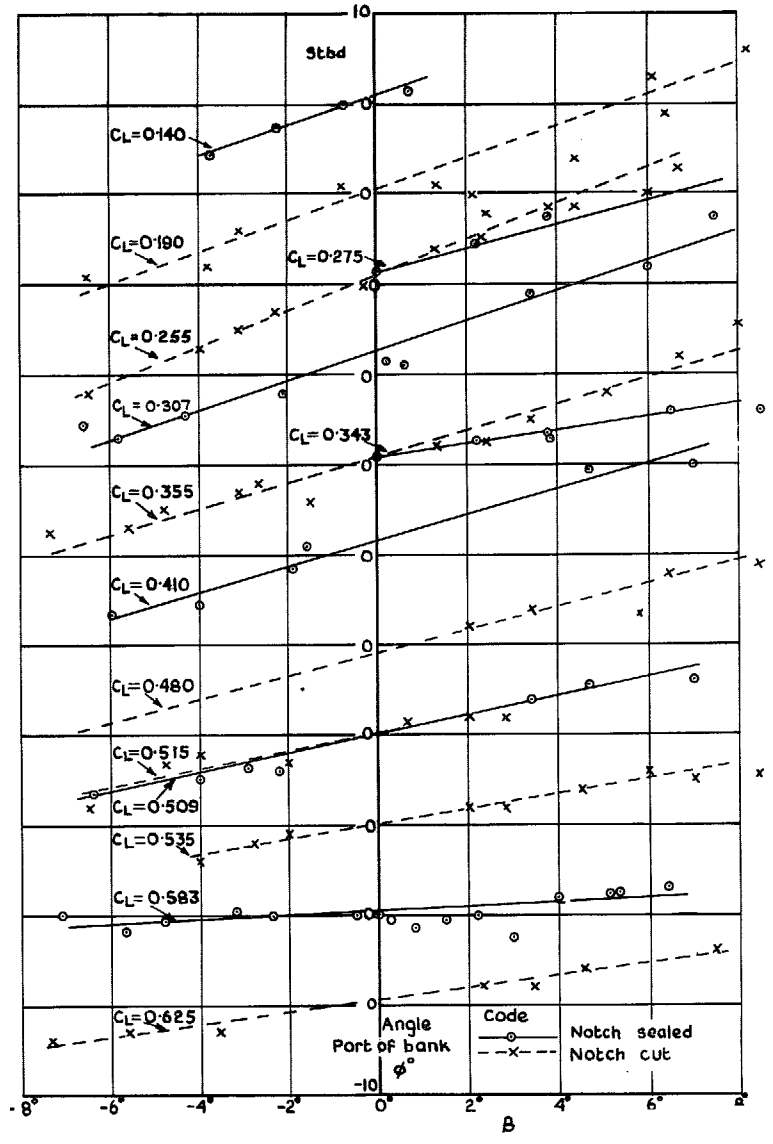

FIG. 62. Angles of bank in straight sideslips, nose flaps 20·2°.

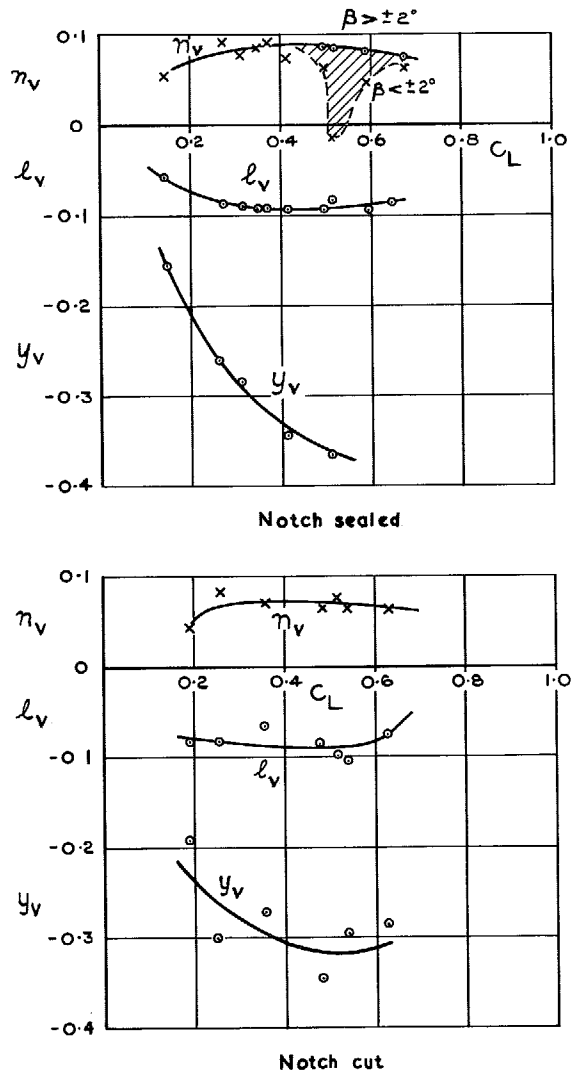

FIG. 63. Sideslip derivatives from steady flights tests (20·2° nose flap), moments corrected to 0·25 $\bar{c}$.

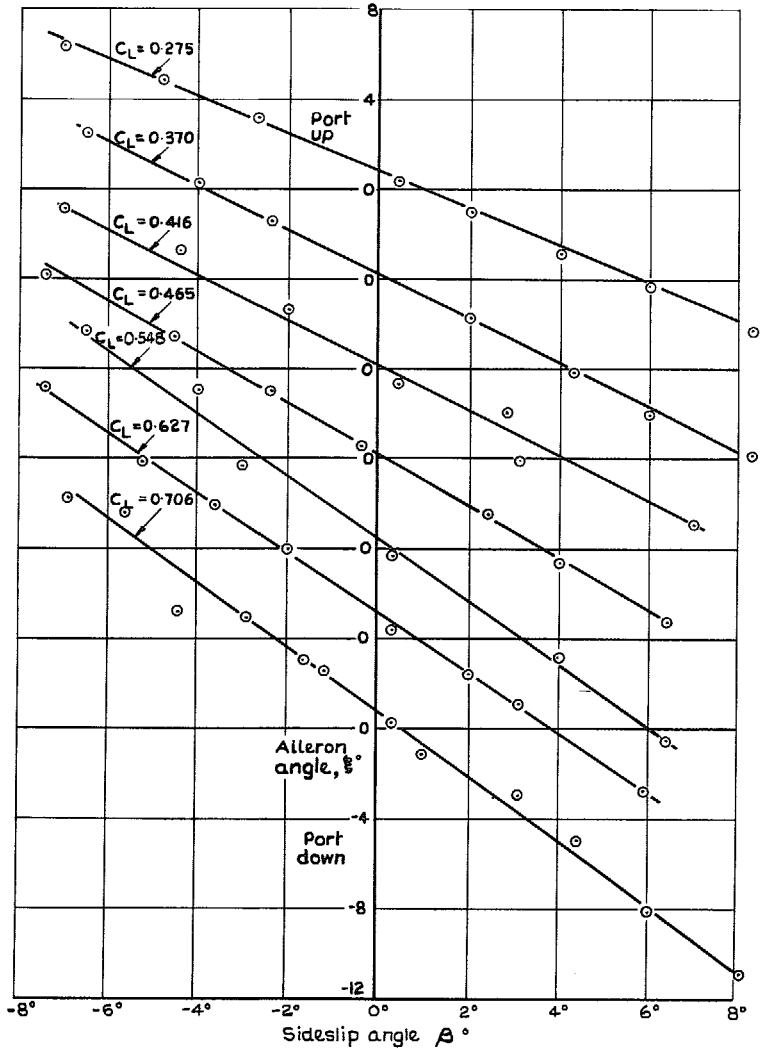

FIG. 64. Aileron angles to trim straight sideslips, 10·7° full span leading edge droop.

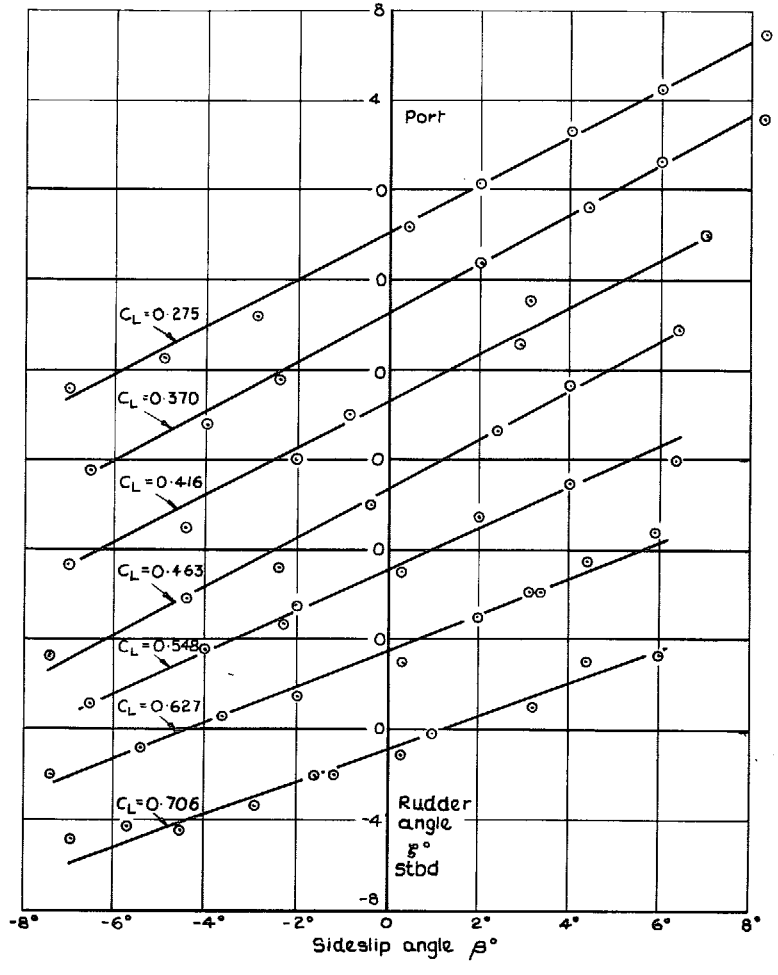

FIG. 65. Rudder angles to trim straight sideslips, 10·7° full-span leading-edge droop.

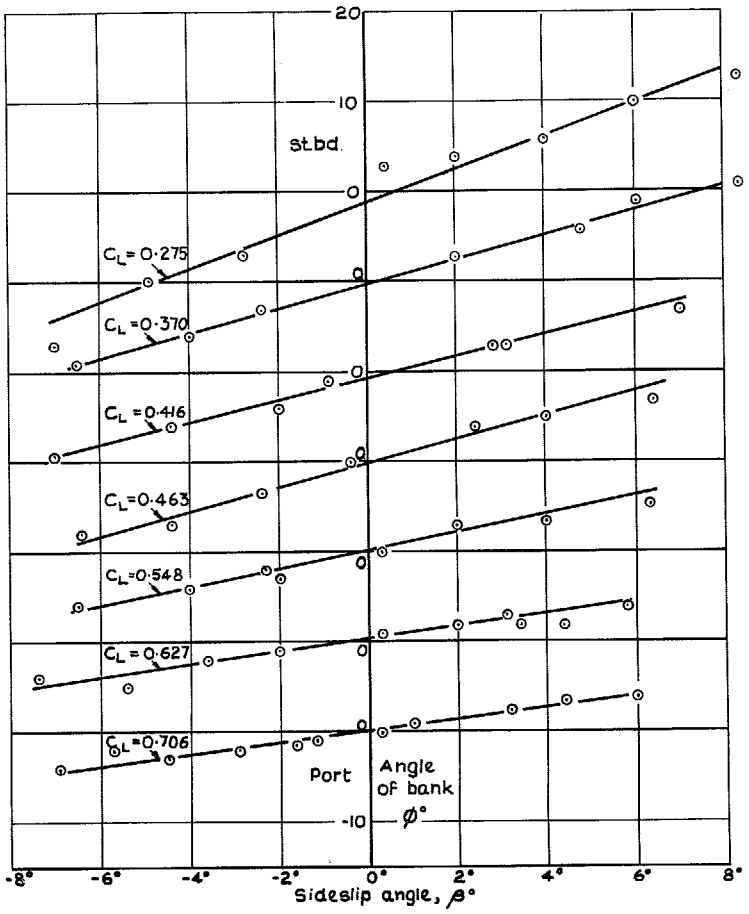

FIG. 66. Angles of bank in straight sideslips, 10·7° full-span leading-edge droop.

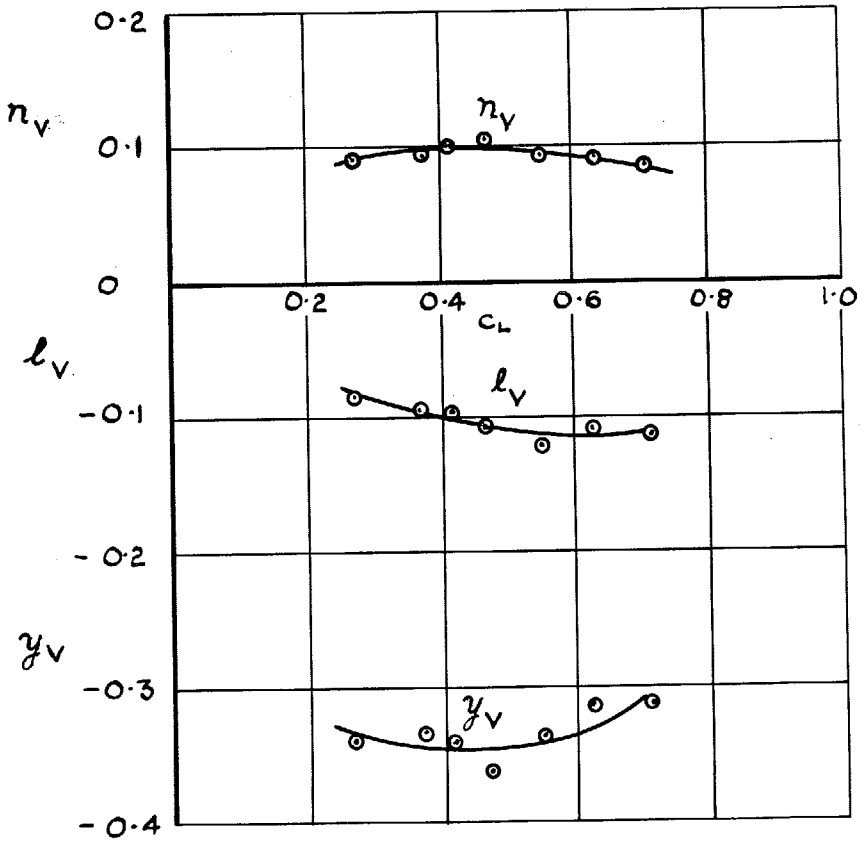

FIG. 67. Sideslip derivatives from steady flight tests (10·7° leading-edge droop), moments corrected to 0·25 $\bar{c}$.

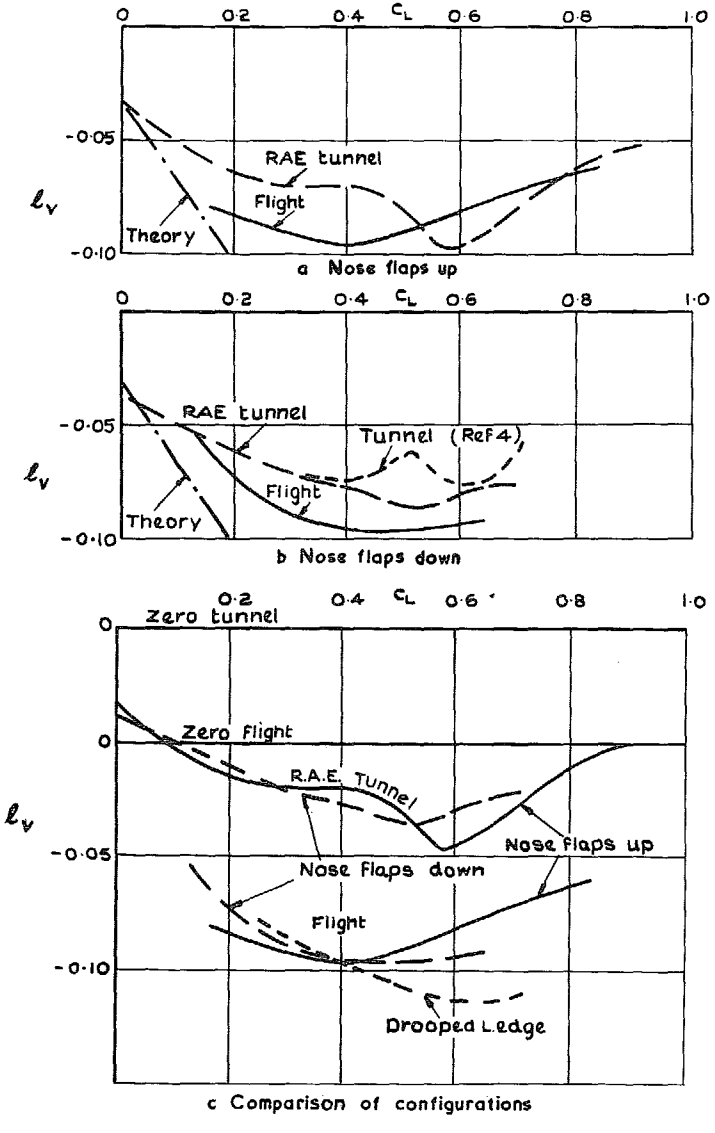

FIG. 68a–c. Comparisons between flight and tunnel results for l_v (notch sealed).

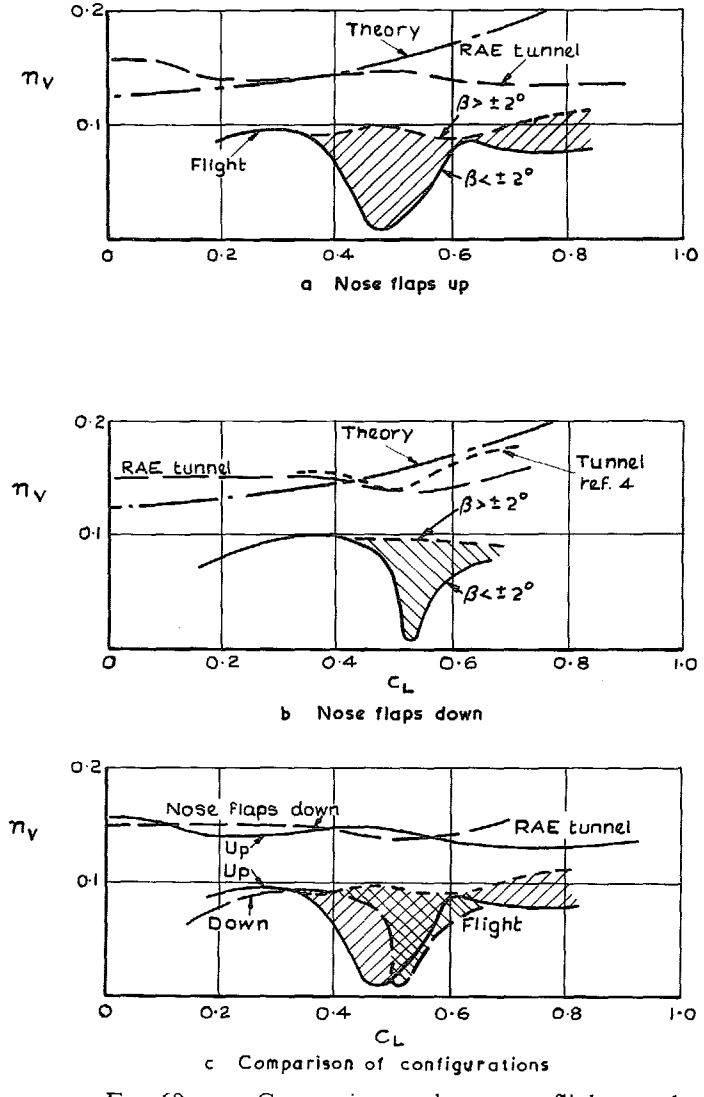

FIG. 69a–c. Comparisons between flight and tunnel results for n_v (notch sealed) referred to 0·25 $\bar{c}$ and corrected for intake momentum.

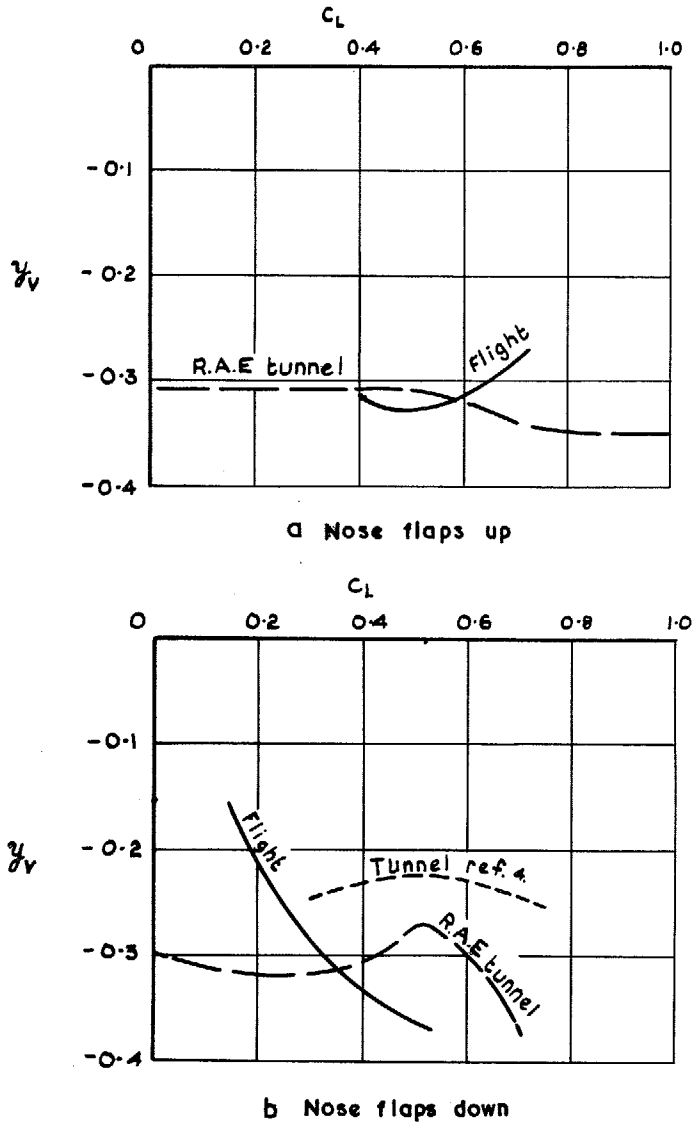

FIG. 70a and b. Comparison between flight and tunnel results for y_v.

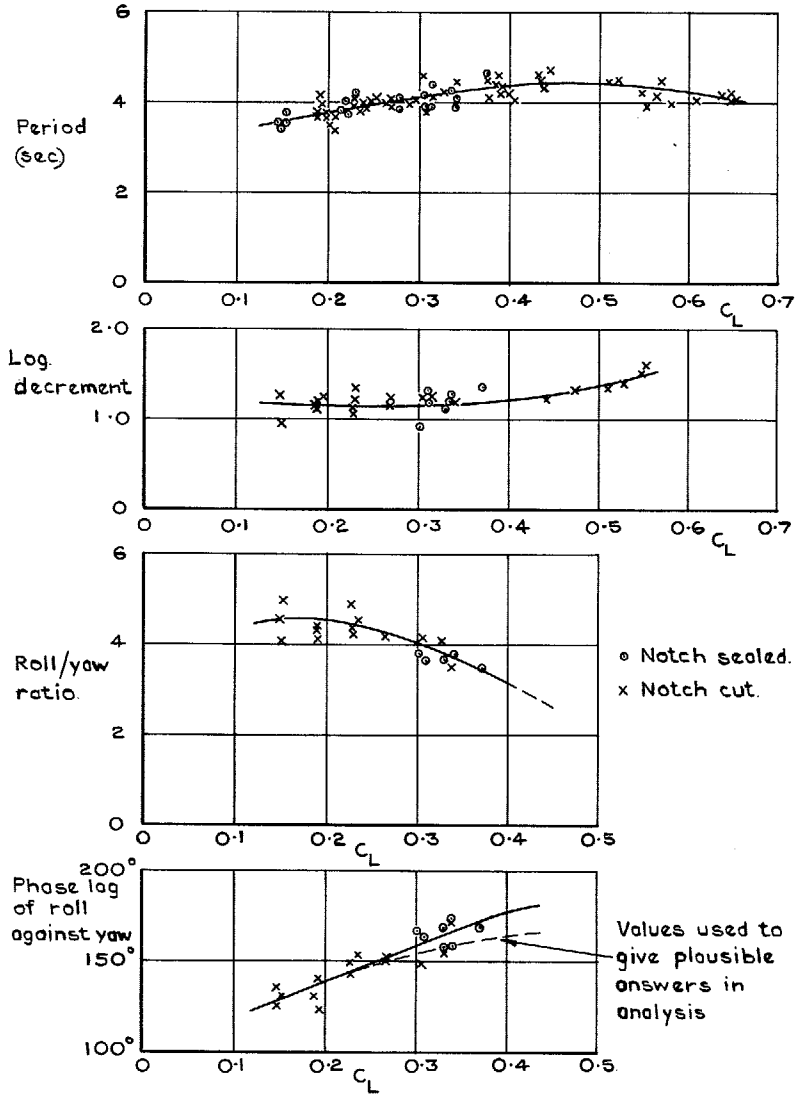

FIG. 71. Characteristics of the lateral oscillation at 5 000 ft altitude, nose flap 0°.

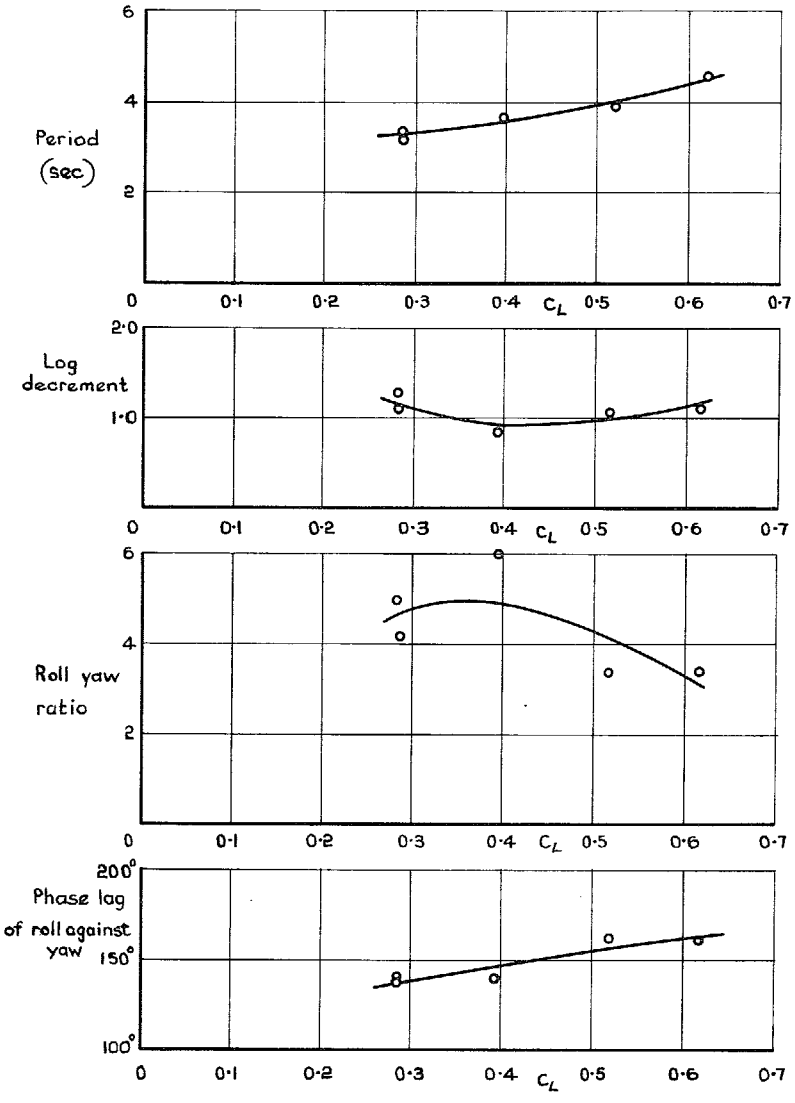

FIG. 72. Characteristics of the lateral oscillation at 5 000 ft altitude, full span leading-edge droop.

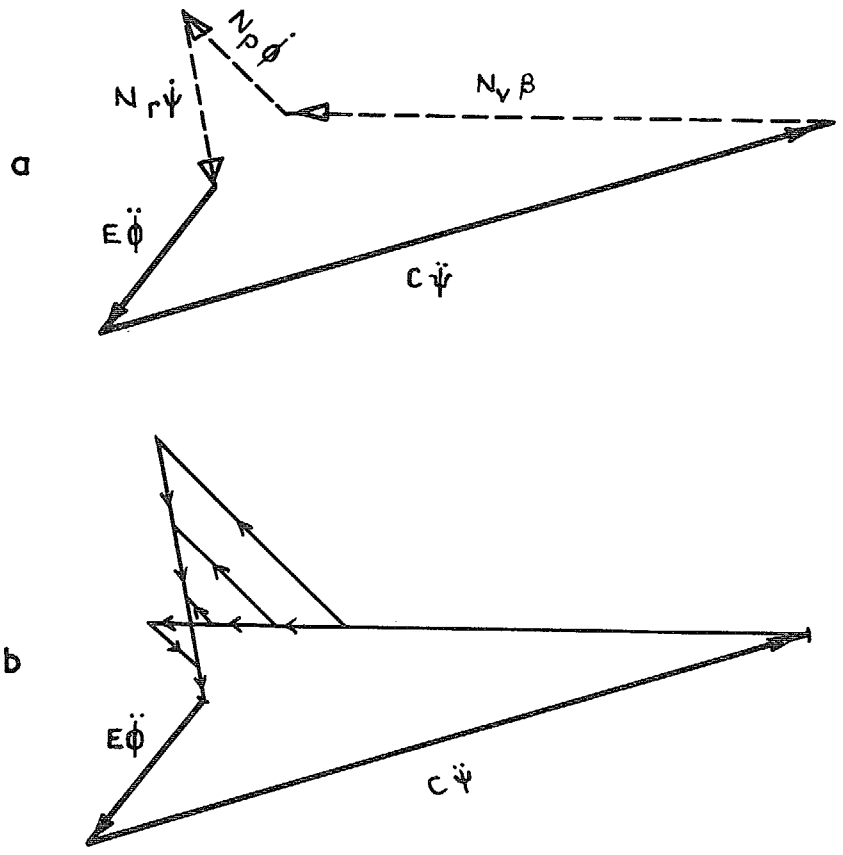

FIG. 73a and b. Typical yawing-moment vector polygon and combination of possible solutions.

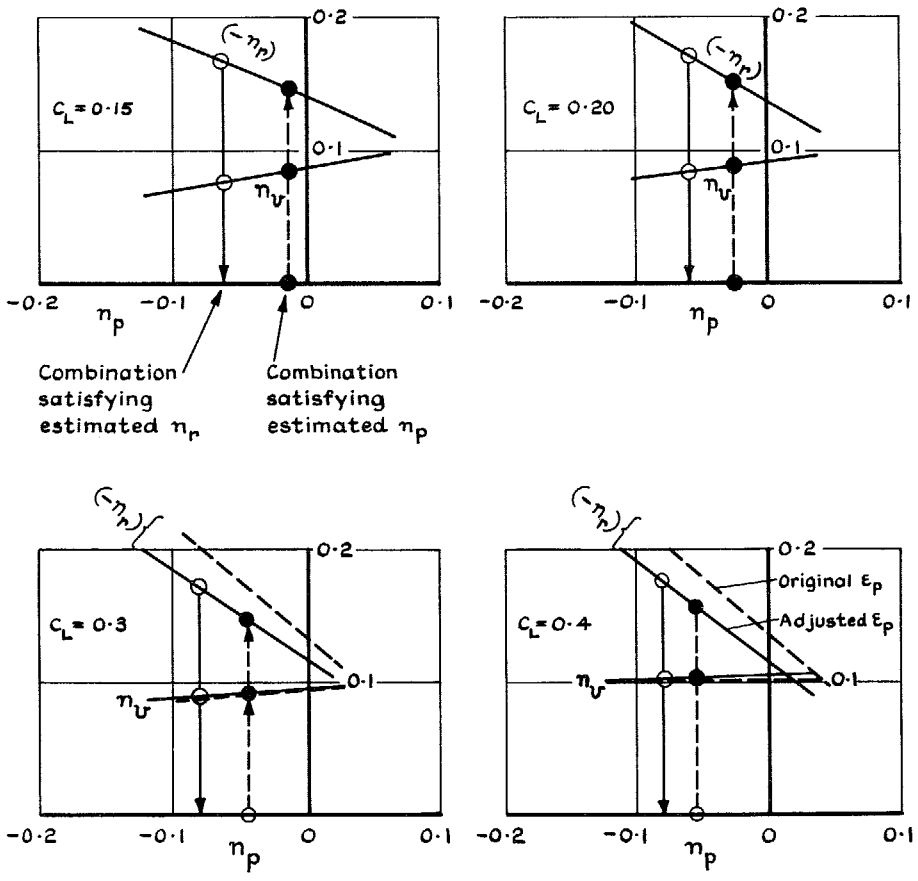

FIG. 74. Possible combinations of yawing-moment derivatives to satisfy measured dutch-roll characteristics, nose flap up. η_v adjusted to 0·25 $\bar{c}$.

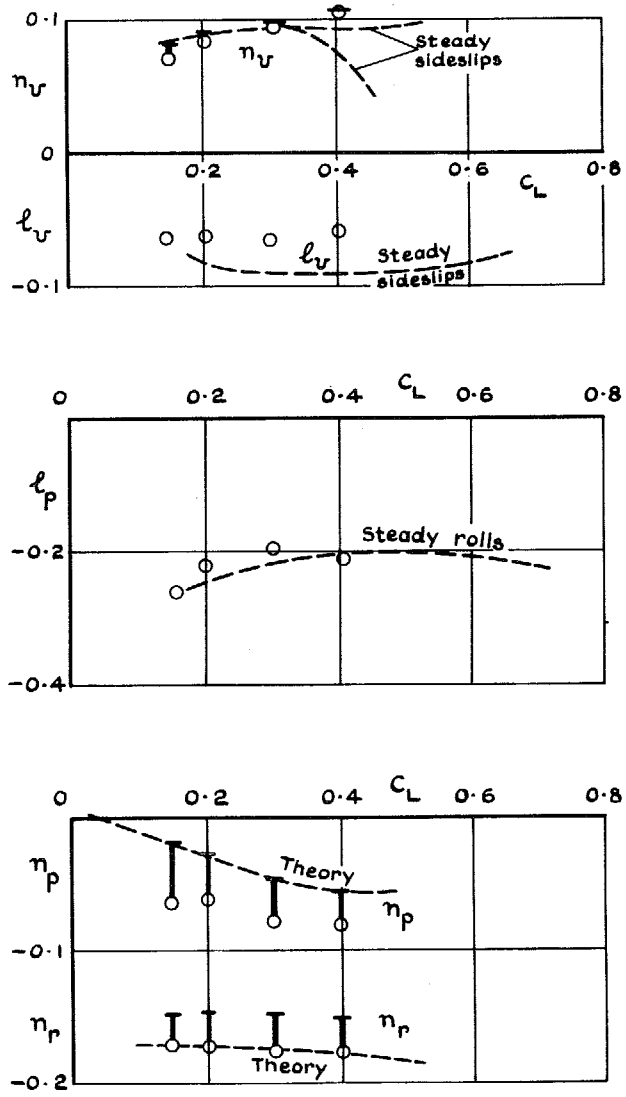

FIG. 75. Later*h*l stability derivatives from vector analysis of dutch rolls compared with steady flight test data or theory (n_v adjusted to 0·25 $\bar{c}$).

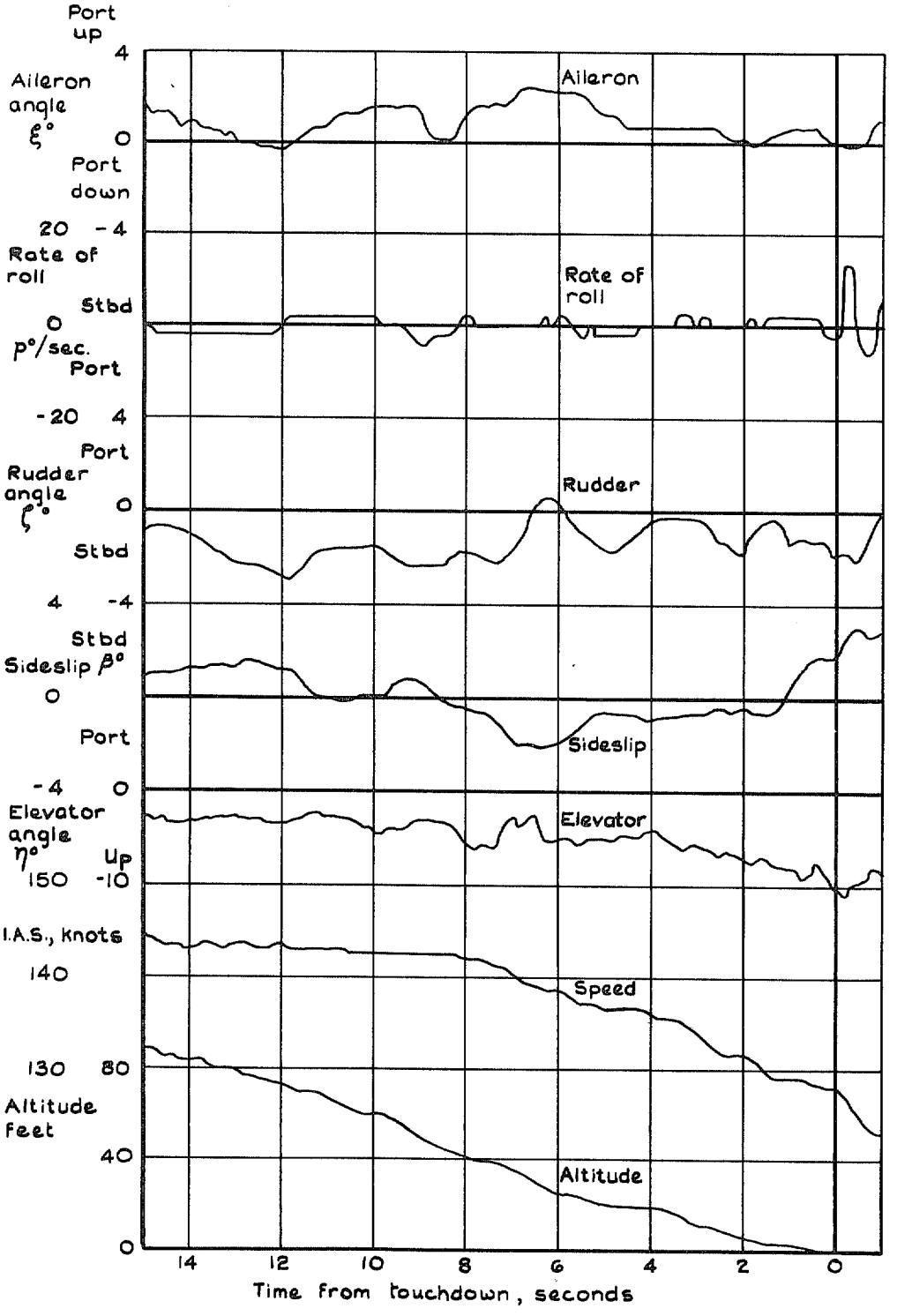

FIG. 76. Typical approach and landing, mild turbulence.

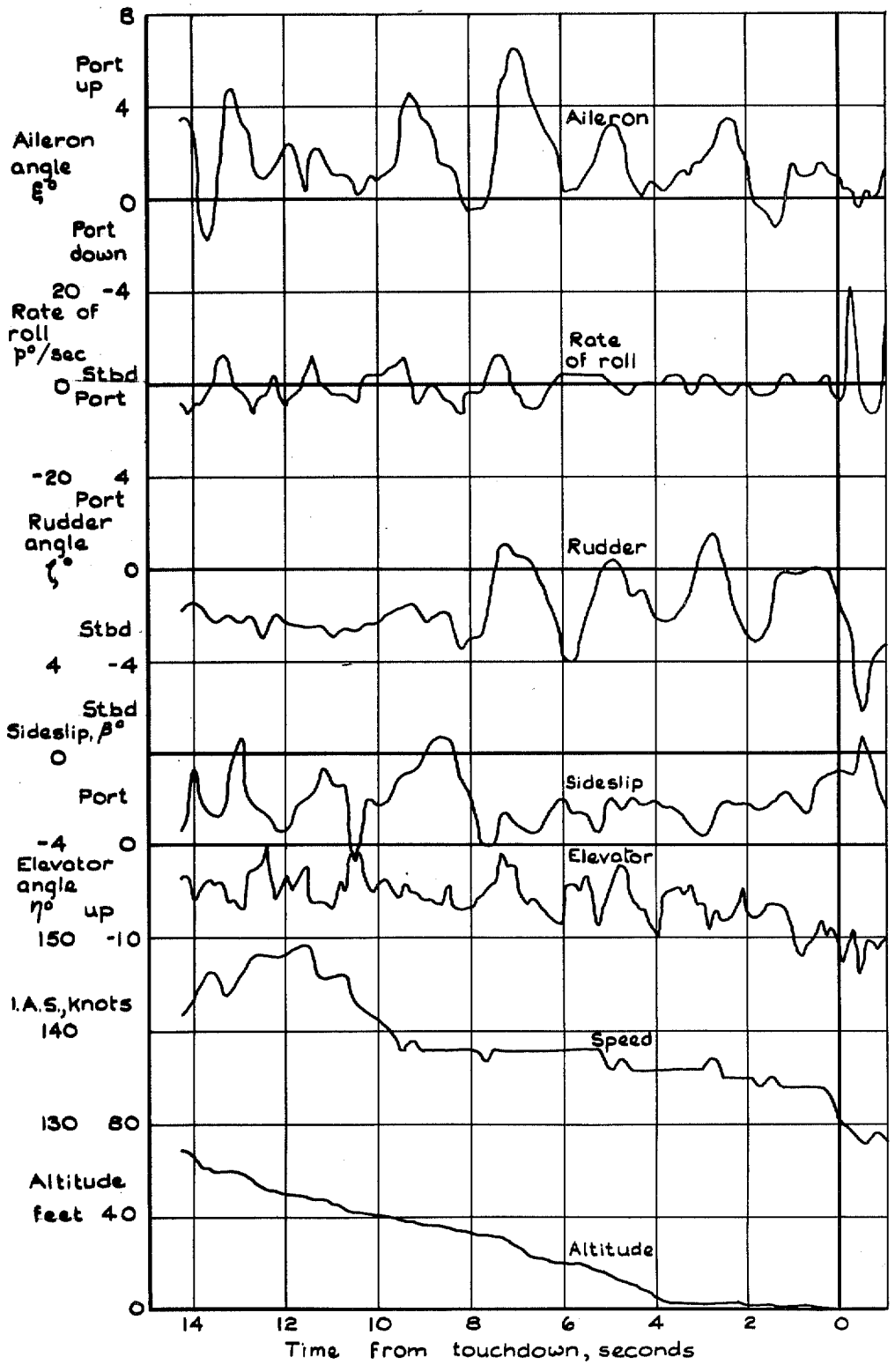

FIG. 77. Typical approach and landing, moderate turbulence.

Printed in Wales for Her Majesty's Stationery Office by Allens Printers (Wales) Limited

Dd. 135646 K 5

Published by
HER MAJESTY'S STATIONERY OFFICE

To be purchased from
49 High Holborn, London W.C.1
13A Castle Street, Edinburgh 2
109 St. Mary Street, Cardiff CF1 1JW
Brazennose Street, Manchester M60 8AS
50 Fairfax Street, Bristol BS1 3DE
258 Broad Street, Birmingham 1
7 Linenhall Street, Belfast BT2 8AY
or through any bookseller

S.O. Code No. 23—35